ORGANIC PHOSPHORUS DYNAMICS AND CONTRIBUTIONS TO EUTROPHICATION IN A SHALLOW, FRESHWATER BAY

Martin Roman Kurek

Submitted to the faculty of the University Graduate School
in partial fulfillment of the requirements
for the degree
Master of Science
in the Department of Earth Sciences,
Indiana University

July 2019

Accepted by the Graduate Faculty of Indiana University, in partial fulfillment of the requirements for the degree of Master of Science.

Master's Thesis Committee

_____
Gregory K. Druschel, PhD, Chair

_____
William P. Gilhooly III, PhD

_____
Gabriel Filippelli, PhD

ACKNOWLEDGEMENT

Completion of this project would not have been possible without the enormous contributions from countless colleagues, advisors, friends, and fellow scientists, all of whom I am very grateful for.

First, I would like to thank my mentor and advisor, Dr. Gregory Druschel for guiding me through both my undergraduate and graduate studies and all the extraordinary opportunities he has provided me with over the years we have been working together. Greg has always pushed me to be a better scientist, a more detail-oriented researcher, and a fluent writer, but at the same time has been the kindest and most understanding advisor I could ever hope for. I am sincerely thankful for all the lengthy sampling trips, late nights, long drives, conferences, presentations, meetings, lunches, dinners, and beers we have shared together all in the pursuit of science. Likewise, I thank my brilliant committee members, Dr. Gabriel Filippelli and Dr. William (Bill) Gilhooly III, for their guidance and knowledge passed down to me during my time at IUPUI and use of their scientific instruments. Particularly, Bill for being the first faculty member in the Earth Science department to meet with me when I first took an interest in geochemistry and for letting me work and learn in his laboratory as an undergraduate.

My research and travel were made possible through the NSF SusChEM grant 1560933 awarded to Dr. Gregory Druschel and the IUPUI graduate fellowship awarded to me in 2017.

I thank our collaborators for their useful feedback and suggestions regarding my research and manuscripts manifested in these chapters. Thank you to Dr. Andrew Schroth, for working with me during this project, allowing us to come sample Missisquoi

Bay, work at the UVM facilities, and all the helpful advice and direction he has given me. His graduate students, Megan Leduc and Austin Wilkes also deserve thanks for their hard work and assistance with sampling and data collection. Most of my work could not have been completed without the sample analyses and data collection from Dr. Philippe Schmitt-Kopplin's lab at the Helmholtz Zentrum in Munich. I sincerely thank him for warmly welcoming me in his lab, allowing me to learn from his extensive expertise, and utilizing his FT-ICR MS instrument. I also greatly appreciate the help from Dr. Mourad Harir over the course of my degree for analyzing samples for me and teaching me about FT-ICR MS data processing. With each email and skype meeting we had, I learned more about organic geochemistry and gained greater confidence in my collaborative abilities. I especially thank John Shukle for all the lab work, field work, R programming help, and ideas we've shared over the course of the Missisquoi Bay project. This degree would have without a doubt been much more difficult if our graduate careers had not overlapped.

I also want to thank all of those in the Earth Science department, particularly those who have helped in any way, including Dr. Catherine Macris, Dr. Pierre-André Jacinthe, and Dr. Lixin Wang for knowledge gained from their courses as well as Cathy Chouinard and Cheryl Montgomery for logistical support. I appreciate the help and comradery from the graduate students in the department, both current and past. I thank my lab group, including Chase Howard and Sarah Denny, for helping me analyze samples, collect field data, and providing me with comments and discussion. The Gilhooly lab group has also assisted me with countless hours of support, both instrumental and personal, especially Alice Bosco-Santos and Evelyn Becerra.

On a more personal level, I want to thank my friends and athletes that I have come to know on the rowing team at IUPUI, namely Taylor Gainey, Inna Ayos, Tara Grayson, Javon Washington, Seth Dalenberg, Trevor Farnsworth, Caleb Corey, Quentin Cooling, Mackenzie Deguch, Jason Kim, Kyle Tompkins, and countless others. They have all shown me immeasurable friendship and made me feel important while I used rowing as an outlet for my graduate work and has now become an important part of my life.

Lastly, I would like to thank my family for their emotional, financial, and spiritual support. My brother, Adam, and sister, Paulina, have always been supportive of my goals and just curious enough about my research to sustain my ego and make me feel like my work carries significance. They are great friends and even better siblings with hearts made of not necessarily gold, but perhaps copper. Both my parents have always done everything in their ability to help me succeed. Whether it was through a home-cooked meal, a stimulating conversation over wine, or just the unconditional love a father and mother have for their son, they have supported me in more ways than I can describe.

Martin Roman Kurek

ORGANIC PHOSPHORUS DYNAMICS AND CONTRIBUTIONS TO EUTROPHICATION IN A SHALLOW, FRESHWATER BAY

Phosphorus (P) is essential for aquatic life; cycling between both inorganic and organic forms to maintain an ecological balance. Its addition into P-scarce freshwaters, either through terrestrial (external) or sedimentary (internal) loading, may disrupt this balance causing blooms of phytoplankton to flourish, often resulting in harmful environmental and anthropogenic consequences. Accordingly, reduction of external P loading has been commonly implemented with a recent focus on sediment-bound legacy P that is mobilized into the water column during dynamic redox conditions. Mobile P species have been identified as both inorganic and organic, with the former representing the most bioavailable fraction, and the latter serving as a source for labile P in freshwaters when in high demand, particularly during blooms. Missisquoi Bay in Lake Champlain, VT experiences harmful cyanobacterial blooms driven by internal P loading and has been the target of numerous geochemical and hydrological studies. This thesis describes a high-resolution investigation of both the organic P and organic matter compositions of the bay with respect to mobility, reactivity, and bioavailability using Fourier Transform-Ion Cyclotron Mass Spectrometry (FT-ICR MS). Sediment from Missisquoi Bay was extracted with a diverse set of reagents, resulting in fractionation of both organic matter and organic P, and illustrating the distribution of various labile and recalcitrant compounds. Many of these molecules are associated with porewater or easily extractable mineral surfaces providing a link to the benthic organic matter and phosphorus fractions available to microorganisms. Additionally, the organic chemistry of

the bay was investigated seasonally from May 2017 to January 2018 revealing biological processing from the spring runoff season through the post-bloom summer season. The transition from late summer to under ice conditions in winter was less severe with a higher commonality between both organic matter and organic P compounds, suggesting reduced biological and abiotic degradation. Moreover, short-term anoxic incubations of sediment cores from each season revealed the presence of diverse organic signatures from sorption processes, and a significant contribution of benthic microbial activity to the benthic organic geochemistry.

Gregory K. Druschel, PhD, Chair

TABLE OF CONTENTS

LIST OF TABLES

LIST OF FIGURES

LIST OF ABBREVIATIONS

AI	Aromaticity index
AMP	Adenosine-5'-monophosphate
APCI	Atmospheric pressure chemical ionization
APPI	Atmospheric pressure photo ionization
BGA	Blue-green algae
Da	Dalton
DBE	Double bond equivalence
DN/TN	Dissolved nitrogen/total nitrogen
DOM	Dissolved organic matter
DOP	Dissolved organic phosphorus
EDTA	Ethylenediaminetetraacetic acid
ESI	Electrospray ionization
EXAFS	Extended X-ray adsorption fine structure
fDOM	Fluorescent dissolved organic matter
FT-ICR MS	Fourier transform-ion cyclotron resonance mass spectrometry
G1P	Glucose-1-phosphate
ICP-OES	Inductively coupled plasma-optical emission spectroscopy
ICP-MS	Inductively coupled plasma-mass spectrometry
KMD	Kendrick mass defect
MLB	Molecular lability boundary
MSCC	Multidimensional stoichiometric compound classification
NMDS	Non-metric multidimensional scaling
NMR	Nuclear magnetic resonance
ODO	Optical dissolved oxygen
OM	Organic matter
PCA	Principal component analysis
pH_{zpc}	pH at zero-point-charge
PPA	Phenylphosphonic acid
SOM	Soil organic matter
SPE	Solid phase extraction

SRFA	Suwannee River fulvic acid
SRP	Soluble reactive phosphorus
SWI	Sediment-water interface
TDP	Total dissolved phosphorus
TRII	Transformed relative intensity index
UV	Ultraviolet

Chapter 1 – A review of relevant literature

Introduction:

Phosphorus mobility and eutrophication:

When the immediate availability of phosphorus (P) is restricted, the cycling between terrestrial and aquatic environments often dictates the extent to which biological activity can thrive or collapse (Smil, 2000). Biological uptake of phosphorus is necessary for life; it is critical in energy storage and release, maintaining cell membrane integrity, signaling between cells, enzyme activity, bone structure, and various other functions (Filippelli, 2008). Anthropogenic overuse and mismanagement of available P through unsustainable mining and agricultural practices has placed great uncertainty in the future supply of accessible sedimentary deposits (Filippelli, 2011) and the health of aquatic ecosystems (Smil, 2000; Cooper et al., 2011; Serediak et al., 2014). The P cycle is primarily composed of terrestrial and aquatic components with no significant atmospheric input (Ruttenberg, 2014). Primary inputs of phosphorus into lakes occur through transfer of terrestrial P adsorbed onto sediment particles and some dissolved species as well (Turner, 2005; Serediak et al., 2014). These inputs result from numerous point and non-point sources of pollution. Examples of point sources include localized inputs such as sewage or outfalls, while non-point sources are comprised of diffuse inputs such as soil runoff, groundwater seepage, or atmospheric particles (Edwards & Withers, 2008; Serediak et al., 2014).

Anthropogenic activities have accelerated P loading with the world's 100 largest lakes experiencing an average of 7% more P input in 2005-2010 than 1990-1995 (Yuan et al., 2018). The trophic status of a lake is characterized by the total concentrations of

limiting nutrients (such as N and P), with elevated concentrations of phosphorus (30-100 mg/m^3) resulting in *eutrophic* conditions (Smith et al., 1999). When phosphorus is scarce in aquatic systems, a sudden input can generate eutrophic conditions resulting in greater organic matter production and excessive plant, algal, and cyanobacterial growth, leading to oxygen depletion and high probabilities of fish kills (Smith et al., 1999; Serediak et al., 2014). These inputs can be from external sources, internally within the lake, or a combination of the two. Lake sediment serves as a large potential reservoir of aquatic P, often more than 100 times higher than the dissolved concentration in the water column (Søndergaard et al., 2003). Sedimentary P is a diverse pool that varies greatly based on the chemical composition of the lake, but generally includes dissolved P species, phosphorus adsorbed onto mineral surfaces, and phosphorus precipitated as minerals (Søndergaard et al., 2003). In addition to sedimentary minerals, colloidal Fe(III) particles can adsorb dissolved P (Yan et al., 2016), increasing the sedimentary P pool. Mobilization of the sedimentary P pool into the water column is known as internal loading, occurring due to changes in chemical conditions. In shallow eutrophic lakes, long term studies have confirmed that warm summer months (May-August) consistently release up to 300% of the external P load from the sediment (Søndergaard et al., 2013) contributing greatly to the eutrophic status.

Orthophosphate, organic P, and other organic matter have high adsorptive affinities for minerals such as iron (Fe) and manganese (Mn) (oxy)hydroxides that are liberated from the sediment upon dissolution of the minerals (Celi & Barberis, 2005; Wang et al., 2013; Chassé & Ohno, 2016). These minerals are insoluble and stable under oxic conditions but undergo reductive dissolution at a circumneutral pH when the

dissolved oxygen concentrations are diminished (Lovley, 1991; Reynolds & Davies, 2001; Christophoridis & Fytianos, 2006; Smith et al., 2011). Reductive dissolution mainly occurs through microbial coupling of organic matter oxidation to Fe(III) and Mn(IV) (oxy)hydroxide dissimilatory reduction, releasing soluble Fe(II) and Mn(II) into the water column (Lovley, 1991). Fe(III) and Mn(IV) can also be reduced abiotically by specific organic compounds, but at much slower rates than enzymatic reduction, making biological reduction a more important mechanism in freshwater sediments (Lovley, 1991). The pH of the lake also contributes significantly to P mobility. Adsorbed phosphate groups can be displaced from oxide surfaces by competing OH^- ions at an alkaline pH, or through anionic repulsion on the mineral surface if the pH is above the mineral zero-point charge (pH_{zpc}) (Lijklema, 1980; Christophoridis & Fytianos, 2006). For some minerals, such as poorly crystalline Fe(III) (oxy)hydroxides, the pH_{zpc} is above neutral (7.0-8.8) (Parks, 1965) making adsorption at circumneutral conditions likely; whereas MnO_2 minerals are much lower (~2.5) (Murray, 1974), but have still been shown to strongly sorb phosphates at a higher pH in the presence of dissolved cations (Kawashima et al., 1986). Thus, the interplay between E_h and pH in freshwater lakes will dictate the release of phosphorus from the sediment, depending on the mineralogy and geochemistry of the lake sediment (Christophoridis & Fytianos, 2006).

Anoxic events driving internal loading of phosphorus have been observed during algal/cyanobacterial bloom events and during winter months where ice cover reduces oxygen penetration (Smith et al., 2011; Giles et al., 2015; Schroth et al., 2015; Joung et al., 2017). In some cases, rapidly changing hydrological conditions can be sufficient to mobilize phosphorus. For instance, Giles et al. (2016) observed rapid (<24 hours)

changes in oxygen stratification and warming leading to sedimentary P and dissolved metal release during summer months. The concurrent release of bioavailable P may then directly lead to excessive microbial, algal, or macrophyte growth which may further prolong anoxic conditions, releasing more phosphorus (Boström et al., 1988; Cullen & Forsberg, 1988; Tyrell, 1999; Mitchel & Baldwin, 2005). During these anoxic periods, mixing events over short time scales such as wind and storm events can entrain oxygen in the bottom water which ceases internal loading by allowing the precipitation of oxide minerals that re-adsorb phosphorus and organic matter (Smith et al., 2011; De Vicente et al., 2012; Schroth et al., 2015). Phosphorus in these systems experiences a hysteresis where it is difficult to remove from the lake by hydrological transport due to its chemical affinity for charged particles and its high demand from residing organisms. Therefore, the cyclic activity of anoxia and reoxygenation are often key to eutrophication and the seasonal mobility of internal P within freshwater lakes.

Cyanobacteria:

Eutrophication driven by nutrient loading has had harmful effects on water quality and ecosystem health (Smith et al., 1999; Yuan et al., 2018). Primary productivity in lakes is mostly due to algal photosynthetic growth. However, during eutrophication trophic shifts from algae and phytoplankton to cyanobacteria occur where the cyanobacteria are equipped to adapt and outcompete other microorganisms (Serediak et al., 2014). Cyanobacteria are highly diverse oxygenic photoautotrophs with many genera able to fix atmospheric nitrogen anaerobically to fulfill their nitrogen needs, while also storing phosphorus and iron to survive in nutrient scarce environments (Paerl & Otten,

2013). These organisms favor warm (25-35° C) surface temperatures, abundant sunlight, and calm, dry air conditions (Paerl & Otten, 2013), as is typical in Northern latitude summer months. A swift influx of nutrients, especially bioavailable P, into a lake where they are limiting can activate rapid biological activity and result in cyanobacteria dominating the photic zone and creating large aggregates of biomass referred to as "blooms" (Mur et al., 1999). Cyanobacterial blooms occur in many aquatic, marine, and estuarine systems impacting millions worldwide, with the potential to increase due to climate change (O'Neil et al., 2012). On a local scale, the ecological effects of blooms are harmful to both residing aquatic life and its consumers who depend on the ecosystem for aquaculture, economic revenue, and drinking water. Biomass from blooms often cause a loss in water clarity suppressing macrophyte and other photoautotrophic activity (Paerl & Otten, 2013). Cyanobacteria can also produce toxic metabolites affecting hepatopancreatic, digestive, endocrine, dermal, and nervous systems in humans (Carmichael, 2001; Kuiper-Goodman et al., 1999; Christoffersen et al., 2002).

Persistence and eventual decomposition of dying biomass results in hypoxic or benthic anoxic events from oxygen depletion beneath the bloom by the rapid oxidation of organic matter, heterotrophic consumption, and limited vertical remixing (Zilius et al., 2014). Anoxia also occurs from light occlusion, when cyanobacteria shift to a heterotrophic metabolism and deplete dissolved oxygen resulting in fish kills and release of sediment-bound P (Smith et al., 2011; Paerl & Otten, 2013). Sustaining blooms is often driven through positive feedback cycles such as the release of sediment-bound P delivering additional nutrients to the cyanobacteria (Giles et al., 2016) and through absorption of solar radiation at the surface which increases the temperature and favors

proliferation (Paerl & Otten, 2013). Other environmental conditions such as low DN:SRP ratios may also be key to sustaining blooms during already anoxic conditions (Pearce et al., 2013) where cyanobacteria can thrive on low TN conditions (Isles et al., 2017). Once initiated, blooms can persist for days or months, long after the external input of nitrogen and phosphorus is reduced (Paerl, 1988). However, they are finite; they can be disturbed and terminated by water column mixing, storm events, or a decrease in surface water temperatures (Bormans et al., 2005) as well through viral cell lysis (Suttle, 1994; Paerl & Otten, 2013).

Dissolved organic matter:

Freshwater systems act as a substantial sink of carbon as inorganic and organic species are transported from terrestrial sources and are buried in lakes, totaling around 5.1 Pg C/ year (Drake et al., 2018). Organic matter can be mineralized to CO_2, stored in sediments, or exported to oceans by rivers (Cole et al., 2007). All these processes are central to the global carbon cycle with inland freshwaters serving as a key intermediate between carbon storage and release into the atmosphere as CO_2 (Cole et al., 2007). Freshwater dissolved organic matter (DOM) is a complex mixture of organic compounds that encompass a diverse mass range, contain various elemental compositions, and possess a set of unique chemical and physical properties (Perdue & Ritchie, 2014). DOM plays a central role in many aquatic cycles by serving as a carbon source in microbial food webs and connecting the carbon cycle to other elemental cycles through consumption and degradation of organics (Aitkenhead-Peterson et al., 2003; Perdue & Ritchie, 2014). The classification of DOM is largely operationally defined as the soluble

fraction of organic matter that passes through a 0.45 μm filter; this fraction can include some colloids and complexes (Nebbioso & Piccolo, 2012), meaning it may not all be "truly dissolved." Frequently, DOM is characterized by its functional groups giving it hydrophobic or hydrophilic-like properties (Perdue & Ritchie, 2014). Within these two categories, molecules are further classified as acidic, neutral, or basic, with most freshwater DOM being composed of hydrophobic acids (Perdue & Ritchie, 2014). Acidic functional groups in DOM are largely from carboxylic and phenolic hydroxyl groups (Perdue & Ritchie, 2003), while basic functional groups include amines (Sleighter & Hatcher, 2007).

DOM transport and reactivity:

Sources of aquatic DOM can be terrestrial (allochthonous) or produced by aquatic plants and microorganisms (autochthonous). Both sources are mixed in the water column as terrestrially-derived DOM is transported from soil and vegetation by the hydrologic cycle (Aitkenhead-Peterson et al., 2003). Terrestrial DOM has a unique molecular signature that is enriched in lignin-like molecules containing randomly branched networks of aromatic and phenolic groups linked by ether bonds (Nebbioso & Piccolo, 2012). These molecules are thought to be more resistant to microbial degradation, compared to most plant debris (Dittmar & Stubbins, 2014), while labile molecules such as proteins and carbohydrates are readily hydrolyzed by enzymes (Nebbioso & Piccolo, 2012). The distribution of allochthonous DOM follows a continuum, where first order streams will contain the most diverse and bioavailable compounds and subsequent higher order streams and water bodies will contain more recalcitrant DOM as it is processed

from the source during transport (Vannote et al., 1980). Transformation continues in freshwater lakes as DOM is consumed throughout the water column and sediment, continually fractionating compounds by degrading the most labile molecules (Meyers & Ishiwatari, 1993). Upon deposition, organic matter is subject to resuspension and bioturbation and in anoxic sediment, methanogenesis can convert labile DOM to methane, ensuring the burial of the most recalcitrant compounds (Meyers & Ishiwatari, 1993). Microbial transformation of DOM is based on bioavailability, or the ability of microorganisms to break carbon bonds and utilize the molecules. Bioavailability is a result of elemental composition and inherent molecular properties; aliphatic carbon molecules with high H/C and N/C ratios and lower O/C ratios have been preferentially consumed by aquatic bacteria to support growth, while unsaturated compounds are less bioavailable (Sun et al., 1997).

Additionally, abiotic transformations can dictate the fate and molecular signatures of DOM. Photobleaching of chromophoric (light absorbing) molecules breaks carbon bonds through electronic excitation and subsequent reactions producing inorganic carbon and transformed organic molecules (Perdue & Ritchie, 2014). Many of these chromophoric molecules are of terrestrial origin containing conjugated aromatic rings from lignins (Fichot et al., 2016). Solar radiation of freshwater riverine DOM has been shown to degrade terrestrial aromatic compounds, producing highly saturated aliphatic molecules that are more photo-resistant (Spencer et al., 2009; Stubbins et al., 2010). Photodegradation of freshwater DOM may also impact the aquatic food web as many of these photo-produced compounds are bioavailable, stimulating microbial growth and activity (Moran & Zepp, 1997; Perdue & Ritchie, 2014). An indirect consequence of

photobleaching is also the abiotic transformation of DOM from the photo-induced production of hydroxyl radicals and other reactive oxygen species (Dittmar & Stubbins, 2014). Radical ions are non-selective and highly reactive towards organic carbon leading to structural alterations of organic molecules including oxygenation, degradation to smaller compounds, and assimilation of substrates and radicals into larger compounds (Sandvik et al., 2000). Hydroxyl radicals can also be formed through Fenton reactions involving photo-reduction of Fe(III) to Fe(II) followed by concurrent Fe(II) oxidation by peroxide to afford the radical (Walling, 1975). These reactions have been suggested as a significant pathway for DOM transformations in Fe-rich aquatic systems, such as discharges from acid-mine drainage (White et al., 2003).

Other abiotic interactions involve complexation with mineral surfaces and dissolved metals, fractionating the deposited DOM and preserving organic matter in sediments (Lalonde et al., 2012). Compounds that are highly oxygenated with aromatic character have been shown to preferentially adsorb onto mineral surfaces including Fe oxides (Coward et al., 2018), aluminum (Al) oxides (Galindo & Del Nero, 2014), and clay minerals (Avneri-Katz et al., 2017). Complexation of DOM to cations through organic ligand interactions sequesters the metal from biological uptake and decreases the pool of bioavailable organic matter (Perdue & Ritchie, 2014). This interaction has biological implications as free toxic metals are chelated (Allen et al., 1980) and biologically essential metals are liberated from organic ligands through competitive displacement with other metals (Harrsion & Morel, 1983).

Organic phosphorus:

As biological processes regulate and consume low concentrations of orthophosphate in lakes (Hudson et al., 2000), it is likely that organisms will turn to organic sources to meet their nutritional demand (Mitchell & Baldwin, 2005). Dissolved organic phosphorus (DOP) molecules are functionally defined by their bonding structure, either containing a phosphate or phosphonate group. Phosphomonoesters contain a single O-C bond from the phosphate group while phosphodiesters contain two O-C bonds, both include the most oxidized state of phosphorus (+5). Phosphonates contain a single P-C bond with the P atom being more reduced (+3). Phosphate ester molecules are considered to be more bioavailable due to the susceptibility of ester bonds to hydrolysis releasing orthophosphate, while the stronger bonding stability of phosphonates limit their degradation (Turner et al., 2005). However, it has been reported that some marine cyanobacteria can outcompete other microorganisms through selective hydrolysis of phosphonates (Baldwin, 2013). The common aquatic phosphoesters can be further classified into DNA/nucleotides, inositol phosphates, and phospholipids (Baldwin, 2013). A summary of the DOP classes are illustrated in figure 1.1.

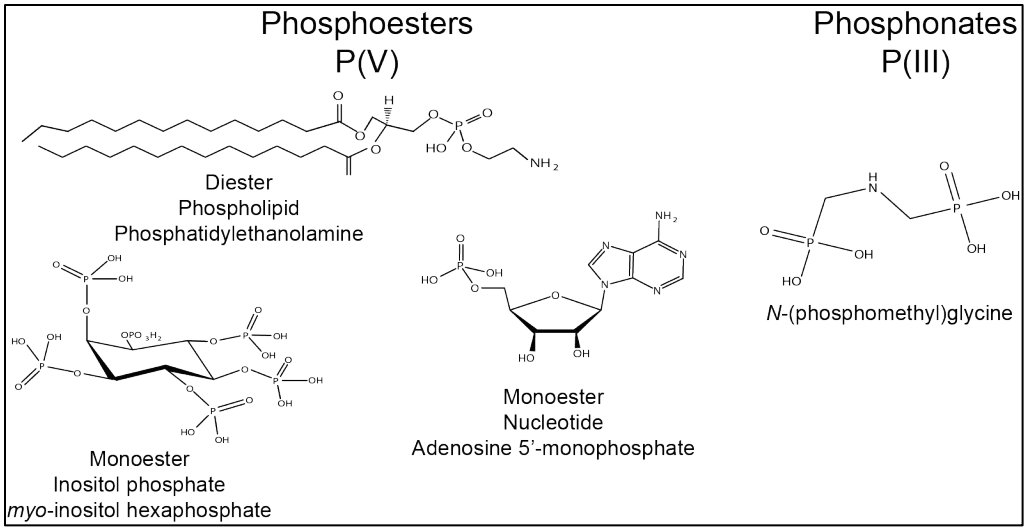

Figure 1.1. Classes of common organic P molecules categorized by bonding structures.

DNA or degraded derivatives frequently represent the most abundant form of DOP in aquatic systems and thus act as a source of phosphorus under nutrient limiting conditions, while their building block nucleotides represent a much lower proportion of DOP (Baldwin, 2013). The many isomers of inositol phosphates represent the most common storage for phosphorus in terrestrial plants and are readily mobilized into aquatic systems through runoff as aggregates associated with sediment particles (Baldwin, 2013). However, their contribution to the bioavailable fraction of DOP is unclear, with evidence of them being used as a source for carbon rather than phosphorus by microorganisms (Siuda & Chrost, 2001; Baldwin, 2013). Furthermore, inositol phosphates are far less abundant in freshwater than in soils due to their high affinity for charged particles (Celi & Barberis, 2005). Phospholipids contain a polar phosphate head group and hydrophobic aliphatic chain causing them to aggregate in the particulate fraction (Baldwin, 2013). The role of phospholipids is not well known in aquatic systems but is thought to be less bioavailable due to their association with particles and cell

surfaces. In some marine systems certain phytoplankton can replace phospholipids in cell membranes with non-P-containing lipids under nutrient limiting conditions, further suggesting that they may have low bioavailability potential (Van Mooy et al., 2009; Baldwin, 2013).

Sources of freshwater DOP is analogous to DOM in the sense that they can be allochthonous or autochthonous. Terrestrial sources account for the majority of allochthonous DOP and include manure, vegetation, pesticides, and soil (Barnett, 1994; Celi & Barberis, 2005; Turner, 2005). DOP distributions vary in different types of soils, but generally phosphomonoesters are the most abundant, followed by diesters, and then phosphonates (Turner, 2005). Most labile forms of DOP are rapidly mineralized to orthophosphate by microorganisms in the soil unless a rainfall or storm event transports them before they are hydrolyzed (Turner, 2005). Terrestrial DOP is more mobile than dissolved orthophosphate because it is not adsorbed as strongly to minerals or organic particles in the soil (Aitkenhead-Peterson, 2003). Even within DOP classes, chemical properties dictate transport; phosphoesters with a lower charge density are displaced into solution from soil particles and result in greater mobility than DOP with a higher charge density (Frossard et al., 1989). Within aquatic systems, autochthonous DOP is intracellularly produced by organisms and released into the water column upon decomposition or cell lysis (Baldwin, 2013). Reductive dissolution of minerals within lakes is also a significant source of DOP as phosphorus molecules are desorbed from sediment and released into the overlying water during reducing conditions (Smith, 2009; Giles et al., 2015).

Aquatic transformations and mineralization:

Degradation of DOP in aquatic systems involves cleavage of the O-P bond producing labile orthophosphate through biotic or abiotic pathways. Biotic degradation occurs via enzyme-catalyzed hydrolysis of the phosphate moiety either through extracellular enzymes or enzymes associated with cell surfaces. Common microbial enzymes present in freshwater lakes include alkaline phosphatases which hydrolyze a wide range of substrates either through an O-P or S-P bond and periplasmic nucleotideases that are responsible for hydrolyzing nucleotide phosphates (Heath, 2005). Both enzymes are subject to different inhibitory effects, which may fractionate the remaining pool of DOP (Heath, 2005). Heterotrophic bacteria can directly uptake certain organic P molecules under non-limiting conditions such as *E. coli* with glycerol-3-phosphate and many other microorganisms assimilating glucose-6-phosphate (Heath, 2005). Direct uptake of low molecular weight DOP through gene regulation has been suggested to satisfy nutritional carbon requirements when phosphorus is not limiting (Heath, 2005; Spohn & Kuzyakov, 2013; Baldwin, 2013), indicating that the bioavailability of DOP is not strictly confined to P need. Similarly, when nitrogen and carbon are limiting, the activity of 5'-nucleotideases increases to satisfy nutritional deficiencies by cleaving phosphate groups from nucleotides, providing a major source of orthophosphate that is not assimilated into biomass while the nucleotides are consumed (Mitchell & Baldwin, 2005).

The primary abiotic reactions of DOP are hydrolysis and photolysis. Hydrolysis can occur either through an associative pathway or dissociative pathway which are both dependent on the phosphate ester, the residual leaving group on the molecule, and pH

(Baldwin et al., 2005). Hydrolysis can also be catalyzed by dissolved metal cations either by neutralizing the negative charge of the phosphate ligand or by shifting electron density from the phosphate group to the metal making it more electrophilic (Baldwin et al., 2005). However, this effect is specific to certain molecules with some compounds, such as phytate, not experiencing any increase in hydrolysis rate after the addition of various metal cations (Bullock et al., 1993; Baldwin et al., 2005). Conversely, some cations may stabilize DOP compounds, preventing hydrolysis, by forming coordination complexes such as Fe(III) and Ca(II) (Celi & Barberis, 2005). Similarly, free DNA fragments have been shown to aggregate with dissolved Fe(III) and Al(III) and precipitate micron-sized particles (Qin et al., 2017). Although complexation may not degrade organic P, it is still an environmentally relevant mechanism that sequesters DOP and affects its water column mobility. Mineral surfaces also contribute to abiotic degradation of DOP through adsorption of compounds directly onto the surface or though facilitation of hydrolysis. Both Mn oxides and Fe oxides have exhibited adsorptive capacities for organic P molecules and promote hydrolysis of the compounds (Dannenberg & Pehkonen, 1998; Baldwin et al., 2001; Baldwin et al., 2005). In a study of p-nitrophenyl phosphate as a model DOP compound, Baldwin et al. (1995) found that Mn oxides catalyzed the hydrolysis most effectively, followed by Fe oxides, and no observable effects for silica, barium sulfate, or clay minerals. However, this increase of hydrolysis will only release bioavailable P upon reductive dissolution of the mineral oxides when the newly formed orthophosphate is desorbed from the surface (Baldwin et al., 2005).

Photolysis of DOP has also been recognized as a paramount pathway for aquatic degradation. Many organic P compounds are susceptible to degradation through

photolysis such as humic-P complexes, various biomolecules including DNA and RNA, and allochthonous pesticides (Baldwin et al., 2005). Reactions occur either directly from DOP molecules containing chromophores that hydrolyze the phosphate group upon excitation, or through formation of radicals on carboxyl and hydroxyl groups associated with humic matter that react with phosphate groups (Kamiya & Kameyama, 1998; Baldwin et al., 2005). Degradation can also occur indirectly, proceeding through photolysis of humic substances that have formed stable aggregates with phosphatase enzymes. These enzymes are then released into the water and can promote further orthophosphate liberation through hydrolysis (Boavida & Wetzel, 1998; Baldwin et al., 2005). Likewise, humic substances complexed to Fe(III) ions can be disrupted through UV photoreduction of Fe(III) to Fe(II), releasing bound orthophosphate, small organic molecules, and possibly DOP compounds (Francko & Heath, 1982). Photolysis can also regulate biological transformations of phosphorus through competitive inhibition of phosphatase enzymes by DOP compounds that are released from UV irradiation (Yiyong, 1996). A summary and visual representation of the discussed DOP reactions is shown in figure 1.2 and table 1.1.

Studying DOP in eutrophic lakes can reveal important processes concerning P mobility, stability, and microbial utilization. Ahlgren et al. (2005) extracted sediment from the moderately-eutrophic Lake Erken to assess DOP transformation from the sediment to the water. Their results indicated a significant loss of biogenic P through degradation or diffusion over time but a retention of highly-recalcitrant biogenic molecules at depth with average half-lives of 21 years for diesters and 23 years for monoesters. Additionally, the presence of pyrophosphate in the upper sediment layers

and the filtered seston samples suggested elevated microbial activity. Transport modelling of DOP from sediment in Lake Kasumigaura by Shinohara et al. (2017) revealed mineralization of phosphomonoesters to be more significant to mobility than diffusion. Further analysis of phosphatase activity led to the conclusion that the degraded DOP molecules in winter could be a likely supply of labile P in the sediment that is released during spring blooms. Compared to the underlying sediment, DOP in the water column is more elusive to characterize due to lower concentrations and higher lability. This portion is significant because the mineralization rates of DOP vary for microorganisms depending on the molecular class (e.g. Wang et al., 2011). Bai et al. (2015) studied the dynamics of particulate P and DOP in the eutrophic lake Taihu by concentrating 20 L of water per sample. Their results illustrated significant differences in the distribution of phosphonates both spatially within the lake, and between the dissolved and particulate fractions, with higher concentrations in the dissolved fraction. The detected particulate phosphonates shared a positive correlation with cyanophyta biomass within the lake suggesting that they originate from cyanobacteria and persist in the dissolved fraction (Bai et al., 2015).

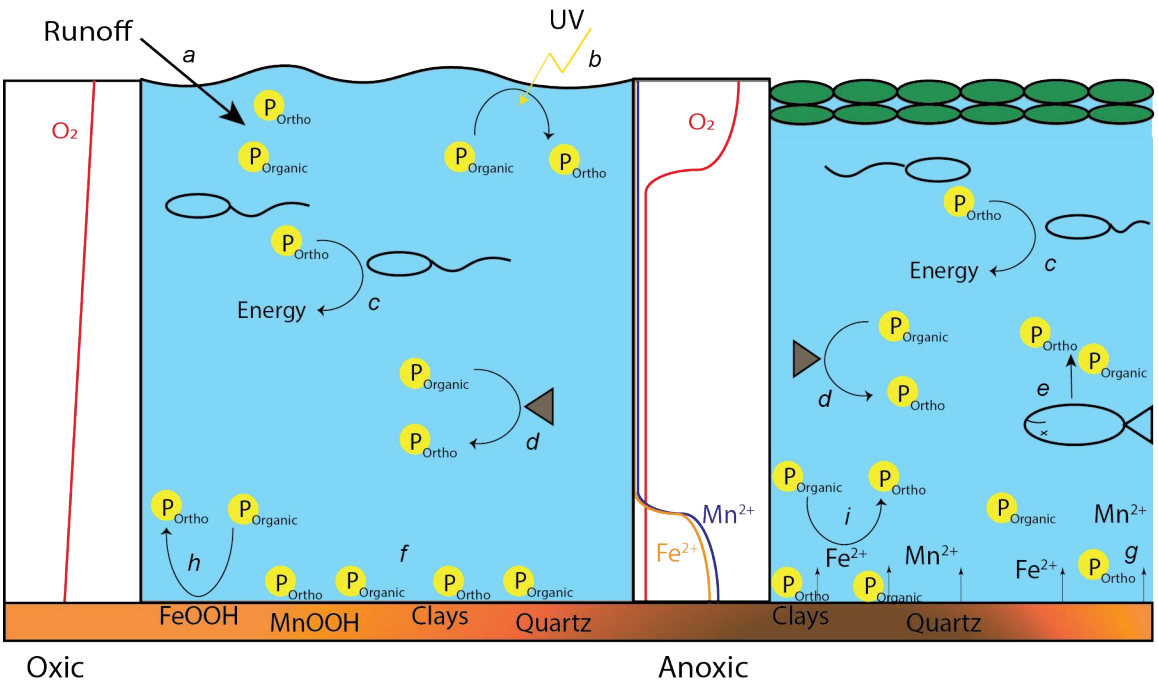

Figure 1.2. Schematic representation of organic phosphorus reactions and mobility within a shallow freshwater lake in oxic (left panel) and anoxic (right panel) conditions. P_{ortho} denotes orthophosphate while $P_{organic}$ denotes organic P. FeOOH represents Fe(III) (oxy)hydroxide minerals, whole MnOOH represents Mn(IV) (oxy)hydroxide minerals. Anoxic conditions assume oxygen depletion in the bottom water and the presence of reduced Mn and Fe cations.

a	Dissolved and particulate organic and inorganic P from runoff
b	Photolysis reactions from sunlight cleave phosphate groups from DOP
c	Organisms consume labile orthophosphate to meet their energy demands
d	Extracellular phosphatase enzymes hydrolyze labile DOP, producing orthophosphate
e	Decomposing organisms release organic and inorganic P into the water
f	Under oxic conditions, inorganic and organic P species adsorb onto mineral surfaces in the sediment
g	Under anoxic conditions, reductive dissolution of Fe and Mn (oxy)hydroxides release inorganic and organic P into the water
h	Oxide mineral surfaces catalyze hydrolysis of labile DOP compounds
i	Dissolved metal cations catalyze hydrolysis of labile DOP compounds

Table 1.1. Summary of DOP reactions and transformations in shallow freshwater lakes from figure 1.2.

Study site:

Lake Champlain basin:

Lake Champlain is a large natural freshwater lake in North America sharing drainage basins with Vermont, New York, and the Province of Quebec, Canada (Figure 1.3). It encompasses a 1,127 km^2 surface area with a mean depth of 22 m and drainage basin of 21,326 km^2 (Smeltzer et al., 2012). The lake is part of the Champlain Valley between the Green Mountains of Vermont in the east and the New York Adirondack Mountains to the west. In general, the primary bedrock of northeastern Lake Champlain consists of Cambrian-Ordovician carbonate platform rocks (Ratcliffe et al., 2011). Specifically, shale and dolomitic siltstone from the Iberville Shale unit compose the majority of the lake bedrock (Smith, 2009). The eastern shore consists of mostly dolomite and sandstone from the Dunham Dolomite formation and is separated from shale by the Champlain thrust fault (Ratcliffe et al., 2011). The sedimentary history of Lake Champlain is a result of the Wisconsinan glaciation. During the event, the advance of the

Laurentide ice sheet through New England carved the Champlain Valley (20,000-12,500 ya) depositing glacial till as the oldest sediments in Lake Champlain overlaying the bedrock (Wright & Larsen, 2004; Smith, 2009). As the ice sheet retreated northward, the Champlain basin was flooded resulting in a large body of water known as Glacial Lake Vermont, which deposited laminated silt and clay on top of the glacial till (Smith, 2009). Most of the lake drained by 12,000 ya and began mixing with Atlantic seawater from the uncovered St. Lawrence estuary, forming the Champlain Sea and resulting in marine sedimentary deposition (Smith, 2009). The surrounding land rebounded from the retreating ice sheet and cut off saltwater input into the Champlain Sea. Since 9,000 ya, glacial melt and precipitation have gradually freshened the water of the Champlain Sea and turned it into the Lake Champlain that exists today (Burgess, 2007). Presently, rivers and tributaries continue to erode and transport glacial till and underlying bedrock into Lake Champlain from the surrounding watershed (Wright & Larsen, 2004).

The lake is well-connected by the Richelieu River to the north and the Champlain Canal and Hudson River to the south, linking it to both the Great Lakes and the Atlantic Ocean. The morphology of the lake is distinct and includes bays and arms that are sheltered from the main basin resulting in various trophic states (Medalie & Smeltzer, 2004; Smeltzer et al., 2012). The variations in morphology result in segments that are both deep and shallow, responding to changes in nutrient fluxes very differently (Isles et al., 2017). In particular, P loading from point and non-point sources has been an issue contributing to eutrophication and blooms of cyanobacteria. Minor contributions originate from atmospheric deposition and point sources, while the majority is attributed to non-point sources, accounting for up to 71% of the total P export into the lake (Meals

& Budd, 1998). Efforts to manage external loading since the 1970s have been attempted, with significant reduction in point-source P loading, yet blooms still persist (Smeltzer & Quinn, 1996; Smeltzer et al., 2012).

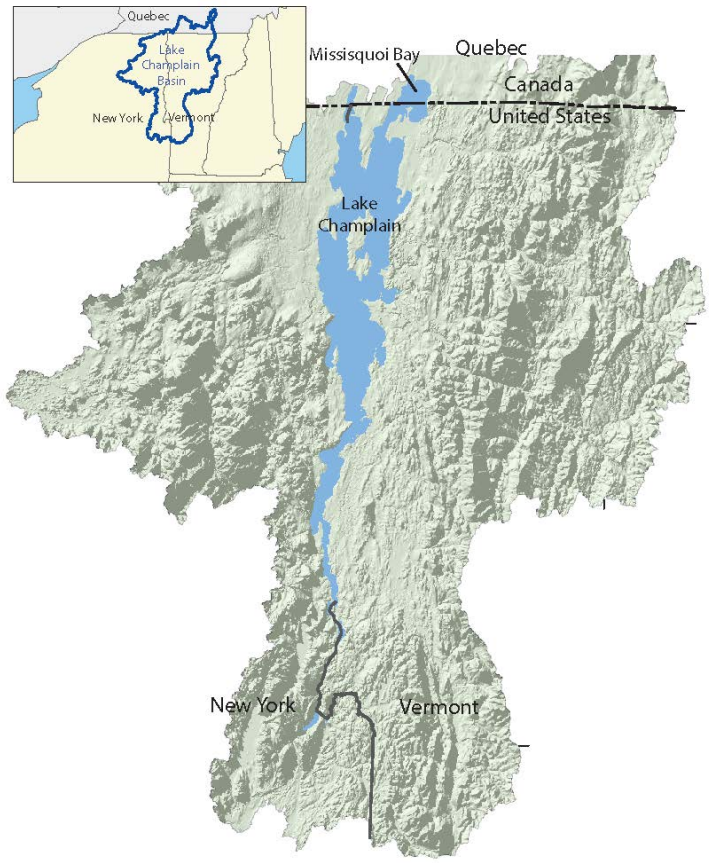

Figure 1.3. Map of Lake Champlain with the surrounding basin. Figure modified from Medalie (2007).

Missisquoi Bay:

Located on the border of Vermont and Quebec, Missisquoi Bay is a eutrophic basin of Lake Champlain experiencing toxic cyanobacterial blooms in late summer months partially due to external and internal nutrient loading (Figure 1.4) (Levine et al., 2012; McCarthy et al., 2013; Schroth et al., 2015). Since 1993 the governments of Quebec and Vermont have worked to reduce P loading into Missisquoi Bay (and all of

Lake Champlain) by setting a target concentration limit of 25 µg/L for the lake segment (Smeltzer et al., 1999). Furthermore, in 2002 a target P load limit of 97 mt/year was established (Smeltzer & Simoneau, 2008); however, total P has greatly exceeded this limit and Missisquoi Bay is still one of highest contributors to total P in the entire lake (Smeltzer et al., 2009). In 2017, total dissolved P levels in Missisquoi Bay spanned 8.8 to 47.2 µg/L with total P ranging from 28 to 71.5 µg/L (VTDEC, 2018). Excess phosphorus allows cyanobacteria such as *Microcystis aeruginosa* and *Microcystis wesenergii* to proliferate and outcompete phytoplankton in the warm summer months that leads to blooms of biomass and release of cyanotoxins in the bay (Watzin et al., 2003). The bay is shallow with a maximum recorded depth of 5 m and a mean depth of 2.8 m, allowing cyanobacteria to scavenge internally cycled nutrients from the sediment (Schroth et al., 2015; Isles et al., 2017). In the winter, the bay usually freezes entirely during December and thaws in April with periodic melt events between; however, Stager and Thill (2010) noted significant inconsistencies with ice cover on Lake Champlain over the last 150 years attributed to a warming climate. Ice cover creates a physical barrier to oxygen diffusion and wave action into the bay resulting in a more thermally and redox-stratified water column in the winter (Schroth et al., 2015). Additionally, persistent cold periods limit physical mixing and oxygenation of the bottom water and result in elevated manganese and total P concentrations from the sediment (Joung et al., 2017). Variations in subfreezing air temperatures may impact how these redox-sensitive species partition between the sediment and affect P biogeochemistry in the spring and summer. As average air temperatures are predicted to increase, the spring thaw period of Missisquoi Bay is expected to occur earlier in the year, supplying nutrients to the bay earlier in spring and

prolonging the dry summer months where stratification occurs and phosphorus is released from the sediment (Isles et al., 2017). Publicly available nutrient and physical data provided by the Lake Champlain Long Term Monitoring Program from 1992-2017 (VTDEC, 2018) has resulted in many studies and publications on Missisquoi Bay (e.g. Smith 2009; Giles et al., 2015; Schroth et al., 2015; Isles et al., 2017; Joung et al., 2017) allowing for direct comparisons between studies.

Figure 1.4. Watershed of Missisquoi Bay with the three river inputs: Pike (red), Rock (black), and Missisquoi (Green). Figure modified from LCBP (2018).

Missisquoi watershed:

The total watershed of the bay is mostly forested (70%) with agricultural (25%) and urban (5%) inputs spanning a total of 3,100 km^2 (Joung et al., 2017). Nutrient

loading is primarily supplied by three river systems: the Missisquoi, Pike, and Rock River (Figure 4) into the bay providing 38% of the P load from agricultural runoff (Smith, 2009). Within the Missisquoi Bay watershed, 73% of land area is dominated by forests but only accounts for 20% of the P load while agricultural lands represent 18% of the watershed, but result in 38% of the total load, partially from streambank erosion (LCBP, 2018). The larger Missisquoi River sub watershed loads more total P into the bay, but high P concentrations from the smaller Pike and Rock River sub watersheds result in greater export rates than from the Missisquoi River when considering land area (Smeltzer & Simoneau, 2008). These sub watersheds are primarily agricultural and are significant sources of non-point loading. For instance, the fertile soil from the Rock River sub watershed allows for extensive crop and dairy farming, with harvested crops comprising 55.4% of land use making only 24% of the total land area responsible for 80% of the P loading (Ghebremichael et al., 2010).

P flux into Missisquoi Bay is also highly dependent on seasonal hydrological events. The greatest episodes of P flux at the mouth of the Pike River have been observed in the spring and fall, accounting for up to 82% of the total annual flux (Adhikari et al., 2010). Spring is characteristic of snowmelt and rain flushing previously frozen sediment and phosphorus into the river from the surrounding landscape, while fall runoff events are due to erosion of post-harvested cropland (Adhikari et al., 2010). A study of the watershed associated with the Missisquoi River revealed that spring melting and flushing events from agricultural lands released high amounts of phosphorus in 2014, but discharge following summer storms released comparable levels of phosphorus as well (Rosenberg & Schroth, 2017). Much of this phosphorus is redox-sensitive and associated

with Fe colloids, allowing for transport and scavenging of phosphorus during high discharge events, such as the onset of spring melt or after sustained summer baseflow (Rosenberg & Schroth, 2017). Although external loading does deliver elevated concentrations of phosphorus into Missisquoi Bay, modelling of data collected over 20 years suggests that the primary drivers of high total P concentrations in the bay were more dependent on calm, dry weather conditions and dissolved P river input during a summer bloom (Isles et al., 2017). This indicates that internal loading of phosphorus from the sediment in summer months is a better predictor for blooms in shallow lakes and will likely make restoration efforts difficult, even after the reduction of point and non-point source pollution. Therefore, future remediation efforts should first focus on greater spatial sampling and analytical methods to identify mobile P sources and sinks, and a subsequent combined approach of best management practices and P recovery techniques from the basin (Giles et al., 2016).

Methodology:

Organic phosphorus quantification:

In water columns and sediments, P concentrations are generally lower than other nutrients such as carbon and nitrogen, making it more difficult to measure organic P with a single analytical procedure (see McKelvie, 2005). In many cases, an estimation for the dissolved fraction of organic P is taken to be the difference between the total dissolved P (TDP) and the orthophosphate defined as soluble reactive phosphorus (SRP). These pools can be measured using several techniques including colorimetry, inductively coupled plasma-optical emission spectroscopy (ICP-OES), or inductively coupled plasma-mass

spectrometry (ICP-MS). SRP can be measured directly without pretreatment using colorimetry assuming careful sample handling and storage (e.g. Turner, 2005). TDP can also be measured directly in some instances with ICP-OES or ICP-MS (Kruse et al., 2015) because they atomize all P-containing molecules (Cooper et al., 2005). However, when using colorimetric methods to determine TDP, samples must first be digested before analysis, usually through a heated persulfate digestion (McKelvie, 2005). When quantification of only specific organic P compounds is desired, select phosphatase enzymes are used to hydrolyze the O-P bond, releasing orthophosphate which can be measured after subtracting background SRP. Such methods have been used colorimetrically by Johnson and Hill (2010) for soil extracts and by Giles et al. (2015) for sediment sampled from Missisquoi Bay. Others have attempted to use enzyme hydrolysis to determine the bioavailability of DOP in aquatic samples with variable results, often attributed to differences in preparations of commercially available enzymes (Mitchell & Baldwin, 2005).

Colorimetric methods are often the simplest and quickest methods to quantify organic P, but suffer from poor sensitivity (Turner, 2005). Measurements are made by complexing orthophosphate with molybdate and quantifying the resulting UV absorbance at a single wavelength. The most common protocols are those developed by Murphy and Riley (1962) using ascorbic acid as a reductant or the malachite green method optimized by D'Angelo et al. (2001). In both approaches SRP is detected through direct complexation while organic P is deemed "unreactive" if the samples is undigested. This method has proven to be robust, but has several limitations, including: overestimation of the amount of SRP due to acid-hydrolysis of some organic compounds during the SRP

acidification step (Monaghan & Ruttenberg, 1999), incomplete recovery of phospholipids and phosphonates during persulfate digestions (Mitchell & Baldwin, 2005), or overestimation of organic P if polyphosphates are present (Turner, 2005). The color complex formation is also subject to positive and negative interferences from the sample matrix including common anions, chelating agents, and Ca(II) (Lowry & Lopez, 1946; Saheki et al., 1984; D'Angelo et al., 2001). Additionally, the enzyme hydrolysis assays are specific to only certain organic P molecules that can be hydrolyzed and are also subject to matrix interferences that can underestimate concentrations (McKelvie, 2005).

ICP-OES and ICP-MS offer unambiguous phosphorus detection with minimal interferences from the sample matrix (De Brabandere et al., 2008; Kruse et al., 2015). In both cases, ionization is achieved by sample introduction to the ICP which reduces all present molecules to their atomic components. Differences between the two arise from their detection methods. ICP-OES relies on quantifying the visible light emitted from elements at high temperatures which increases linearly with atomic concentration (Olesik, 1991). ICP-MS uses a mass spectrometer to detect P atoms at 30.974 Da varying in sensitivity depending on the analytical capabilities of the instrument. Since mass differences of only 1 Da are required to differentiate between elements, low resolution spectrometers are often sufficient for these analyses (Cooper et al., 2005). Although both methods have been used to determine phosphorus concentrations in soil and sediment extracts, ICP-OES cannot detect phosphorus below 100 μg/L (Rowland & Haygarth, 1997) with even poorer detection limits if the background signal is sufficiently high (Olesik, 1991). In contrast, ICP-MS has been used to measure phosphorus in natural waters and can quantify as little as 1.7 μg/L (Cooper et al., 2005), making it more

favorable for these lower concentration environments. Despite the instrument sensitivity, ICP-MS is purely quantitative and provides no qualitative information about the classes of organic P molecules.

FT-ICR MS instrumentation and theory:

Analytical methods such as time of flight and quadrupole mass spectrometry have demonstrated resolving power of up to 10,000, but still do not have the adequate resolution necessary to describe DOM (Sleighter & Hatcher, 2007). Fourier transform-ion cyclotron resonance mass spectrometry (FT-ICR MS) provides unprecedented resolving power reported in ranges from 300,000 to 600,000 allowing for many molecular ions to be identified in a given single nominal mass in parallel (Sleighter & Hatcher, 2007). Conceptually, integer peaks in a mass spectrum represent nominal molecular masses and conventional mass spectrometers can resolve peaks that differ by at least one nominal mass unit (1 Da). Natural organic matter contains many molecules within a single nominal mass, making good peak resolution critical for characterization. FT-ICR MS has been used successfully in many studies to characterize DOM including complex heteroatomic compounds (e.g. Herzsprung et al., 2014; D'Andrilli et al., 2015; Gonsior et al., 2016). DOM is composed of tens of thousands of unique molecular formulae and by studying the distributions of these formulae, one can connect the transformations of organic carbon with many elemental cycles (Hertkorn et al., 2007).

Rigorous descriptions concerning the theory and mechanics of FT-ICR MS have been reviewed by Marshall et al. (1998) and Nikolaev et al. (2016). Molecules can only be detected as ions, and thus must be treated as charged species. An ion moving in the

presence of a uniform magnetic field (B) will have a corresponding force (mass, m, times acceleration, a) called the Lorentz force (F) (Equation 1.1), where q is the charge and v is the velocity (Marshall et al., 1998). The cross product denotes the Lorentz force will be perpendicular to the plane defined by B and v.

Equation 1.1: $$F = ma = qv \times B$$

At a constant velocity, the magnetic field will bend the ion path into a circular motion of radius, r, with an angular velocity of ω equal to v/r. Acceleration can be defined in centrifugal terms as v^2/r, and substituted for a into equation 1.1 to yield equation 1.2.

Equation 1.2: $$\frac{mv^2}{r} = qvB$$

Adding in ω into equation 1.2 and rearranging gives equation 1.3, where ω is now defined as the cyclotron frequency. This equation is only dependent on q, m, and B stating that every unique ion (m/q) will have its own corresponding cyclotron frequency (Marshall et al., 1998).

Equation 1.3: $$\omega = \frac{qB}{m}$$

A schematic of ion excitation and detection is shown in figure 1.5. Circulating ions are excited by rf pulses from an oscillating electric field that increase the orbital radius of the ions (Nikolaev et al., 2016). As the radius increases, ions move closer to the detector

plates and induce image charges that change the potential of the plates (Nikolaev et al., 2016). The signals are recorded in a time domain spectrum, which is transformed to a frequency spectrum using a Fourier transform and then finally converted to a mass spectrum with equation 1.3.

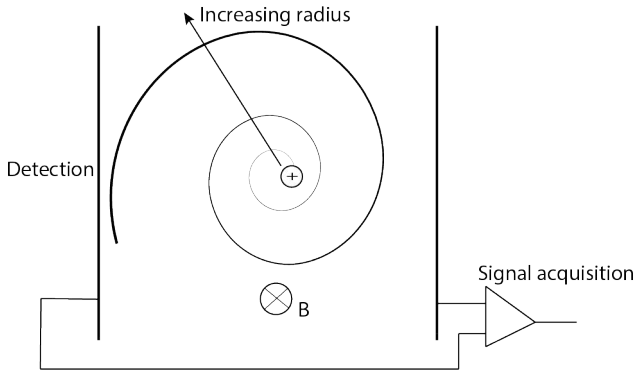

Figure 1.5. Schematic of ion excitation and detection during FT-ICR MS analysis. *B* is the magnetic field going into the plane. Figure adapted from figure 1 in Nikolaev et al. (2016).

Prior to sample introduction into the instrument cell, molecules are ionized using several techniques. Soft ionization techniques are preferred, meaning the molecules are unfragmented, for DOM analysis and routinely include electrospray ionization (ESI), atmospheric pressure photo ionization (APPI), or atmospheric pressure chemical ionization (APCI) (Hertkorn et al., 2008). These techniques can produce either negative (-) or positive (+) ions. Both ESI and APPI have been used extensively to investigate DOM, but differ in their selection of ionizable compounds based on functional groups (Sleighter & Hatcher, 2007; Sleighter & Hatcher, 2011). The techniques are complementary with minimal overlap; ESI primarily ionizes polar functional groups, while APPI selects for more aromatic and nonpolar molecules (Sleighter & Hatcher, 2011). Ion introduction into the instrument during ESI can be described in three steps:

sample nebulization into charged droplets from a high electric field, release of the ions from the droplets, and ion transport into the vacuum of the mass analyzer (Bruins, 1998). Within ESI, molecules are selectively ionized depending on the mode employed. Negative mode preferentially ionizes acidic functional groups containing alcohols and carboxylic acids while positive mode selects for basic functional groups including N-containing amines (Sleighter & Hatcher, 2007). Most DOM analyses to date have used negative ionization partly due to the assumption that DOM contains mainly acidic functional groups and the complication of the mass spectrum from the inclusion of sodium adducts with positive ionization (Sleighter & Hatcher 2007; Ohno et al., 2016). Methods to isolate and desalt DOM for ESI-FT-ICR MS analysis have included the implementation of various resins for solid phase extractions and have been successfully used on fresh- and saltwater samples (Dittmar et al., 2008; Li et al., 2016).

Data processing and visualization techniques:

Analysis of DOM using FT-ICR MS typically follows a sequence of sample collection, concentration, isolation/desalting, ionization, instrumental analysis, and data processing (Appendix A). Tens of thousands of peaks are present in the raw spectrum of a single DOM sample after data acquisition and calibration with internal and/or external standards. Visualization is key to meaningful analysis; the data is often converted from ion intensity peaks to molecular formulae for examination of detected molecules. These calculations can be performed manually for each peak, but would be unnecessarily tedious given the high volume of peaks. Many research groups have developed proprietary algorithms and software that assign and filter molecular formulae from mass

spectrum peaks. They operate within a specified error tolerance based on fundamental principles of chemical bonding, valency, and element probability described in great detail (e.g. Kind & Fiehn, 2007; Koch et al., 2007; Tziotis et al., 2011; Herzsprung et al., 2014; Green & Perdue, 2015). Processing should begin with reasonable constraints for the maximum number of elements (N, S, P, Cl etc.) allowed in a given formula, too few and many important molecules may be omitted from the mass list, too many and the possibility of false assignments increases (Kind & Fiehn, 2007; Koch et al., 2007). Although false assignments can be minimized by constraining the number of allowable atoms in the mass list, artifacts of the sample matrix can still complicate formulae assignments. For instance, Dvorski (2016) analyzed DOM at an alkaline pH and found that many of the assigned condensed aromatic CHOS molecules were actually sodium adducts of CHO compounds. In this case desalting the sample would further minimize false assignments by removing adducts. Additional constraints can be achieved by identifying corresponding ^{13}C molecular peak patterns for each assignment, realistic atomic ratios within each molecule, and filtering by molecular mass (Kind & Fiehn, 2007). Such processing significantly reduces the number of assignments but also increases confidence in the formulae assigned to peaks. It should be stressed that DOM isolation, ionization, acquisition, and data processing all introduce possible fractionations and thus no technique will unequivocally describe all present molecules; however, great certainty of assignments can be achieved through careful filtering of the molecules that were ionized and detected by the instrument (Herzsprung et al., 2014). Figure 1.6 describes a typical mass spectrum data filtering workflow of DOM isolated from the Missisquoi River in September 2017 (ESI negative) with the goal of describing organic P.

An allowed error range for the peak fittings are defined as ±0.2 ppm, element counts are defined ($N_{0\text{-}5}$,$S_{0\text{-}1}$,$P_{0\text{-}3}$) and a corresponding ^{13}C peak is searched for each molecule. Then, formulae are further filtered by stoichiometric ratios and multiple formulae assigned to a single peak are discarded.

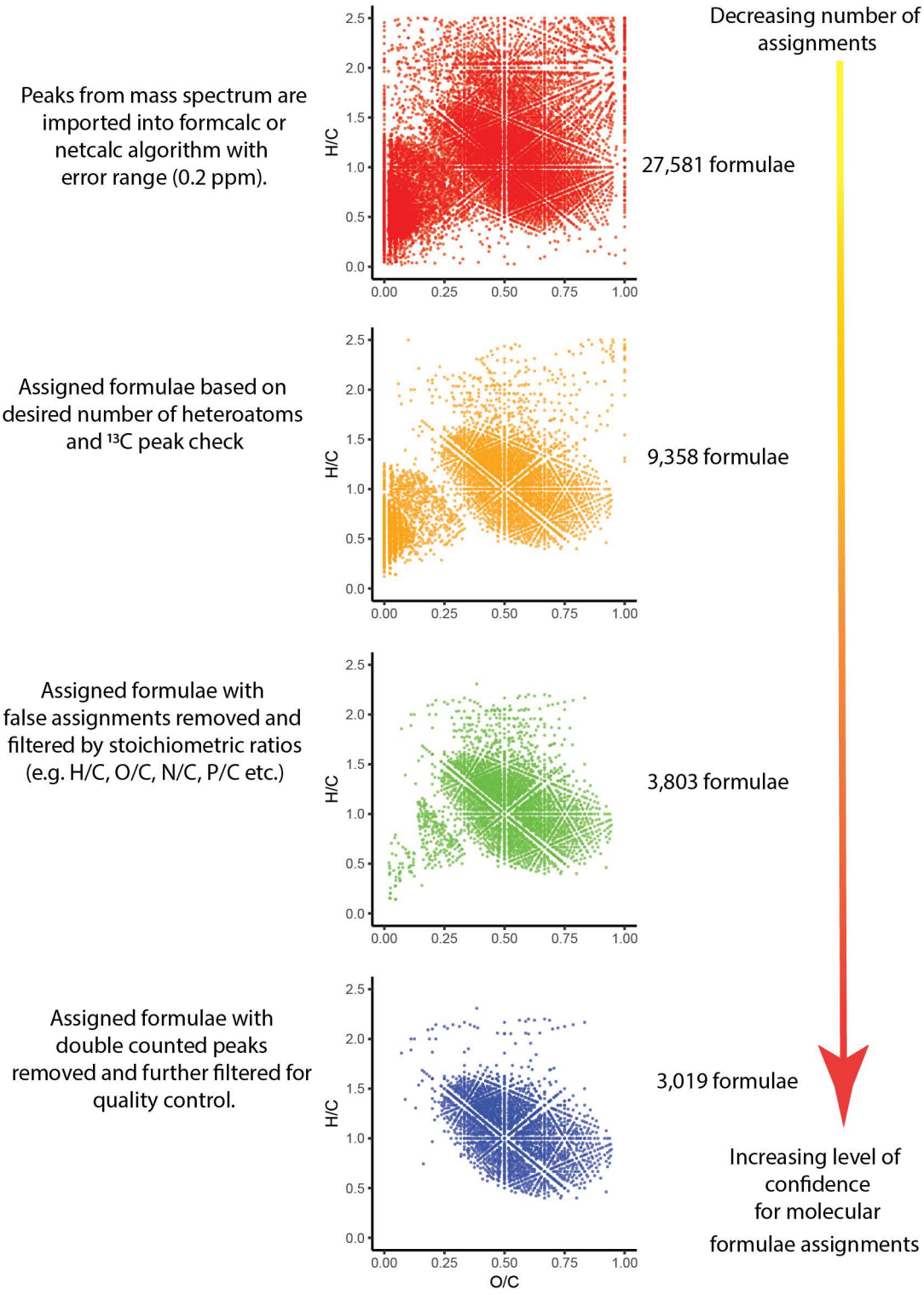

Figure 1.6. FT-ICR MS data processing workflow of formula assignments obtained from an algorithm. Each dot in the diagrams represent an assigned formula.

Assigned formulae are traditionally visualized in 2-D space using a van Krevelen diagram which plots the stoichiometric H/C ratio versus the O/C ratio of all considered molecules (Van Krevelen, 1950; Kim et al., 2003; Sleighter & Hatcher, 2007). This technique allows for the classification of various functional compounds (e.g. lipids, proteins, lignins etc.) from their regions in 2-D space and identification of homologous series and reaction pathways of related molecules (Sleighter & Hatcher 2007; D'Andrilli et al., 2015). Van Krevelen regions are useful for data visualization, but overlap with each other and yield ambiguous characterization, despite efforts to strictly define specific regions (Sleighter & Hatcher, 2007; Hockaday et al., 2009). Recent efforts have attempted to modify van Krevelen regions by classifying compounds based on other stochiometric ratios in addition to H/C and O/C values (Rivas-Ubach et al., 2018). Another powerful data visualization technique, often used together with the van Krevelen diagram, is the Kendrick Mass Defect plot. A functional group (usually CH_2) is chosen as the base unit and all molecular masses are converted into a new scale utilizing the mass defect (i.e. the exact difference between the nominal and measured atomic masses of each element) of that functional group (Hughey et al., 2001; Sleighter & Hatcher 2007). This new scale produces networks of homologous series that all differ by the chosen functional group. Other approaches have experimented with multivariate ordination techniques such as PCA (Wagner et al., 2015), clustering (Guigue et al., 2016), and NMDS (Kellerman et al., 2015) to correlate changes in DOM composition to other observable variables. Although abundant with information, current FT-ICR MS methods still offer limited compound quantification, make differentiating between isomers difficult, and only reveal molecules that are ionizable, thus giving the false impression

that the detected pool is truly representative of all DOM molecules in the system (Hertokorn et al., 2007).

FT-ICR MS applications to DOP analysis:

The application of FT-ICR MS to study organic P present in DOM is limited for several reasons. First, in uncontaminated aquatic systems the total P concentration is relatively low, typically around 10 µg/L with the dissolved organic P representing only a fraction of the total (ppb range) (Llewelyn et al., 2002; Celi & Barberis, 2005). Therefore, only specific aquatic systems with a high nutrient loading will have a significant P contribution to the total DOM molecular signature. Second, in ESI there is a fixed amount of positive or negative charge that can be applied to molecules in the sample resulting in the most ionizable molecules receiving most of the charge and subsequently arriving at the detector. While acidic functional groups are efficiently ionized in negative mode (alcohols and carboxylic acids) and basic functional groups (amines) ionize well in positive mode, phosphate functional groups are not preferentially ionized in either mode (Cooper et al., 2005; Sleighter & Hatcher, 2007). To efficiently ionize and detect organic P molecules in a DOM mixture, they should contain abundant ionizable functional groups in addition to the P moiety. Third, with increasing molecular mass the amount of possible formula solutions for each mass peak increases if non-oxygen heteroatoms are considered in the algorithm (Koch et al., 2007; Herzsprung et al., 2014). The increase in possible formulae increases the system complexity and make false assignments of mass peaks more probable, which results in an inaccurate description of the system. These reasons limit the amount and type of organic P that can be observed in

natural samples, but with the resolving power and precise molecular information FT-ICR MS provides, there are still a remarkable number of molecules worth investigating.

Llewelyn et al. (2002) overcame low P concentrations and poor ionization efficiencies by separating large-fraction organic matter from the Florida Everglades using tangential cross-flow filtration and precipitating organic phosphorus with barium acetate after concentration. The precipitate was dissolved and analyzed using FT-ICR MS in ESI positive mode revealing highly resolved organic P peaks that would have otherwise been obscured by the background DOM signatures (Llewelyn et al., 2002). Since this study, P-centered analysis of DOM has been severely lacking, but the peripheral contributions of organic P to DOM in other studies have been reported. For instance, in several studies P-containing formulae were included in FT-ICR MS analysis of DOM and shown to be a dynamic molecular class within the aquatic systems (Sleighter et al., 2009; Gonsior et al., 2011; Altieri et al., 2012; Minor et al., 2012). Sleighter et al. (2009) was able to detect CHOP, CHONP, CHOSP, and CHONSP molecules from natural waters with low DOM concentrations and observed relative increases in the classes after each sample was concentrated. CHOP signatures were also detected in marine waters off the coast of the South Island, New Zealand in ESI negative, but were only present in the winter indicating seasonal differences in terrestrial input and biological consumption (Gonsior et al., 2011). Similarly, water samples from the oligotrophic Lake Superior were sampled and ionized in negative mode revealing the presence of many P-containing molecules (Minor et al., 2012). Despite the system being P-limited, CHONP molecules represented as much as 9.4% of the total DOM assignments in some water samples and are thought to be a key component of the bulk organic matter (Minor et al., 2012). Seasonal rainwater collected

from Bermuda ionized in positive mode afforded CHONP and CHONSP compounds that were highly condensed based on their double bond equivalence and were confirmed with EXAFS to be mainly phosphate groups (Altieri et al., 2012). Multiple approaches utilizing FT-ICR MS in tandem with other targeted analytical techniques could prove useful to making confident DOP assignments in systems with low phosphorus concentrations.

DOP has also been detected with FT-ICR MS while studying the molecular composition of estuaries. Analysis of surface waters from the Chesapeake Bay area revealed that most negatively ionized organic P molecules shared stoichiometries similar to carbohydrate- and protein-like compounds; very few had similarities with lipid-like molecules (Abdulla et al., 2013). Furthermore, watershed samples of a tributary feeding into the bay ionized hundreds of DOP molecules, many of which shared characteristics with lipid-like molecules that were highly labile and decomposed within several days (Killberg-Thoreson et al., 2013). In the nearby Delaware Bay, Osterholz et al. (2016) correlated a salinity gradient to increasing amounts of detected DOP molecules, suggesting autochthonous production of the highly aliphatic molecules outward from the bay and into the Atlantic Ocean.

Recently, Brooker et al. (2018) identified specific organic P signatures from point and non-point pollution sources leeching into Lake Erie using FT-ICR MS in a unique study focused solely on DOP. The authors demonstrated high similarity of organic P compounds present between three pollution sources and showed that organic P degradation is slower in the system due to non-limiting levels of orthophosphate (Brooker et al., 2018). Additionally, a new procedure for solid phase extraction of the analyte at pH

10, rather than pH 2 as per the manufacturer's recommendation, was implemented selecting specifically for the hydrophilic compounds, while the latter selects for the hydrophobic components (Brooker et al., 2018). This study confirmed that FT-ICR MS can be reliably used to study organic P molecules but was only implemented on extracted sediment and manure samples; a study targeting freshwater DOP using the SPE procedure has yet to be published. Clearly, it has been demonstrated that this mass spectrometry technique can detect significant amounts of organic P molecules present in DOM, but also that their occurrence, distribution, and characteristics are dynamic; they vary greatly from sample site and seasonally.

References:

Abdulla, H. A., Sleighter, R. L., & Hatcher, P. G. (2013). Two dimensional correlation analysis of Fourier transform ion cyclotron resonance mass spectra of dissolved organic matter: A new graphical analysis of trends. *Analytical chemistry*, *85*(8), 3895-3902.

Adhikari, B. K., Madramootoo, C. A., & Sarangi, A. (2010). Temporal variability of phosphorus flux from Pike River watershed to the Missisquoi Bay of Quebec. *Current Science*, 58-64.

Ahlgren, J., Tranvik, L., Gogoll, A., Waldebäck, M., Markides, K., & Rydin, E. (2005). Sediment depth attenuation of biogenic phosphorus compounds measured by ^{31}P NMR. *Environmental Science & Technology*, *39*(3), 867-872.

Aitkenhead-Peterson, J. A., McDowell, W. H., & Neff, J. C. (2003). Sources, production, and regulation of allochthonous dissolved organic matter inputs to surface waters. In *Aquatic Ecosystems* (pp. 25-70). Academic Press.

Allen, H. E., Hall, R. H., & Brisbin, T. D. (1980). Metal speciation. Effects on aquatic toxicity. *Environmental science & technology*, *14*(4), 441-443.

Altieri, K. E., Hastings, M. G., Peters, A. J., & Sigman, D. M. (2012). Molecular characterization of water soluble organic nitrogen in marine rainwater by ultra-high resolution electrospray ionization mass spectrometry. *Atmospheric Chemistry and Physics*, *12*(7), 3557-3571.

Avneri-Katz, S., Young, R. B., McKenna, A. M., Chen, H., Corilo, Y. E., Polubesova, T., ... & Chefetz, B. (2017). Adsorptive fractionation of dissolved organic matter (DOM) by mineral soil: Macroscale approach and molecular insight. *Organic Geochemistry*, *103*, 113-124.

Bai, X. L., Zhou, Y. K., Sun, J. H., Ma, J. H., Zhao, H. Y., & Liu, X. F. (2015). Classes of dissolved and particulate phosphorus compounds and their spatial distributions in the water of a eutrophic lake: a ^{31}P NMR study. *Biogeochemistry*, *126*(1-2), 227-240.

Baldwin, D. S. (2013). Organic phosphorus in the aquatic environment. *Environmental Chemistry*, *10*(6), 439-454.

Baldwin, D. S., Beattie, J. K., Coleman, L. M., & Jones, D. R. (1995). Phosphate ester hydrolysis facilitated by mineral phases. *Environmental science & technology*, *29*(6), 1706-1709.

Baldwin, D. S., Beattie, J. K., Coleman, L. M., & Jones, D. R. (2001). Hydrolysis of an organophosphate ester by manganese dioxide. *Environmental science & technology*, *35*(4), 713-716.

Baldwin, D., Howitt, J., & Beattie, J. (2005). Abiotic degradation of organic phosphorus compounds in the environment. In *Organic phosphorus in the environment* (pp. 75-88). Wallingford, UK: CABI Publishing.

Barnett, G. M. (1994). Phosphorus forms in animal manure. *Bioresource Technology*, *49*(2), 139-147.

Boavida, M. J., & Wetzel, R. G. (1998). Inhibition of phosphatase activity by dissolved humic substances and hydrolytic reactivation by natural ultraviolet light. *Freshwater Biology*, *40*(2), 285-293.

Bormans, M., Ford, P. W., & Fabbro, L. (2005). Spatial and temporal variability in cyanobacterial populations controlled by physical processes. *Journal of plankton Research*, *27*(1), 61-70.

Boström, B., Persson, G., & Broberg, B. (1988). Bioavailability of different phosphorus forms in freshwater systems. In *Phosphorus in Freshwater Ecosystems* (pp. 133-155). Dordrecht, NL: Springer.

Brooker, M. R., Longnecker, K., Kujawinski, E. B., Evert, M., & Mouser, P. J. (2018). Discrete Organic Phosphorus Signatures are Evident in Pollutant Sources within a Lake Erie Tributary. *Environmental science & technology*, *52*(12), 6771-6779.

Bruins, A. P. (1998). Mechanistic aspects of electrospray ionization. *Journal of Chromatography A*, *794*(1-2), 345-357.

Bullock, J. I., Duffin, P. A., & Nolan, K. B. (1993). In vitro hydrolysis of phytate at 95 C and the influence of metal ion on the rate. *Journal of the Science of Food and Agriculture*, *63*(2), 261-263.

Burgess, H. (2007). *Geochemical indicators of productivity change in Lake Champlain, USA-Canada*. (Graduate College Dissertations and Theses). Retrieved from https://scholarworks.uvm.edu

Carmichael, W. W. (2001). Health effects of toxin-producing cyanobacteria:"The CyanoHABs". *Human and ecological risk assessment: An International Journal*, *7*(5), 1393-1407.

Celi, L., & Barberis, E. (2005). Abiotic stabilization of organic phosphorus in the environment. In *Organic phosphorus in the environment* (pp. 113-132). Wallingford, UK: CABI Publishing.

Chassé, A. W., & Ohno, T. (2016). Higher molecular mass organic matter molecules compete with orthophosphate for adsorption to iron (oxy) hydroxide. *Environmental science & technology*, *50*(14), 7461-7469.

Christoffersen, K., Lyck, S., & Winding, A. (2002). Microbial activity and bacterial community structure during degradation of microcystins. *Aquatic Microbial Ecology*, *27*(2), 125-136.

Christophoridis, C., & Fytianos, K. (2006). Conditions affecting the release of phosphorus from surface lake sediments. *Journal of Environmental Quality*, *35*(4), 1181-1192.

Cole, J. J., Prairie, Y. T., Caraco, N. F., McDowell, W. H., Tranvik, L. J., Striegl, R. G., ... & Melack, J. (2007). Plumbing the global carbon cycle: integrating inland waters into the terrestrial carbon budget. *Ecosystems*, *10*(1), 172-185.

Cooper, J., Lombardi, R., Boardman, D., & Carliell-Marquet, C. (2011). The future distribution and production of global phosphate rock reserves. *Resources, Conservation and Recycling*, *57*, 78-86.

Cooper, W. T., Llewelyn, J. M., Bennett, G. L., Stenson, A. C., & Salters, V. J. (2005). Organic phosphorus speciation in natural waters by mass spectrometry. In *Organic phosphorus in the environment* (pp. 45-74). Wallingford, UK: CABI Publishing.

Coward, E. K., Ohno, T., & Plante, A. F. (2018). Adsorption and Molecular Fractionation of Dissolved Organic Matter on Iron-Bearing Mineral Matrices of Varying Crystallinity. *Environmental science & technology*, *52*(3), 1036-1044.

Cullen, P., & Forsberg, C. (1988). Experiences with reducing point sources of phosphorus to lakes. *Hydrobiologia*, *170*(1), 321-336.

D'Andrilli, J., Cooper, W. T., Foreman, C. M., & Marshall, A. G. (2015). An ultrahigh-resolution mass spectrometry index to estimate natural organic matter lability. *Rapid Communications in Mass Spectrometry*, *29*(24), 2385-2401.

D'Angelo, E., Crutchfield, J., & Vandiviere, M. (2001). Rapid, sensitive, microscale determination of phosphate in water and soil. *Journal of environmental quality*, *30*(6), 2206-2209.

Dannenberg, A., & Pehkonen, S. O. (1998). Investigation of the heterogeneously catalyzed hydrolysis of organophosphorus pesticides. *Journal of agricultural and food chemistry*, *46*(1), 325-334.

De Brabandere, H., Forsgard, N., Israelsson, L., Petterson, J., Rydin, E., Waldebäck, M., & Sjöberg, P. J. (2008). Screening for organic phosphorus compounds in aquatic sediments by liquid chromatography coupled to ICP-AES and ESI-MS/MS. *Analytical chemistry*, *80*(17), 6689-6697.

De Vicente, I., López, R., Pozo, I., & Green, A. J. (2012). Nutrient and sediment dynamics in a Mediterranean shallow lake in southwest Spain. *Limnetica, 31*(2), 231-250.

Dittmar, T., & Stubbins, A. (2014). 12.6 - Dissolved organic matter in aquatic systems. In *Treatise on Geochemistry, 2nd edn* (pp. 125-156). Oxford, UK: Elsevier Science.

Dittmar, T., Koch, B., Hertkorn, N., & Kattner, G. (2008). A simple and efficient method for the solid-phase extraction of dissolved organic matter (SPE-DOM) from seawater. *Limnology and Oceanography: Methods*, *6*(6), 230-235.

Drake, T. W., Raymond, P. A., & Spencer, R. G. (2018). Terrestrial carbon inputs to inland waters: A current synthesis of estimates and uncertainty. *Limnology and Oceanography Letters*, *3*(3), 132-142.

Dvorski, S. E. M. (2017). *Linking the sulfur and carbon cycle by ultrahigh resolution characterization of dissolved organic matter.* (Doctoral dissertation). Retrieved from https://mediatum.ub.tum.de

Edwards, A. C., & Withers, P. J. A. (2008). Transport and delivery of suspended solids, nitrogen and phosphorus from various sources to freshwaters in the UK. *Journal of Hydrology*, *350*(3-4), 144-153.

Fichot, C. G., Benner, R., Kaiser, K., Shen, Y., Amon, R. M., Ogawa, H., & Lu, C. J. (2016). Predicting dissolved lignin phenol concentrations in the coastal ocean from chromophoric dissolved organic matter (CDOM) absorption coefficients. *Frontiers in Marine Science*, *3*, 7.

Filippelli, G. M. (2008). The global phosphorus cycle: past, present, and future. *Elements*, *4*(2), 89-95.

Filippelli, G. M. (2011). Phosphate rock formation and marine phosphorus geochemistry: the deep time perspective. *Chemosphere*, *84*(6), 759-766.

Francko, D. A., & Heath, R. T. (1982). UV-sensitive complex phosphorus: Association with dissolved humic material and iron in a bog lake 1. *Limnology and Oceanography*, *27*(3), 564-569.

Frossard, E., Stewart, J. W. B., & St. Arnaud, R. J. (1989). Distribution and mobility of phosphorus in grassland and forest soils of Saskatchewan. *Canadian Journal of Soil Science*, *69*(2), 401-416.

Galindo, C., & Del Nero, M. (2014). Molecular level description of the sorptive fractionation of a fulvic acid on aluminum oxide using electrospray ionization Fourier transform mass spectrometry. *Environmental science & technology*, *48*(13), 7401-7408.

Ghebremichael, L. T., Veith, T. L., & Watzin, M. C. (2010). Determination of critical source areas for phosphorus loss: Lake Champlain basin, Vermont. *Transactions of the ASABE*, *53*(5), 1595-1604.

Giles, C. D., Isles, P. D., Manley, T., Xu, Y., Druschel, G. K., & Schroth, A. W. (2016). The mobility of phosphorus, iron, and manganese through the sediment–water continuum of a shallow eutrophic freshwater lake under stratified and mixed water-column conditions. *Biogeochemistry*, *127*(1), 15-34.

Giles, C. D., Lee, L. G., Cade-Menun, B. J., Hill, J. E., Isles, P. D., Schroth, A. W., & Druschel, G. K. (2015). Characterization of organic phosphorus form and bioavailability in lake sediments using ^{31}P nuclear magnetic resonance and enzymatic hydrolysis. *Journal of environmental quality*, *44*(3), 882-894.

Gonsior, M., Peake, B. M., Cooper, W. T., Podgorski, D. C., D'Andrilli, J., Dittmar, T., & Cooper, W. J. (2011). Characterization of dissolved organic matter across the Subtropical Convergence off the South Island, New Zealand. *Marine Chemistry*, *123*(1-4), 99-110.

Gonsior, M., Valle, J., Schmitt-Kopplin, P., Hertkorn, N., Bastviken, D., Luek, J., ... & Enrich Prast, A. (2016). Chemodiversity of dissolved organic matter in the Amazon Basin. *Biogeosciences*, *13*(14), 4279-4290.

Green, N. W., & Perdue, E. M. (2015). Fast Graphically Inspired Algorithm for Assignment of Molecular Formulae in Ultrahigh Resolution Mass Spectrometry. *Analytical chemistry*, *87*(10), 5086-5094.

Guigue, J., Harir, M., Mathieu, O., Lucio, M., Ranjard, L., Lévêque, J., & Schmitt-Kopplin, P. (2016). Ultrahigh-resolution FT-ICR mass spectrometry for molecular characterisation of pressurised hot water-extractable organic matter in soils. *Biogeochemistry*, *128*(3), 307-326.

Harrison, G. I., & Francois, M. M. (1983). NTAGONISM BETWEEN CADMIUM AND IRON IN THE MARINE DIATOM THALASSIOSIRA WEISSFLOGII[1]. *Journal of phycology*, *19*(4), 495-507.

Heath, R. T. (2005). Microbial turnover of organic phosphorus in aquatic systems. In *Organic phosphorus in the environment* (pp. 185-204). Wallingford, UK: CABI Publishing.

Hertkorn, N., Frommberger, M., Witt, M., Koch, B. P., Schmitt-Kopplin, P., & Perdue, E. M. (2008). Natural organic matter and the event horizon of mass spectrometry. *Analytical chemistry*, *80*(23), 8908-8919.

Hertkorn, N., Ruecker, C., Meringer, M., Gugisch, R., Frommberger, M., Perdue, E. M., ... & Schmitt-Kopplin, P. (2007). High-precision frequency measurements: indispensable tools at the core of the molecular-level analysis of complex systems. *Analytical and bioanalytical chemistry*, *389*(5), 1311-1327.

Herzsprung, P., Hertkorn, N., von Tümpling, W., Harir, M., Friese, K., & Schmitt-Kopplin, P. (2014). Understanding molecular formula assignment of Fourier transform ion cyclotron resonance mass spectrometry data of natural organic

matter from a chemical point of view. *Analytical and bioanalytical chemistry*, *406*(30), 7977-7987.

Hockaday, W. C., Purcell, J. M., Marshall, A. G., Baldock, J. A., & Hatcher, P. G. (2009). Electrospray and photoionization mass spectrometry for the characterization of organic matter in natural waters: a qualitative assessment. *Limnology and Oceanography: Methods*, *7*(1), 81-95.

Hudson, J. J., Taylor, W. D., & Schindler, D. W. (2000). Phosphate concentrations in lakes. *Nature*, *406*(6791), 54.

Hughey, C. A., Hendrickson, C. L., Rodgers, R. P., Marshall, A. G., & Qian, K. (2001). Kendrick mass defect spectrum: a compact visual analysis for ultrahigh-resolution broadband mass spectra. *Analytical Chemistry*, *73*(19), 4676-4681.

Isles, P. D., Xu, Y., Stockwell, J. D., & Schroth, A. W. (2017). Climate-driven changes in energy and mass inputs systematically alter nutrient concentration and stoichiometry in deep and shallow regions of Lake Champlain. *Biogeochemistry*, *133*(2), 201-217.

Johnson, N. R., & Hill, J. E. (2010). Phosphorus species composition of poultry manure-amended soil using high-throughput enzymatic hydrolysis. *Soil Science Society of America Journal*, *74*(5), 1786-1791.

Joung, D., Leduc, M., Ramcharitar, B., Xu, Y., Isles, P. D., Stockwell, J. D., ... & Schroth, A. W. (2017). Winter weather and lake-watershed physical configuration drive phosphorus, iron, and manganese dynamics in water and sediment of ice-covered lakes. *Limnology and Oceanography*, *62*(4), 1620-1635.

Kamiya, M., & Kameyama, K. (1998). Photochemical effects of humic substances on the degradation of organophosphorus pesticides. *Chemosphere*, *36*(10), 2337-2344.

Kawashima, M., Tainaka, Y., Hori, T., Koyama, M., & Takamatsu, T. (1986). Phosphate adsorption onto hydrous manganese (IV) oxide in the presence of divalent cations. *Water research*, *20*(4), 471-475.

Kellerman, A. M., Kothawala, D. N., Dittmar, T., & Tranvik, L. J. (2015). Persistence of dissolved organic matter in lakes related to its molecular characteristics. *Nature Geoscience*, *8*(6), 454.

Killberg-Thoreson, L., Sipler, R. E., & Bronk, D. A. (2013). Anthropogenic nutrient sources supplied to a Chesapeake Bay tributary support algal growth: a bioassay and high-resolution mass spectrometry approach. *Estuaries and coasts*, *36*(5), 966-980.

Kim, S., Kramer, R. W., & Hatcher, P. G. (2003). Graphical method for analysis of ultrahigh-resolution broadband mass spectra of natural organic matter, the van Krevelen diagram. *Analytical Chemistry*, *75*(20), 5336-5344.

Kind, T., & Fiehn, O. (2007). Seven Golden Rules for heuristic filtering of molecular formulas obtained by accurate mass spectrometry. *BMC bioinformatics*, *8*(1), 105.

Koch, B. P., Dittmar, T., Witt, M., & Kattner, G. (2007). Fundamentals of molecular formula assignment to ultrahigh resolution mass data of natural organic matter. *Analytical Chemistry*, *79*(4), 1758-1763.

Kruse, J., Abraham, M., Amelung, W., Baum, C., Bol, R., Kühn, O., ... & Santner, J. (2015). Innovative methods in soil phosphorus research: A review. *Journal of plant nutrition and soil science*, *178*(1), 43-88.

Kuiper-Goodman, T., Falconer, I., & Fitzgerald, J. (1999). Human Health Aspects. In *Toxic Cyanobacteria In Water: A Guide To Their Public Health Consequences, Monitoring And Management* (pp. 113-154). CRC Press.

Lake Champlain Basin Program (LCBP). (2018). State of the Lake and Ecosystem Indicators Report. http://sol.lcbp.org/en/

Lalonde, K., Mucci, A., Ouellet, A., & Gélinas, Y. (2012). Preservation of organic matter in sediments promoted by iron. *Nature*, *483*(7388), 198.

Levine, S. N., Lini, A., Ostrofsky, M. L., Bunting, L., Burgess, H., Leavitt, P. R., ... & Gilles, E. (2012). The eutrophication of Lake Champlain's northeastern arm: Insights from paleolimnological analyses. *Journal of Great Lakes Research*, *38*, 35-48.

Li, Y., Harir, M., Lucio, M., Kanawati, B., Smirnov, K., Flerus, R., ... & Hertkorn, N. (2016). Proposed guidelines for solid phase extraction of Suwannee River dissolved organic matter. *Analytical chemistry*, *88*(13), 6680-6688.

Lijklema, L. (1980). Interaction of orthophosphate with iron (III) and aluminum hydroxides. *Environmental Science & Technology*, *14*(5), 537-541.

Llewelyn, J. M., Landing, W. M., Marshall, A. G., & Cooper, W. T. (2002). Electrospray ionization Fourier transform ion cyclotron resonance mass spectrometry of dissolved organic phosphorus species in a treatment wetland after selective isolation and concentration. *Analytical chemistry*, *74*(3), 600-606.

Lovley, D. R. (1991). Dissimilatory Fe (III) and Mn (IV) reduction. *Microbiological reviews*, *55*(2), 259-287.

Lowry, O. H., & Lopez, J. A. (1946). The determination of inorganic phosphate in the presence of labile phosphate esters. *Journal of Biological Chemistry*, *162*, 421-428.

Marshall, A. G., Hendrickson, C. L., & Jackson, G. S. (1998). Fourier transform ion cyclotron resonance mass spectrometry: A primer. *Mass Spectrometry Reviews*, *17*, 1-35.

McCarthy, M. J., Gardner, W. S., Lehmann, M. F., & Bird, D. F. (2013). Implications of water column ammonium uptake and regeneration for the nitrogen budget in temperate, eutrophic Missisquoi Bay, Lake Champlain (Canada/USA). *Hydrobiologia*, *718*(1), 173-188.

McKelvie, I. D. (2005). Separation, preconcentration and speciation of organic phosphorus in environmental samples. In *Organic phosphorus in the environment* (pp. 1-20). Wallingford, UK: CABI Publishing.

Meals, D. W., & Budd, L. F. (1998). LAKE CHAMPLAIN BASIN NONPOINT SOURCE PHOSPHORUS ASSESSMENT[1]. *JAWRA Journal of the American Water Resources Association*, *34*(2), 251-265.

Medalie, L. (2007). Concentrations and Loads of Nutrients and Suspended Sediments in Englesby Brook and Little Otter Creek, Lake Champlain Basin, Vermont, 2000-2005. U.S. Geological Survey Scientific Investigations Report 2007–5074. https://pubs.usgs.gov/sir/2007/5074/pdf/SIR2007-5074.pdf

Medalie, L., & Smeltzer, E. (2004). Status and trends of phosphorus in Lake Champlain and its tributaries, 1990–2000. In *Lake Champlain: partnerships and research in the new millennium* (pp. 191-219). Boston, MA: Springer.

Meyers, P. A., & Ishiwatari, R. (1993). Lacustrine organic geochemistry—an overview of indicators of organic matter sources and diagenesis in lake sediments. *Organic geochemistry*, *20*(7), 867-900.

Minor, E. C., Steinbring, C. J., Longnecker, K., & Kujawinski, E. B. (2012). Characterization of dissolved organic matter in Lake Superior and its watershed using ultrahigh resolution mass spectrometry. *Organic Geochemistry*, *43*, 1-11.

Mitchell, A. M., & Baldwin, D. S. (2005). Organic phosphorus in the aquatic environment: Speciation, transformations and interactions with nutrient cycles. In *Organic phosphorus in the environment* (pp. 309-324). Wallingford, UK: CABI Publishing.

Monaghan, E. J., & Ruttenberg, K. C. (1999). Dissolved organic phosphorus in the coastal ocean: Reassessment of available methods and seasonal phosphorus profiles from the Eel River Shelf. *Limnology and Oceanography*, *44*(7), 1702-1714.

Moran, M. A., & Zepp, R. G. (1997). Role of photoreactions in the formation of biologically labile compounds from dissolved organic matter. *Limnology and Oceanography*, *42*(6), 1307-1316.

Mur, R., Skulberg, O. M., & Utkilen, H. (1999). CYANOBACTERIA IN THE ENVIRONMENT. In *Toxic Cyanobacteria In Water: A Guide To Their Public Health Consequences, Monitoring And Management* (pp. 15-40). CRC Press.

Murphy, J., & Riley J. (1962) A modified single solution method for the determination of phosphate in natural water. *Analytica chimica acta, 27*, 31-36

Murray, J. W. (1974). The surface chemistry of hydrous manganese dioxide. *Journal of Colloid and Interface Science*, *46*(3), 357-371.

Nebbioso, A., & Piccolo, A. (2013). Molecular characterization of dissolved organic matter (DOM): a critical review. *Analytical and bioanalytical chemistry*, *405*(1), 109-124.

Nikolaev, E. N., Kostyukevich, Y. I., & Vladimirov, G. N. (2016). Fourier transform ion cyclotron resonance (FT ICR) mass spectrometry: Theory and simulations. *Mass spectrometry reviews*, *35*(2), 219-258.

O'neil, J. M., Davis, T. W., Burford, M. A., & Gobler, C. J. (2012). The rise of harmful cyanobacteria blooms: the potential roles of eutrophication and climate change. *Harmful algae*, *14*, 313-334.

Ohno, T., Sleighter, R. L., & Hatcher, P. G. (2016). Comparative study of organic matter chemical characterization using negative and positive mode electrospray ionization ultrahigh-resolution mass spectrometry. *Analytical and bioanalytical chemistry*, *408*(10), 2497-2504.

Olesik, J. W. (1991). Elemental analysis using ICP-OES and ICP/MS. *Analytical Chemistry*, *63*(1), 12A-21A.

Osterholz, H., Kirchman, D. L., Niggemann, J., & Dittmar, T. (2016). Environmental drivers of dissolved organic matter molecular composition in the Delaware Estuary. *Frontiers in Earth Science*, *4*, 95.

Paerl, H. W. (1988). Nuisance phytoplankton blooms in coastal, estuarine, and inland waters[1]. *Limnology and Oceanography*, *33*(4, part 2), 823-843.

Paerl, H. W., & Otten, T. G. (2013). Harmful cyanobacterial blooms: causes, consequences, and controls. *Microbial ecology*, *65*(4), 995-1010.

Parks, G. A. (1965). The isoelectric points of solid oxides, solid hydroxides, and aqueous hydroxo complex systems. *Chemical Reviews*, *65*(2), 177-198.

Pearce, A. R., Rizzo, D. M., Watzin, M. C., & Druschel, G. K. (2013). Unraveling associations between cyanobacteria blooms and in-lake environmental conditions in Missisquoi Bay, Lake Champlain, USA, using a modified self-organizing map. *Environmental science & technology*, *47*(24), 14267-14274.

Perdue, E. M., & Ritchie, J. D. (2014). 7.8 - Dissolved organic matter in freshwaters. In *Treatise on Geochemistry, 2nd edn* (pp. 237-272). Oxford, UK: Elsevier Science.

Qin, C., Kang, F., Zhang, W., Shou, W., Hu, X., & Gao, Y. (2017). Environmentally-relevant concentrations of Al (III) and Fe (III) cations induce aggregation of free DNA by complexation with phosphate group. *Water research*, *123*, 58-66.

Ratcliffe, N. M., Stanley, R. S., Gale, M. H., Thompson, P. J., & Walsh, G. J. (2011). Bedrock Geologic Map of Vermont: USGS Scientific Investigations Series Map 3184, 3 sheets, scale 1:100,000.

Reynolds, C. S., & Davies, P. S. (2001). Sources and bioavailability of phosphorus fractions in freshwaters: a British perspective. *Biological reviews*, *76*(1), 27-64.

Ritchie, J. D., & Perdue, E. M. (2003). Proton-binding study of standard and reference fulvic acids, humic acids, and natural organic matter. *Geochimica et Cosmochimica Acta*, *67*(1), 85-96.

Rivas-Ubach, A., Liu, Y., Bianchi, T. S., Tolić, N., Jansson, C., & Paša-Tolić, L. (2018). Moving beyond the van Krevelen Diagram: A New Stoichiometric Approach for Compound Classification in Organisms. *Analytical chemistry*, *90*(10), 6152-6160.

Rosenberg, B. D., & Schroth, A. W. (2017). Coupling of reactive riverine phosphorus and iron species during hot transport moments: impacts of land cover and seasonality. *Biogeochemistry*, *132*(1-2), 103-122.

Rowland, A. P., & Haygarth, P. M. (1997). Determination of total dissolved phosphorus in soil solutions. *Journal of Environmental Quality*, *26*(2), 410-415.

Ruttenberg, K.C. (2014). 10.13 - The global phosphorus cycle. In *Treatise on Geochemistry, 2nd edn* (pp. 499-558). Oxford, UK: Elsevier Science.

Saheki, S., Takeda, A., & Shimazu, T. (1985). Assay of inorganic phosphate in the mild pH range, suitable for measurement of glycogen phosphorylase activity. *Analytical biochemistry*, *148*(2), 277-281.

Sandvik, S. L. H., Bilski, P., Pakulski, J. D., Chignell, C. F., & Coffin, R. B. (2000). Photogeneration of singlet oxygen and free radicals in dissolved organic matter isolated from the Mississippi and Atchafalaya River plumes. *Marine chemistry*, *69*(1-2), 139-152.

Schroth, A. W., Giles, C. D., Isles, P. D., Xu, Y., Perzan, Z., & Druschel, G. K. (2015). Dynamic coupling of iron, manganese, and phosphorus behavior in water and sediment of shallow ice-covered eutrophic lakes. *Environmental science & technology*, *49*(16), 9758-9767.

Serediak N.A., Prepas E.E., Putz G.J. (2014). 11.8 - Eutrophication of freshwater systems. In *Treatise on Geochemistry, 2nd edn* (pp. 305-323). Oxford, UK: Elsevier Science.

Shinohara, R., Hiroki, M., Kohzu, A., Imai, A., Inoue, T., Furusato, E., ... & Miura, S. (2017). Role of organic phosphorus in sediment in a shallow eutrophic lake. *Water Resources Research*, *53*(8), 7175-7189.

Siuda, W., & Chróst, R. J. (2001). Utilization of selected dissolved organic phosphorus compounds by bacteria in lake water under non-limiting orthophosphate conditions. *Polish Journal of Environmental Studies*, *10*(6), 475-484.

Sleighter, R. L., & Hatcher, P. G. (2007). The application of electrospray ionization coupled to ultrahigh resolution mass spectrometry for the molecular characterization of natural organic matter. *Journal of Mass Spectrometry*, *42*(5), 559-574.

Sleighter, R. L., & Hatcher, P. G. (2011). Fourier transform mass spectrometry for the molecular level characterization of natural organic matter: Instrument capabilities, applications, and limitations. In *Fourier Transforms-Approach to Scientific Principles* (pp. 295-320). Rijeka, Croatia: InTech.

Sleighter, R. L., McKee, G. A., & Hatcher, P. G. (2009). Direct Fourier transform mass spectral analysis of natural waters with low dissolved organic matter. *Organic Geochemistry*, *40*(1), 119-125.

Smeltzer, E. (1999). Phosphorus management in Lake Champlain. *Water Science and Applications*, *1*, 435-451.

Smeltzer, E., & Quinn, S. (1996). A phosphorus budget, model, and load reduction strategy for Lake Champlain. *Lake and Reservoir Management*, *12*(3), 381-393.

Smeltzer, E., & Simoneau, M. (2008). Phosphorus loading to Missisquoi Bay from sub-basins in Vermont and Québec, 2002–2005. Report submitted to the Lake Champlain Steering Committee. http://www.wwwalker.net/champ/tmdl/references/Missisquoi%20Bay/MissBay%20P%20Loading%202002-2005%20(Smeltzer2008).pdf

Smeltzer, E., Dunlap, F. & Simoneau, M. (2009). Lake Champlain phosphorus concentrations and loading rates, 1990–2008. Technical Report 57. http://www.lcbp.org/techreportPDF/57_Phosphorus_Loading_1990-2008.pdf. Lake Champlain Basin Program.

Smeltzer, E., d Shambaugh, A., & Stangel, P. (2012). Environmental change in Lake Champlain revealed by long-term monitoring. *Journal of Great Lakes Research*, *38*, 6-18.

Smil, V. (2000). Phosphorus in the environment: natural flows and human interferences. *Annual review of energy and the environment*, *25*(1), 53-88.

Smith, L. (2009). *Missisquoi Bay sediment phosphorus cycling: the role of organic phosphorus and seasonal redox fluctuations.* (Graduate College Dissertations and Theses). Retrieved from https://scholarworks.uvm.edu

Smith, L., Watzin, M. C., & Druschel, G. (2011). Relating sediment phosphorus mobility to seasonal and diel redox fluctuations at the sediment–water interface in a eutrophic freshwater lake. *Limnology and Oceanography*, *56*(6), 2251-2264.

Smith, V. H., Tilman, G. D., & Nekola, J. C. (1999). Eutrophication: impacts of excess nutrient inputs on freshwater, marine, and terrestrial ecosystems. *Environmental pollution*, *100*(1-3), 179-196.

Søndergaard, M., Bjerring, R., & Jeppesen, E. (2013). Persistent internal phosphorus loading during summer in shallow eutrophic lakes. *Hydrobiologia*, *710*(1), 95-107.

Søndergaard, M., Jensen, J. P., & Jeppesen, E. (2003). Role of sediment and internal loading of phosphorus in shallow lakes. *Hydrobiologia*, *506*(1-3), 135-145.

Spencer, R. G., Stubbins, A., Hernes, P. J., Baker, A., Mopper, K., Aufdenkampe, A. K., ... & Six, J. (2009). Photochemical degradation of dissolved organic matter and dissolved lignin phenols from the Congo River. *Journal of Geophysical Research: Biogeosciences*, *114*(G3).

Spohn, M., & Kuzyakov, Y. (2013). Phosphorus mineralization can be driven by microbial need for carbon. *Soil Biology and Biochemistry*, *61*, 69-75.

Stager, J. C., & Thill, M. (2010). Climate change in the Champlain Basin. *The Nature Conservancy*.

Stubbins, A., Spencer, R. G., Chen, H., Hatcher, P. G., Mopper, K., Hernes, P. J., ... & Six, J. (2010). Illuminated darkness: molecular signatures of Congo River dissolved organic matter and its photochemical alteration as revealed by ultrahigh precision mass spectrometry. *Limnology and Oceanography*, *55*(4), 1467-1477.

Sun, L., Perdue, E. M., Meyer, J. L., & Weis, J. (1997). Use of elemental composition to predict bioavailability of dissolved organic matter in a Georgia river. *Limnology and Oceanography*, *42*(4), 714-721.

Suttle, C. A. (1994). The significance of viruses to mortality in aquatic microbial communities. *Microbial ecology*, *28*(2), 237-243.

Turner, B. L. (2005). Organic phosphorus transfer from terrestrial to aquatic environments. In *Organic phosphorus in the environment* (pp. 269-294). Wallingford, UK: CABI Publishing.

Tyrrell, T. (1999). The relative influences of nitrogen and phosphorus on oceanic primary production. *Nature*, *400*(6744), 525.

Tziotis, D., Hertkorn, N., & Schmitt-Kopplin, P. (2011). Kendrick-analogous network visualisation of ion cyclotron resonance Fourier transform mass spectra: improved options for the assignment of elemental compositions and the classification of organic molecular complexity. *European Journal of Mass Spectrometry*, *17*(4), 415-421.

Van Krevelen, D. W. (1950). Graphical-statistical method for the study of structure and reaction processes of coal. *Fuel*, *29*, 269-284.

Van Mooy, B. A., Fredricks, H. F., Pedler, B. E., Dyhrman, S. T., Karl, D. M., Koblížek, M., ... & Rappé, M. S. (2009). Phytoplankton in the ocean use non-phosphorus lipids in response to phosphorus scarcity. *Nature*, *458*(7234), 69.

Vannote, R. L., Minshall, G. W., Cummins, K. W., Sedell, J. R., & Cushing, C. E. (1980). The river continuum concept. *Canadian journal of fisheries and aquatic sciences*, *37*(1), 130-137.

Vermont Department of Environmental Conservation (VTDEC). (2018). Lake Champlain long-term monitoring. Vermont Department of Environmental Conservation. http://dec.vermont.gov/watershed

Wagner, S., Riedel, T., Niggemann, J., Vähätalo, A. V., Dittmar, T., & Jaffé, R. (2015). Linking the molecular signature of heteroatomic dissolved organic matter to watershed characteristics in world rivers. *Environmental science & technology*, *49*(23), 13798-13806.

Walling, C. (1975). Fenton's reagent revisited. *Accounts of chemical research*, *8*(4), 125-131.

Wang, X., Liu, F., Tan, W., Li, W., Feng, X., & Sparks, D. L. (2013). Characteristics of phosphate adsorption-desorption onto ferrihydrite: comparison with well-crystalline Fe (hydr) oxides. *Soil Science*, *178*(1), 1-11.

Wang, Z. H., Liang, Y., & Kang, W. (2011). Utilization of dissolved organic phosphorus by different groups of phytoplankton taxa. *Harmful Algae*, *12*, 113-118.

Watzin, M. C, Shambaugh, A. D., & Brines, E. (2003). Monitoring and evaluation of cyanobacteria in Burlington Bay, Lake Champlain: Summer 2002. Report prepared for Lake Champlain Basin Program. http://www.lcbp.org/wp-content/uploads/2013/04/41_BGA_Summer_2002.pdf

White, E. M., Vaughan, P. P., & Zepp, R. G. (2003). Role of the photo-Fenton reaction in the production of hydroxyl radicals and photobleaching of colored dissolved organic matter in a coastal river of the southeastern United States. *Aquatic Sciences*, *65*(4), 402-414.

Wright, S. & Larsen, F. (2004). Surficial Geology of the Barre-Montpelier Region. www.anr.state.vt.us/dec/geo/pdfdocs/BarreWestwright.pdf

Yan, J., Jiang, T., Yao, Y., Wang, J., Cai, Y., Green, N. W., & Wei, S. (2017). Underestimation of phosphorus fraction change in the supernatant after

phosphorus adsorption onto iron oxides and iron oxide–natural organic matter complexes. *Journal of Environmental Sciences*, *55*, 197-205.

Yiyong, Z. (1996). UV-sensitive P compounds: release mechanism, seasonal fluctuation and inhibitory effects on alkaline phosphatase activity in a shallow Chinese freshwater lake (Donghu Lake). *Hydrobiologia*, *335*(1), 55-62.

Yuan, Z., Jiang, S., Sheng, H., Liu, X., Hua, H., Liu, X., & Zhang, Y. (2018). Human perturbation of the global phosphorus cycle: changes and consequences. *Environmental science & technology*, *52*(5), 2438-2450.

Zilius, M., Bartoli, M., Bresciani, M., Katarzyte, M., Ruginis, T., Petkuviene, J., ... & Razinkovas-Baziukas, A. (2014). Feedback mechanisms between cyanobacterial blooms, transient hypoxia, and benthic phosphorus regeneration in shallow coastal environments. *Estuaries and coasts*, *37*(3), 680-694.

Chapter 2 – Chemical fractionation of organic matter and organic phosphorus extractions from freshwater lake sediment

Introduction:

Organic matter (OM) represents a sometimes minor, but critical, portion of lake sediment serving as a nutrition source for organisms, controlling oxygen concentrations in porewater, and providing reducing potential to inorganic ions in redox reactions (Meyers & Ishiwatari, 1993). Sediment-associated OM acts as a freshwater carbon sink containing organic compounds from allochthonous (terrestrially derived) and autochthonous (algal and microbially derived) sources linked with the N, S, and P cycles (Aitkenhead-Peterson et al., 2003; Perdue & Ritchie, 2014). Terrestrial OM is transported to lakes through runoff and streams where the most labile compounds are degraded (through bio- or photochemical reactions) and the most recalcitrant compounds enter the system (Dittmar & Stubbins, 2014). Further consumption occurs throughout the water column as allochthonous and autochthonous sources are mixed and variably mineralized by microorganisms as they settle (Aitkenhead-Peterson et al., 2003; Kritzberg et al., 2005). Compared to deep lakes, shallow lake sediment would be more enriched in OM due to shorter transport times (Meyers & Ishiwatari, 1993). Upon incorporation into the sediment, labile OM continues the degradation process through biotic and abiotic pathways, leaving behind large aromatic plant material and lipids while labile amino-sugars and carbohydrates are consumed (Kemp & Johnston, 1979; Meyers & Ishiwatari, 1993).

The diversity of OM associated with soil and sediment is governed by the structural and molecular binding properties of its constituent parts, varying from

environmental settings and through time (Hertkorn et al., 2007, Guigue et al. 2016, Herzsprung et al. 2017, Valle et al. 2018,). Characterization of this OM is largely operationally defined as humic and fulvic acids, both soluble in alkali solution. Fulvic acids retain solubility upon acidification, while humics are precipitated below pH 2 (Schlesinger & Bernhardt, 2013). Further detailed characterizations have been described using targeted extractions of specific OM pools. For instance, extraction of soil sediments with water affords microbially labile organic carbon (Sparling et al., 1998; Guigue et al., 2016) and extraction with more acidic reagents, such as HCl-dithionite, selects for Fe mineral-associated OM (Coward et al., 2018). Association of OM onto mineral oxide surfaces is generally dependent on molecular functionality; typically, with minerals sequestering more aromatic and oxygen-rich molecules while aliphatics are adsorbed to a lesser extent (Galindo & Del Nero, 2014; Riedel et al., 2013; Dadi et al., 2017). A subset of functionalized OM includes organic P that also follows predictable fractionations from targeted chemical extractions (Turner et al., 2005).

Excess bioavailable P input into eutrophic freshwater lakes from dissolved and particulate fractions can trigger harmful cyanobacterial blooms resulting in fish kills from anoxia, toxin production, and excessive algal growth (Serediak et al., 2014). Organic P greatly contributes to bioavailable P pools through microbial and abiotic degradation allowing it to be utilized by microorganisms and adsorbed onto lake sediment (Mitchell & Baldwin, 2005; Giles et al., 2015). Much like the inorganic form, organic P adsorbs onto various Fe, Mn, and Al (oxy)hydroxides and clays in oxic sediments through ligand exchange of the charged phosphate groups onto positive mineral surface sites (Søndergaard et al., 2003; Smith, 2009). During anoxic periods, reductive dissolution of

Fe and Mn (oxy)hydroxides releases the previously bound P into the water column and sediment porewater, increasing the pool of bioavailable P (Smith et al., 2011; Li et al., 2015), which can be utilized by harmful cyanobacteria for sustained growth during blooms (Giles et al., 2015).

Fourier transform-ion cyclotron resonance mass spectrometry (FT-ICR MS) provides unprecedented resolving power and detailed characterization of complex mixtures of natural OM (Hertkorn et al., 2007, 2013, 2016; Sleighter & Hatcher, 2007, Gonsior et al. 2016). It can also be used to give detailed information on organic P molecules that are often not detected by other methods such as ^{31}P NMR spectroscopy and other lower-resolution mass spectrometers (Cooper et al., 2005; El-Rifai et al., 2008). ^{31}P NMR has been routinely used to characterize organic P from soil (e.g. Cade-Menun et al., 2018), sediments (e.g. Giles et al., 2015), and water (e.g. Bai et al., 2015), but is limited by the signal detection limit, about 1 mg P/g (Magid et al., 1996; Cade-Menun et al., 2002), and line broadening from sediments containing high amounts of paramagnetic ions (Hawkesd et al., 1984; Cade-Menun & Preston, 1996). Furthermore, identification of individual organic P compounds (if present in appreciable amounts) requires spiking standard refence material into the matrix and long acquisition times. In contrast, FT-ICR MS can provide information on several thousand m/z ion signals from a single spectrum. The use of this technique to study organic P has been limited by the ionization efficiency of organic phosphates in complex mixtures relative to other ionizable functional groups (Cooper, 2005). Nevertheless, Brooker et al. (2018) recently showed that water extractions of dry manure can yield hundreds of extractable organic P compounds (10.9-12.8% of assigned peaks) with various functionalities. Despite the low ionization

efficiency, FT-ICR MS can still provide unparalleled qualitative information on previously uncharacterized P compounds. The goals of this study were: 1) to evaluate the fractionation of lake sediment OM with parallel extractions of various solvents and 2) to use the parallel extractions to determine the quality and composition of organic P molecules in lake sediments using FT-ICR MS. By investigating the extractable components of lake sediment, we seek to provide an unparalleled glimpse into benthic freshwater OM and organic P cycling by clearly identifying common extraction pools which may assist future research efforts in optimizing site-specific extraction schemes driven by distinct objectives.

Methods:

Site description and sampling:

Missisquoi Bay is in the northeast corner of Lake Champlain and borders both Vermont and Quebec, Canada. The Bay is isolated from the rest of Lake Champlain encompassing an area of 77.5 km^2 (Levine et al., 2012) and is considered shallow with a maximum depth of 5 m (Schroth et al., 2015). The system has undergone anthropogenic eutrophication due to a current and past human-enhanced nutrient loading from its watershed, with persistent summer cyanobacteria blooms occurring every summer in recent decades (Isles et al. 2015, Levine et al. 2012). However, the duration and severity of cyanobacteria blooms are thought to be strongly controlled by the flux of benthic P during summer months, typically starting in early August (Isles et al. 2017a,b). The top 30 cm of the sediment contains between 2 and 3% organic carbon and silt interspersed with plant material and mussels (Burgess, 2007). Down to 60 cm, the sediment becomes

darker and enriched in fine-grained clay (Burgess, 2007). Redox-sensitive Fe and Mn are present in the sediment with average concentrations of total Fe ranging from 40.50-53.43 mg/g and Mn from 0.80-1.60 mg/g (Smith, 2009). Bulk sediment from Missisquoi Bay was sampled on September 14, 2017 using a Ponar grab dredge and sifted for mussels on site. The sediment was kept on ice until transported to the laboratory and subsequently frozen at -20 °C prior to lyophilization.

Sediment extraction protocol:

Freeze-dried sediment was ground and homogenized in a mortar and pestle and divided into 3 g portions for extractions. Extractant volumes were 45 mL and included: 1 M NaOH, 1 M HCl, 1 M acetic acid, a 1:2 mixture of chloroform: methanol (modified from White et al., 1979), and 0.5 M $NaHCO_3$ at pH 10. All aqueous solvents were made using Milli-Q (DI) water. The chloroform-methanol mixture was evaporated under air and redissolved in DI water (designated H_2O organic extract) with another portion dissolved in 1 M NaOH (designated NaOH organic extract). The sediment extracts were centrifuged at 3500 rpm for 20 minutes and the supernatants were filtered through 0.22 µm sterile syringe filters for solid phase extraction.

Solid phase extractions:

Samples were concentrated and desalted using solid phase extractions immediately after filtration to minimize hydrolysis and sample alterations. Solid phase extraction (SPE) procedures were adapted from Dittmar et al. (2008). Samples were acidified to pH 2 with dropwise addition of HCl and passed through an Agilent Bond Elut

PPL column under air pressure. Columns were previously activated with 3 mL of methanol and washed with acidified water at pH 2. After sample addition, columns were rinsed with acidified water at pH 2 and stored at -20 °C until analysis. The columns were then eluted with 5 mL of methanol and diluted accordingly for FT-ICR MS analysis.

Fourier transform-ion cyclotron mass spectrometry:

Methanolic extracts were analyzed using a Bruker Solarix 12 Tesla (Bruker Daltonics, Bremen, Germany) Fourier Transform-Ion Cyclotron Resonance Mass Spectrometer (FT-ICR MS) with electrospray ionization in negative mode. The concentrations of the samples were prepared in methanol using a microliter pump at a flow rate of 120 μL h^{-1} with a nebulizer gas pressure of 138 kPa and a drying gas pressure of 103 kPa. A source heater temperature of 200 °C was kept ensuring rapid desolvation of the ionized droplets. The spectra were zero filled to a processing size of 4 megawords in ESI(−) and 500 scans were accumulated for each mass spectrum. All spectra were internally calibrated using an appropriate reference mass list to obtain a mass accuracy of less than 0.2 ppm. Data processing was conducted using Compass Data Analysis 4.0 (Bruker, Bremen, Germany) and formula assignment was processed by in-house software. The exact masses of the compounds were defined (FT-ICR MS), and their molecular composition was batch calculated by a software tool, written in-house (mass error: 0.2 ppm). The generated formulas were validated by setting sensible chemical constraints (N rule, oxygen-to-carbon (O/C) ratio ≤ 1, hydrogen-to-carbon (H/C) ratio ≤ 2n+2(C_nH_{2n+2}), element counts: C≤80, H unlimited, O≤60, N≤5, S≤1, P≤2) in conjunction with an automated theoretical isotope pattern comparison. Formulae with

heteroatomic assignments in the range of N_{0-5}, S_{0-1}, and P_{0-2} were considered only if they had a corresponding ^{13}C peak. Final molecular formula assignments were combined into groups containing CHO(P), CHON(P), CHOS(P), and CHONS(P) molecular compositions, which were used to reconstruct the group-selective mass spectra. Post processing and statistical analysis of the filtered mass lists were conducted using Microsoft Excel and R with the ggplot2 package (Wickham, 2016).

Geochemical analysis:

Samples were diluted accordingly with DI water and analyzed on a Perkin Elmer ICP-OES for total extractable S and P. Sample reproducibility, calculated from three measurements of the same extract, was within 5% for all elements. The same extracts were diluted further with DI water, acidified with 85% phosphoric acid, and measured in duplicate for extractable organic carbon by wet combustion at 850˚C using a Vario-Cube analyzer (Elementar Americas). Bulk sediment was measured for total inorganic and organic carbon as well as total sulfur using a total carbon and sulfur determinator (Eltra). Dry Sediment (200 mg) was combusted at 1350 ˚C and quantified for total carbon and sulfur using a standard reference calibration (Alpha Resources LLC). The concentrations for both extractable organic carbon and sediment organic carbon were determined as the difference between total combusted carbon and acidified inorganic carbon. The sediment mineral composition was examined using X-Ray Diffraction with a Bruker D8 Discover X-Ray Diffractometer, sample diffraction patterns were matched to candidate patterns in the Crystallography Open Database (http://www.crystallography.net/cod/) using Bruker EVA software.

Results:

Sediment geochemistry:

Extraction yield for organic carbon varied widely between different extractions (Table 2.1). NaOH extracted the most organic carbon from the sediment (10.4 mg C/g) while the lowest organic carbon was from the H_2O organic extract (0.6 mg C/g). The organic carbon concentrations for the acetic acid extract could not be determined due to analytical interference from the acetic acid during combustion. NaOH extracted the highest total sulfur (821.9 µg S/g) whereas both organic extracts yielded substantially lower sulfur at 10.9 and 11.8 µg S/g for the H_2O and NaOH organic extracts, respectively. Total P extractions spanned a dynamic range from 1148.6 µg P/g for the HCl extract, to 6.2 µg P/g for the NaOH organic extract. The concentration of total P for the H_2O organic extract was detected but below the quantification limit for the instrument. X-ray diffraction analysis of the sediment confirmed the presence of mainly quartz and clay (muscovite and kaolinite) minerals with some iron (oxy)hydroxides (goethite).

FT-ICR MS analysis of sediment extracts:

The filtered mass lists for each extractant were separated into two groups: a list with molecules containing at least 1 P atom and the remaining molecules not containing any P atoms. The analysis of non-P-containing molecules are plotted in van Krevelen diagrams classified according to their atomic compositions (Figure 2.1A) and their double bond equivalence (DBE) (Figure 2.1B). Fractionation of OM is evident as the HCl and NaOH organic extracts exhibit higher O/C and lower H/C distributions while the

molecular space of $NaHCO_3$ and the H_2O organic extracts cover lower O/C and higher H/C ratios (Figure 2.1A,B). Qualitatively, acetic acid and NaOH extracts cover a more extensive region in the van Krevelen diagrams covering most of the H/C and O/C ranges between all extracts (Figure 2.1A,B). DBE values are much higher for molecules extracted using HCl and the NaOH organic extract and lower for the acetic acid, $NaHCO_3$, and H_2O organic extracts; the NaOH extraction includes molecules that cover the whole range of observed DBE values (Figure 2.1B).

Assigned molecules common in all the extractions ("shared pool") were classified by their atomic compositions and were found to be primarily CHO-containing molecules (66.5%), followed by CHOS (15.9%), CHON (14.5%), and CHONS (3.2%). However, each extraction scheme produced a unique molecular composition that differed significantly from the portions of common molecules within the shared pool, resulting in great variability between the samples (Figure B-2.1). The largest group of compounds, CHO-containing molecules, represented 74.8-87.0% of all relative assignments, with the HCl and NaOH organic extractions contributing the most CHO-containing molecules (87.0% and 82.7%, respectively) (Figure B-2.1). The smallest group was CHONS compounds with the highest proportions (>2%) found only in the alkali extractions, while both CHON and CHOS varied between treatments.

Sample	Total extracted P (µg P/g) [ppm]	Total extracted S (µg S/g) [ppm]	Total extracted organic C (mg C/g)	FT-ICR MS formulae assignments	Total S (µg S/g) [ppm]	Total organic C (mg C/g)
1 M HCl	1148.6 ± 14.3	585.9 ± 3.1	1.9 ± 0.1	1,181		
1 M NaOH	709.2 ± 29.5	821.9 ± 21.7	10.4 ± 0.4	2,103		
1 M Acetic acid	32.3 ± 0.7	508.4 ± 23.2	-	2,401		
0.5 M $NaHCO_3$ at pH 10	265.3 ± 6.0	591.1 ± 7.3	3.7 ± 0.8	1,113		
Organic extract redissolved in DI H_2O	Below quantification	10.9 ± 0.3	0.6 ± 0.1	1,601		
Organic extract redissolved in 1 M NaOH	6.2 ± 0.2	11.8 ± 0.1	2.1 ± 0.1	1,425		
Dry sediment					1130.3 ± 76.8	23.5 ± 0.2

Table 2.1. Mean total extracted P, S, organic C, and FT-ICR MS formulae assignments for each sample. Total sediment combustible S and organic C are also included. Total S and P means are calculated using three replicate measurements, organic C means are calculated using duplicates. Analytical uncertainties are presented as ± 1σ standard deviations. “Below quantification” indicates P concentrations were detected but not reliably quantified due to the signal being below instrument calibration.

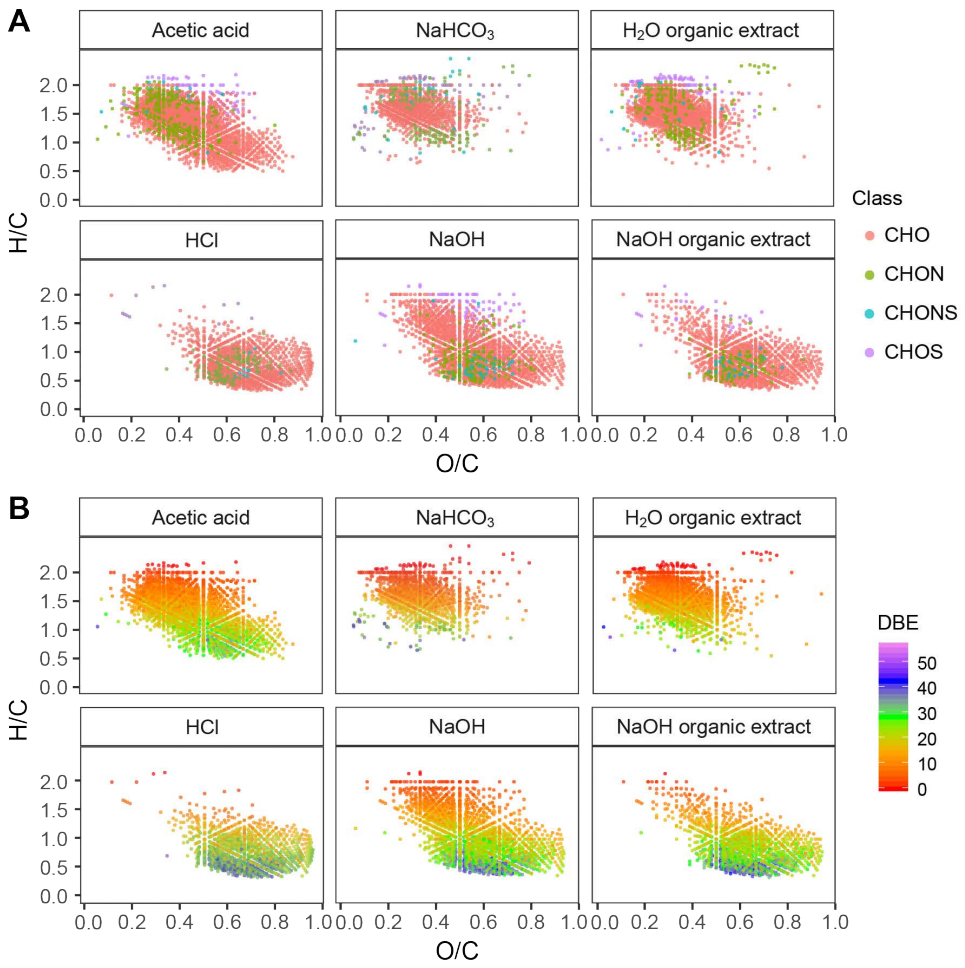

Figure 2.1. Van Krevelen diagrams of non-P-containing molecules in bulk sediment from Missisquoi Bay extracted with aqueous and organic solvents related to (A) compounds classified by their atomic compositions and (B) molecules colored by their calculated DBE values.

Pairwise presence-absence comparisons between peaks from the mass spectra were conducted to investigate molecular similarity between sediment extractions. Between all extractions, there were 1,632 common molecules corresponding to 16.6% of the entire dataset. The highest percent similarities were between HCl and NaOH organic extracts (928 molecules, 35.6%), NaOH and NaOH organic extracts (1,211 molecules, 34.3%), and $NaHCO_3$ and H_2O organic extracts (862 molecules, 31.8%) (Table B-2.1). The lowest percent similarities were between HCl and $NaHCO_3$ extracts (80 molecules,

3.5%), HCl and H_2O organic extracts (138 molecules, 5.0%), and $NaHCO_3$ and NaOH organic extracts (177 molecules, 7.0%) (Table B-2.1). Acetic acid and NaOH extracts had the highest mean pairwise similarity between all samples (905 and 887 shared molecules, respectively), while $NaHCO_3$ and HCl had the lowest (468 and 532 molecules, respectively). Both organic extracts had intermediate mean similarities; 671 molecules for the extract redissolved in NaOH, and 589 for the extract dissolved in DI water.

Median experimental mass distributions differed significantly for the HCl and $NaHCO_3$ extracts compared to the others (Figure B-2.2, Table B-2.2). HCl had the highest m/z at 461.0573, while $NaHCO_3$ was lower at 389.1606 Da. The other extracts were in the narrow range of 413.3272-425.0150 Da mean experimental mass distributions. NaOH resulted in very uniform mass range while $NaHCO_3$ and the H_2O organic extracts had a unique almost-bimodal distribution pattern that was more pronounced with $NaHCO_3$ (Figure B-2.2). Despite the difference, the two extracts had similar bulk molecular characteristics (Table B-2.2). Median H/C values were 1.56 and 1.53, respectively with O/C ratios for both being 0.33. Aromaticity index (AI) values were calculated to describe the extent of aromatic rings that could be present from the assigned molecular formulae (Koch & Dittmar, 2006); median AI was -0.10 ad -0.09, respectively and they both had median DBE values of 12. HCl, NaOH, and NaOH organic extracts had lower median H/C ratios of 0.82, 0.96, and 0.83, respectively, and higher O/C ratios of 0.67, 0.56, and 0.61, respectively. Median AI was higher at 0.00, -0.08, and 0.00, respectively with DBE values also greater (24, 20, 24, respectively). Molecules extracted using acetic acid had intermediate median H/C and O/C ratios of 1.36 and 0.44, respectively, with a calculated AI of -0.13 and DBE of 16.

Dissolved organic phosphorus:

The organic P distribution of the sediment extracts varied significantly. Relative organic P molecular assignments for each extractant are displayed in figure 2.2. The highest relative assignments of organic P are from the $NaHCO_3$ extract at 8.0% while the lowest was in the NaOH extract at 0.6%. The H_2O organic extract also afforded a high relative composition at 4.2%, while the organic NaOH extract resulted in only 1.2% organic P assignments, even though both originated from the same initial organic sediment extract. The $NaHCO_3$ and H_2O organic extracts also had the most assigned organic P molecules, with various molecular classes, out of all the extractants (100 and 70, respectively), while the HCl and NaOH extracts had the lowest (13 each) (Figure B-2.3). Assigned P molecules were plotted in van Krevelen space according to their atomic compositions (Figure 2.3). In general, they were found within the same regions of the van Krevelen diagrams of the non-P-containing molecules from the same extractions (Figure 2.1). The most dominant molecular classes containing P atoms for the acetic acid, $NaHCO_3$, and H_2O organic extracts were CHOP molecules (accounting for 51.7-64.3% of total P). A significant contribution was observed from CHONSP molecules (20.6% of total P) in $NaHCO_3$ and many CHONP molecules in the acetic acid extract (34.5% of total P) (Figure 2.3, Figure B-2.3). HCl, NaOH, and NaOH organic extracts had less contributions from CHOP molecules and greater relative proportions of N and S-containing molecules. Pairwise presence-absence comparisons between peaks from the mass spectra revealed $NaHCO_3$ and H_2O organic extracts shared the most organic P molecules (12 peaks, or 7.2% of the combined molecules) The second most shared peaks were between the acetic acid and the H_2O organic extracts (7 peaks, or 7.0% of the

combined molecules) and acetic acid with $NaHCO_3$ (7 peaks, or 5.6% of the combined molecules) (Table B-2.3). The NaOH extract had the lowest similarity between other extracts, only sharing 1 organic P molecule with acetic acid and 1 with the NaOH organic extract. HCl was also dissimilar, sharing 1 molecule with acetic acid, the H_2O organic extract, and $NaHCO_3$ (Table B-2.3).

Molecular properties from the $NaHCO_3$ and H_2O organic extracts, such as stoichiometric O/C and H/C ratios, saturation, and aromaticity, were quite similar (Table B-2.4). Their mass distributions also spanned the same range with median experimental masses of 469.1997 and 472.2126 Da, respectively. Median H/C values were 1.65 and 1.67 and median O/C values for both were 0.36, respectively. Calculated median AI values were -0.21 and -0.29 and DBE values were both 10 for the $NaHCO_3$ and H_2O organic extracts. Median experimental masses for both NaOH extracts were well within the distribution range of the previously mentioned samples, however the HCl extract was significantly higher with a median mass of 573.0544 Da (Table B-2.4). The HCl, NaOH, and NaOH organic extracts all had statistically lower median H/C values in the range of 0.87-1.1 and higher O/C values ranging from 0.43-0.44. Median AI was also higher ranging from 0.00-0.36 as well as DBE values from 24-28. Molecules from acetic acid extracts generally fell between the two groups with median H/C and O/C values at 1.61 and 0.32, respectively, and median AI and DBE values of -0.14 and 12, respectively.

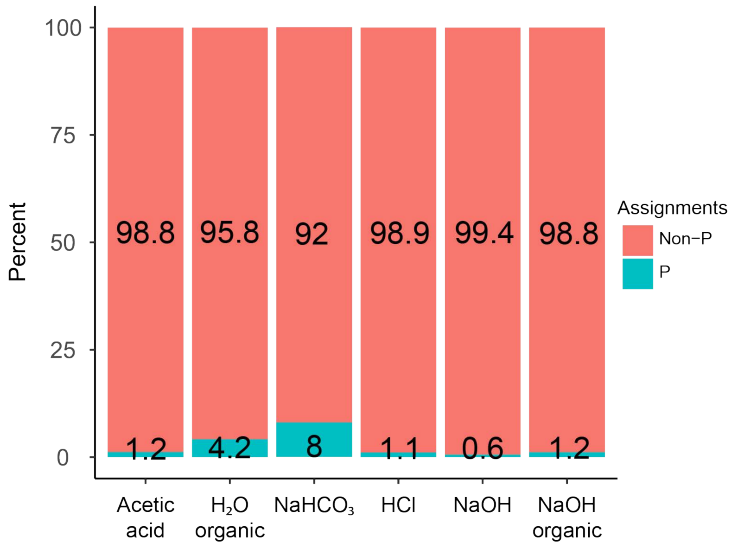

Figure 2.2. Percent composition of assigned P molecules for each extraction relative to the total extracted assignments.

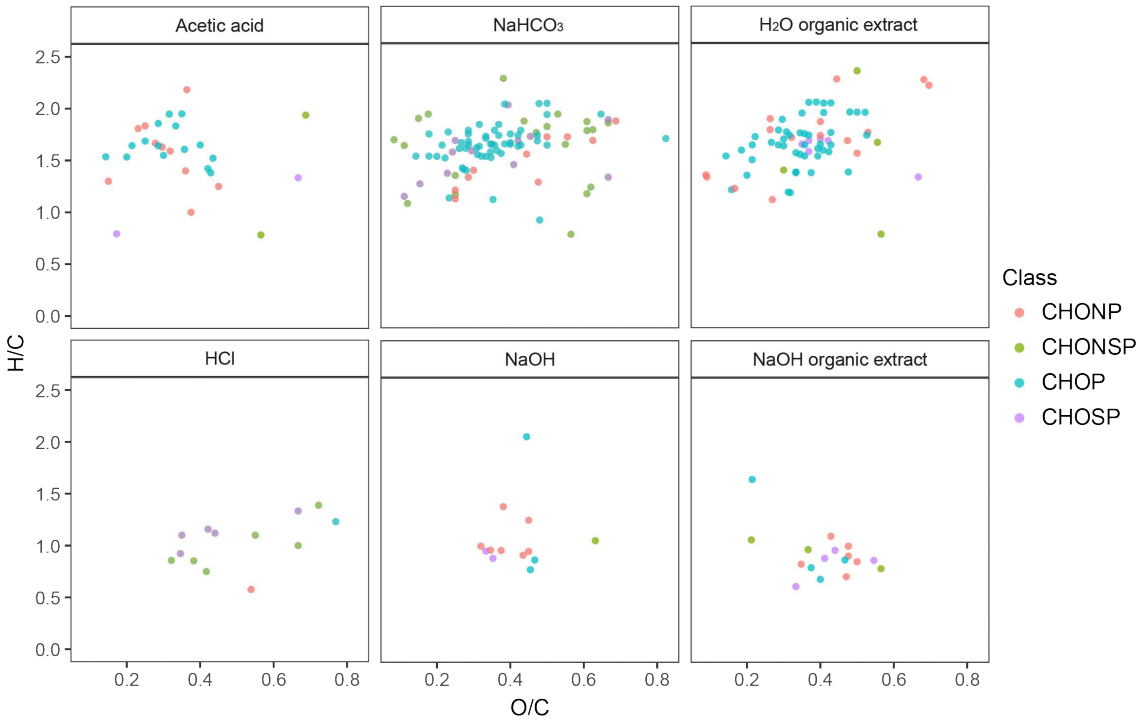

Figure 2.3. Van Krevelen diagrams of P-containing molecules in bulk sediment from Missisquoi Bay extracted with aqueous and organic solvents. Classifications are colored by atomic compositions.

Combined molecular characterization:

The filtered mass lists were grouped into biomolecular classes using the same procedure and modified R code from Rivas-Ubach et al. (2018). Multidimensional stoichiometric compound classification (MSCC) was done as opposed to classification using regions from the van Krevelen diagram to 1) minimize overlap and subjectivity from van Krevelen regions that have not been standardized and 2) to test this approach on complex environmental samples containing mixtures of molecules from many sources. The analysis does not aim to unequivocally identify biomolecules, but rather group molecules into representative classes that share common features with specified biomolecules. Details of classification constraints can be found in Rivas-Ubach et al. (2018). Compounds were grouped into lipid-like, proteins, amino sugars, carbohydrates, oxy-aromatic compounds, and a "not matched" category. Figure 2.4 shows the MSCC results from the sediment extracts. Despite molecular heterogeneity, compound matching was comprehensive with only a small number of molecules that could not be matched, 0.9-2.3%, while Rivas-Ubach et al. (2018) reported 7.5-9.6% molecules as not matched in their biological extracts. Relative percentages of less than 0.5% are omitted from labeling in Figure 2.4. The 3 most significant compound classes were lipid-like, oxy-aromatic compounds, and proteins, with the former two being the most abundant between all extracts. Lipid-like molecules broadly represent the most highly saturated and least oxygenated compounds, while the oxy-aromatic class is more unsaturated and oxygenated, representing molecules similar to lignin and tannin-like compounds. The $NaHCO_3$ and H_2O organic extracts displayed similar compositions with 75.2-77.1% lipid-like molecules, 18.2-20.3% oxy-aromatic compounds, and 2.6-3.4% proteins (Figure

2.4). Whereas HCl, NaOH, and the NaOH organic extracts had greater contributions from oxy-aromatic compounds, far less from the lipid-like, and almost none from proteins (Figure 2.4). In the case of the HCl extract, 94.6% of the total was classified as oxy-aromatics while only 3.8% as lipid-like. The acetic acid extract had a more balanced composition of oxy-aromatics and lipids (43.7% and 50.1%, respectively) and 4.0% from proteins.

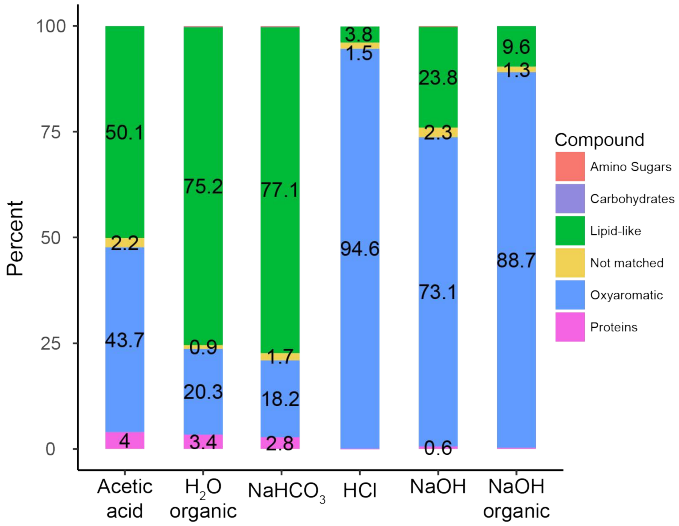

Figure 2.4. Multidimensional stoichiometric compound classification (MSCC) of molecules detected using FT-ICR MS on bulk sediment extractions from Missisquoi Bay. Values are computed percentages relative to the total assigned formulae.

Discussion:

Organic matter selectivity:

Coprecipitation and adsorption of sedimentary OM with Fe(III) minerals in aquatic systems (Lalonde et al., 2012) and with soil clay minerals (Kaiser & Guggenberger, 2000) have been suggested to promote long term carbon storage. While the exact structure of mineral-associated OM is unknown, terrestrial aromatic molecules have been shown to associate with Fe(III) mineral phases in redox-dynamic porewaters

(Riedel et al., 2013), likely being released upon dissolution of Fe-rich sediments, as well as to clays in soils (Kaiser & Guggenberger, 2000; Kaiser & Zech, 2000; Fox et al., 2017). Selective extractions were conducted to explore the chemical properties of this mineral-associated OM pool in Missisquoi Bay lake sediment. Although an implied fractionation is implemented by using PPL columns in the SPE procedure, selecting for more hydrophobic and certain polar compounds (Dittmar et al., 2008; Li et al., 2016), the choice of solvent for sediment extractions selects for compositionally distinct molecular classes (Figure 2.1). It is important to note that these extractions were carried out in parallel and resulting OM represent end-member compositions, while sequential extractions would likely isolate subsets of the total DOM. For instance, the compounds present in the NaOH extractions represent a combination of operationally defined humic and fulvic acids; further acidification of the extract would select for fulvic acids which are partially represented in the HCl extraction. Missisquoi Bay sediment is composed of various Fe oxides and clays, likely resulting in surface adsorption and aggregation of OM to minerals and macromolecules. Treatment of the sediment with alkaline extractants isolated this portion by disrupting mineral and organic aggregates and hydrolyzed the more labile fraction (von Lützow et al., 2007) (Figure 2.1). Diverse OM extracted with NaOH, ranging from aliphatics to aromatics, have been shown to associate with different clay minerals in soil, with many more aliphatics present that could not be extracted with NaOH (Wattel-Koekkoek et al., 2001). Similarly, extractions in HCl dissolves amorphous Fe-bound minerals, but only selects for OM that is soluble in HCl itself (Fox et al., 2017). In contrast, the milder extractants (acetic acid and $NaHCO_3$) preferentially removed the loosely adsorbed or porewater fraction of sediment OM with acetic acid contributing to

some mineral dissolution as evidenced by the high pairwise similarity between the stronger extractants (NaOH and HCl) (Table B-2.1). Generally speaking, the milder aqueous treatments extracted lower molecular weight aliphatic compounds, while stronger extractants targeted larger, more aromatic, molecules (Figure B-2.2, Table B-2.2) possibly representing vascular plant-derived compounds with terrestrial origins (Kellerman et al., 2015). Consistent with these findings, a study of permafrost soil treated with both water and NaOH resulted in mass differences between the two with NaOH yielding a higher mass distribution of compounds (Mann et al., 2015).

The acetic acid and $NaHCO_3$ extracts displayed a great deal of commonality, despite their differences in pH. Both extractants target many saturated, lipid-like molecules with higher H/C ratios and lower DBE values (Figure 2.1A,B) as well as comparable amounts of total sulfur from the sediment (Table 2.1) making them analogous to methanol as an extractant for SOM and SRFA (Tfailey et al., 2015). However, acetic acid extracted far more organic carbon from the sediment (Table 2.1) also demonstrated by over twice as many molecular formulae assignments than $NaHCO_3$ (2,401 and 1,113, respectively). Acetic acid also extracted more oxy-aromatic compounds than $NaHCO_3$ (Figure 2.4) resulting in greater chemical diversity and representing many of the same compounds present in the HCl extraction, likely acid-soluble plant material (Ryan et al., 1990). The diversity of the extracted OM is partially due to acetic acid chelating polyvalent cations associated with OM and dissolving certain mineral phases, thereby releasing previously insoluble OM. The selectivity from both these extractants can be comparable to the selectivity of pyrophosphate, previously used to extract chelated and dispersed Fe phases (Fox et al., 2017; Coward et al., 2018), and the selectivity of

water, whose extracted molecules often represent the labile OM pool in soils (Guigue et al., 2016).

Organic sediment extractions, modified from White et al. (1979) were primarily done to isolate hydrophobic molecules and phospholipids; redissolution in aqueous media was done to isolate the molecules that could be present in both sediment and in water column or porewater DOM. There is overlap of molecules between the NaOH and H_2O organic extracts, but overall, they extract structurally different molecules. H_2O organic extract molecules are mostly saturated with lower O/C and DBE values, while NaOH organic extract molecules have higher O/C, lower H/C, and greater calculated DBE values (Figure 2.1B). Chemically, these molecules are also distinct with H_2O solubilizing more heteroatom-containing compounds and a greater diversity of biomolecules than NaOH from the organic extraction (Figure B-2.1, Figure 2.4). The H_2O organic extract shared more molecules with acetic acid than $NaHCO_3$ (1,103 and 862, respectively) but was closer in heteroatomic composition and biomolecular distribution to $NaHCO_3$, primarily extracting highly saturated molecules (Table B-2.1, Figure 2.1A, Figure 2.4). The combination of methanol and chloroform as an extractant resulted in a range of polarities selecting for various polar and nonpolar compounds that are present upon solvent evaporation. Redissolution with water dissolved more polar and labile molecules, while NaOH likely hydrolyzed some of the labile compounds and released particle and metal-associated macromolecules. This is evidenced by an increase in median mass and almost 4-fold gain of organic carbon content in the NaOH redissolved fraction (Table B-2.1). Although hydrolysis cannot completely explain the absence of the many saturated molecules from the NaOH organic extract, ion suppression from highly acidic carboxylic

functional groups (higher O/C, lower H/C; Figure 2.1A) likely outcompeted the saturated molecules for charge, thus underrepresenting their contribution.

Interestingly, the NaOH organic and HCl extractions selected for similar OM. Both consisted of primarily oxy-aromatic compounds with low chemical diversity and had the highest percentage of shared molecules (35.6%). The organic extract was also similar to the NaOH aqueous extract (1,211 shared molecules) but did not have the same amount of heteroatomic or biomolecular diversity (Figure B-2.4, Figure 2.1A, Figure 2.4). Between HCl, NaOH, and the NaOH organic extract, 855 molecules were shared, but more unique molecules were shared between NaOH aqueous and the organic than the organic extract and HCl (Table B-2.1). The commonality between the three indicates a core of recalcitrant, carboxylic-rich, aromatic molecules that are water-insoluble and only extractable with chemical solvents (Figure B-2.4). The NaOH organic extract still contained 10% of its total assignments that were unique from the other two extractants, meaning the organic treatment targeted a pool of OM unavailable to aqueous solvents. Additionally, out of the three extractions, HCl had the least number of assignments with 84.8% shared between the other two, and the lowest organic carbon content overall (Table 2.1), suggesting HCl represents the most recalcitrant plant-derived molecules (Lützow et al., 2007). Tfailey et al. (2015) obtained similar fractionations of SOM and SRFA using acetonitrile and water as extractants. However, their extractions covered a large range of the van Krevelen diagram while HCl, NaOH, and NaOH organic extracts from this study concentrate molecules from the lignin and tannin-like region with much higher median O/C ratios and lower H/C median ratios. Similarly, Coward et al. (2018) obtained fractionation of many lignin-like molecules associated with Fe minerals using

HCl—hydroxylamine and HCl-dithionite extractions, but also extracted other molecules spanning a wide range of the van Krevelen diagram.

Extraction of organic phosphorus:

Several aqueous solvents were tested to study the selectivity of organic P extractions from lake sediment. Parallel extractions resulted in the identification of various functionally distinct organic P compounds present in the sediment (Figure B-2.3, Figure 2.3). Previously, Cade-Menun and Preston (1996) optimized a high yield extraction procedure for soil total P for ^{31}P NMR after Bowman and Moir (1993) using a one-step NaOH-EDTA extraction. EDTA chelates metal ions such as Fe and Mn that are associated with P, increasing the extraction efficiency. NaOH alone extracted 22-34% of total P from the soil, while the addition of EDTA increased recovery to 71-90% (Cade-Menun & Preston, 1996). This extraction was considered for this study using similar samples from the same site, but the high EDTA concentration in solution resulted in ion suppression and a decrease in detected peaks in the mass spectra (Figure B-2.5). NaOH and HCl sequential extracts of lake sediment have historically been combined and used to determine organic P content (Williams et al., 1976) and also partitioned out to investigate different organic P pools separately (De Groot & Golterman, 1993). Additionally, methods to fractionate organic P from soils using $NaHCO_3$, H_2SO_4/HCl, and NaOH for operationally defined classes have been extensively used and modified (Bowman & Cole, 1978; Ivanoff et al., 1998).

Although the HCl and NaOH extracts result in the highest yield of total P (Table 2.1), they have the lowest assignments of organic P molecules from the FT-ICR MS data

(Figure 2.2). This is likely due to significant contributions from inorganic P phases to the total P pool, variable solubilities of organic P in acidic and alkali phases, and hydrolysis of organic P during extraction (Chang & Jackson, 1957; Bowman & Cole, 1978; Turner et al., 2005). $NaHCO_3$-extractable P from soil is proposed to be labile (Bowman & Cole, 1978; Turner et al., 2005) and in this study, produced the highest proportion of assigned organic P molecules relative to the other extractants. Indeed, D'Andrilli et al. (2015) described the concept of a "Molecular Lability Boundary" (MLB) defining molecules with $H/C \geq 1.5$ as being more labile. In the $NaHCO_3$ extract 78 of the assigned 100 molecules are located above the MLB, in agreement with the definition of labile organic P employed by Bowman and Cole (1978). This extraction mostly affords saturated CHOP molecules that are probably lipid- or protein-like, while HCl and NaOH extractions select for more oxygenated and unsaturated organic P compounds (Figure 2.3). The absence of these saturated molecules and low abundance of organic P assignments could be indicative of hydrolysis or extraction of fundamentally less soluble molecules, such as highly aromatic organic P associated with humic and fulvic acids. Acetic acid also targets saturated organic P molecules, but with a much lower extraction efficiency (Table 2.1), historically used for extracting authigenic apatite, calcite-bound P, and biogenic apatite rather than organic P (Ruttenberg, 1992).

Even after being redissolved from the same chloroform-methanol extraction, organic P from the NaOH and H_2O organic extractions had minimal commonality with each other, sharing only 2 peaks. The NaOH organic extraction shared similar van Krevelen compositional space with HCl and NaOH extracts, while the H_2O extract occupied saturated space common with $NaHCO_3$ and acetic acid extracts (Figure 2.3).

Although phosphate group hydrolysis can be a significant degradation pathway in alkali media (Golterman, 1988; Turner et al., 2003; Turner et al., 2005) and likely contributes to differences in organic P molecular distributions between the samples, the greatest distribution differences are due to solubility. Minimal van Krevelen overlap and large shifts in calculated AI/DBE values indicate structurally different organic P molecules are solubilized from the organic extract depending on aqueous solvent, similarly to the non-P containing molecules. Organic P bound from the stronger extractants is likely associated with larger macromolecular aggregates that are broken apart during electrospray ionization (Llewelyn et al., 2002). In the case of the HCl and NaOH extracts selecting for more acidic functional groups, charge competition between carboxyl and phosphate groups would be even greater and result in less ionization of organic P. Differences in organic P composition from each extraction reveal the chemical diversity and complexity within the sediments, which is in agreement with the findings of Giles et al. (2015) who provided evidence for both terrestrial and algal derived organic P in Missisquoi Bay sediment. Furthermore, these results confirm their observations of bio-labile organic P depletion during summer bloom months and retention of refractory compounds post bloom, as evidenced by the coexistence of both types of molecular signatures in the late summer sediment from this study (Figure 2.3). The surface (0-1 cm) has been suggested as the most redox-active portion of the lake sediment mobilizing large amounts of bio-labile P, whereas recalcitrant compounds accumulate at depth (Smith et al., 2009, Giles et al., 2015); however, further work is required to identify the spatial distribution of these extracted organic P compounds and how they partition based on their chemical properties.

Recommendations and limitations:

When considering the non-P pool of OM, the acetic acid extract spanned the most inclusive van Krevelen space (Figure 2.1A), resulted in the most molecular assignments, had the highest proportion of extractable N and S-containing compounds (Figure B-2.1), and the greatest chemical diversity of biomolecules (Figure 2.4). Acetic acid also had the highest mean pairwise similarity with all other extractants (905 assignments). From a purely qualitative perspective, $NaHCO_3$ extracted the most assigned organic P molecules out of all the extractants and resulted in the third highest total P yield (Table 2.1). The extracted P molecules are mostly labile and consist of saturated compounds, probably protein or lipid-like (Figure 2.3). Therefore, it is recommended that 1.0 M acetic acid be used to extract OM from sediment as a basis for comparisons, whereas other extractants can be used to selectively target specific classes, such as $NaHCO_3$ for organic P. From a purely quantitative perspective, NaOH extracted the highest concentrations of organic carbon and total sulfur with the second most formulae assignments (Table 2.1), meaning it should be considered for bulk extractions when sediment geochemistry is of interest. Although all these targeted extraction protocols hold great potential for sediment and soil characterizations, the fractionation of OM is inherently biased due to desalting with the SPE procedure, and charge competition in negative electrospray ionization (Sleighter & Hatcher, 2007). Different procedures for desalting with SPE and ionization modes should be considered to ensure these fractionations are chemically inherent and not a result of sample preparation. Also, comparisons for this study are limited due to similar published FT-ICR MS studies focusing on soil samples rather than lake sediments, which may explain many differences in OM lability and distributions. Future studies using similar

targeted extractions across a range of lake sediments and soil-stream-lake continua could be valuable in determining the lability and recalcitrance of OM as it is transported from soil to lacustrine sediment, specifically organic P classes.

References:

Aitkenhead-Peterson, J. A., McDowell, W. H., & Neff, J. C. (2003). Sources, production, and regulation of allochthonous dissolved organic matter inputs to surface waters. In *Aquatic Ecosystems* (pp. 25-70). Academic Press.

Bai, X. L., Zhou, Y. K., Sun, J. H., Ma, J. H., Zhao, H. Y., & Liu, X. F. (2015). Classes of dissolved and particulate phosphorus compounds and their spatial distributions in the water of a eutrophic lake: a ^{31} P NMR study. *Biogeochemistry*, *126*(1-2), 227-240.

Bowman, R. A., & Cole, C. V. (1978). An exploratory method for fractionation of organic phosphorus from grassland soils. *Soil Science*, *125*(2), 95-101.

Bowman, R. A., & Moir, J. O. (1993). Basic EDTA as an extractant for soil organic phosphorus. *Soil Science Society of America Journal*, *57*(6), 1516-1518.

Brooker, M. R., Longnecker, K., Kujawinski, E. B., Evert, M., & Mouser, P. J. (2018). Discrete Organic Phosphorus Signatures are Evident in Pollutant Sources within a Lake Erie Tributary. *Environmental science & technology*, *52*(12), 6771-6779.

Burgess, H. (2007). *Geochemical indicators of productivity change in Lake Champlain, USA-Canada*. (Graduate College Dissertations and Theses). Retrieved from https://scholarworks.uvm.edu

Cade-Menun, B. J., & Preston, C. M. (1996). A comparison of soil extraction procedures for ^{31}P NMR spectroscopy. *Soil Science*, *161*(11), 770-785.

Cade-Menun, B. J., Elkin, K. R., Liu, C. W., Bryant, R. B., Kleinman, P. J., & Moore, P. A. (2018). Characterizing the phosphorus forms extracted from soil by the Mehlich III soil test. *Geochemical transactions*, *19*(1), 7.

Cade-Menun, B. J., Liu, C. W., Nunlist, R., & McColl, J. G. (2002). Soil and litter phosphorus-31 nuclear magnetic resonance spectroscopy. *Journal of Environmental Quality*, *31*(2), 457-465.

Chang, S.C., and M.L Jackson. (1957). Fractionation of soil phosphorus. *Soil Science*, *84*, 133-144.

Cooper, W. T., Llewelyn, J. M., Bennett, G. L., Stenson, A. C., & Salters, V. J. (2005). Organic phosphorus speciation in natural waters by mass spectrometry. In *Organic phosphorus in the environment* (pp. 45-74). Wallingford, UK: CABI Publishing.

Coward, E. K., Ohno, T., & Plante, A. F. (2018). Adsorption and Molecular Fractionation of Dissolved Organic Matter on Iron-Bearing Mineral Matrices of Varying Crystallinity. *Environmental science & technology*, *52*(3), 1036-1044.

D'Andrilli, J., Cooper, W. T., Foreman, C. M., & Marshall, A. G. (2015). An ultrahigh-resolution mass spectrometry index to estimate natural organic matter lability. *Rapid Communications in Mass Spectrometry*, *29*(24), 2385-2401.

Dadi, T., Harir, M., Hertkorn, N., Koschorreck, M., Schmitt-Kopplin, P., & Herzsprung, P. (2017). Redox Conditions Affect Dissolved Organic Carbon Quality in Stratified Freshwaters. *Environmental science & technology*, *51*(23), 13705-13713.

De Groot, C. J., & Golterman, H. L. (1993). On the presence of organic phosphate in some Camargue sediments: evidence for the importance of phytate. *Hydrobiologia*, *252*(1), 117-126.

Dittmar, T., & Stubbins, A. (2014). 12.6 - Dissolved organic matter in aquatic systems. In *Treatise on Geochemistry, 2nd edn* (pp. 125-156). Oxford, UK: Elsevier Science.

Dittmar, T., Koch, B., Hertkorn, N., & Kattner, G. (2008). A simple and efficient method for the solid-phase extraction of dissolved organic matter (SPE-DOM) from seawater. *Limnology and Oceanography: Methods*, *6*(6), 230-235.

El-Rifai, H., Heerboth, M., Gedris, T. E., Newman, S., Orem, W., & Cooper, W. T. (2008). NMR and mass spectrometry of phosphorus in wetlands. *European journal of soil science*, *59*(3), 517-525.

Fox, P. M., Nico, P. S., Tfaily, M. M., Heckman, K., & Davis, J. A. (2017). Characterization of natural organic matter in low-carbon sediments: Extraction and analytical approaches. *Organic Geochemistry*, *114*, 12-22.

Galindo, C., & Del Nero, M. (2014). Molecular level description of the sorptive fractionation of a fulvic acid on aluminum oxide using electrospray ionization Fourier transform mass spectrometry. *Environmental science & technology*, *48*(13), 7401-7408.

Giles, C. D., Lee, L. G., Cade-Menun, B. J., Hill, J. E., Isles, P. D., Schroth, A. W., & Druschel, G. K. (2015). Characterization of organic phosphorus form and bioavailability in lake sediments using ^{31}P nuclear magnetic resonance and enzymatic hydrolysis. *Journal of environmental quality*, *44*(3), 882-894.

Golterman, H. L. (1998). The distribution of phosphate over iron-bound and calcium-bound phosphate in stratified sediments. *Hydrobiologia*, *364*(1), 75-81.

Gonsior, M., Valle, J., Schmitt-Kopplin, P., Hertkorn, N., Bastviken, D., Luek, J., Harir, M., Bastos, W., & Enrich Prast, A. (2016). Chemodiversity of dissolved organic matter in the Amazon Basin. *Biogeosciences*, *13*(14), 4279-4290.

Guigue, J., Harir, M., Mathieu, O., Lucio, M., Ranjard, L., Lévêque, J., & Schmitt-Kopplin, P. (2016). Ultrahigh-resolution FT-ICR mass spectrometry for molecular characterisation of pressurised hot water-extractable organic matter in soils. *Biogeochemistry*, *128*(3), 307-326.

Hawkesd, G. E., Powlson, D. S., Randall, E. W., & Tate, K. R. (1984). A ^{31}P nuclear magnetic resonance study of the phosphorus species in alkali extracts of soils from long-term field experiments. *Journal of Soil Science*, *35*(1), 35-45.

Hertkorn, N., Ruecker, C., Meringer, M., Gugisch, R., Frommberger, M., Perdue, E. M., ... & Schmitt-Kopplin, P. (2007). High-precision frequency measurements: indispensable tools at the core of the molecular-level analysis of complex systems. *Analytical and bioanalytical chemistry*, *389*(5), 1311-1327.

Hertkorn, N., Harir, M., Koch, B., Michalke, B., & Schmitt-Kopplin, P. (2013). High-field NMR spectroscopy and FTICR mass spectrometry: powerful discovery tools for the molecular level characterization of marine dissolved organic matter. *Biogeosciences*, *10*, 1583-1624.

Hertkorn, N., Harir, M., Cawley, K. M., Schmitt-Kopplin, P., & Jaffé, R. (2015). Molecular characterization of dissolved organic matter from subtropical wetlands: a comparative study through the analysis of optical properties, NMR and FTICR/MS. *Biogeosciences Discussions*, *12*(16).

Herzsprung, P., von Tümpling, W., Wendt-Potthoff, K., Hertkorn, N., Harir, M., Schmitt-Kopplin, P., & Friese, K. (2017). High field FT-ICR mass spectrometry data sets enlighten qualitative DOM alteration in lake sediment porewater profiles. *Organic Geochemistry*, *108*, 51-60.

Isles, P. D., Giles, C. D., Gearhart, T. A., Xu, Y., Druschel, G. K., & Schroth, A. W. (2015). Dynamic internal drivers of a historically severe cyanobacteria bloom in Lake Champlain revealed through comprehensive monitoring. *Journal of Great Lakes Research*, *41*(3), 818-829.

Isles, P. D., Rizzo, D. M., Xu, Y., & Schroth, A. W. (2017a). Modeling the drivers of interannual variability in cyanobacterial bloom severity using self-organizing maps and high-frequency data. *Inland Waters*, *7*(3), 333-347.

Isles, P. D., Xu, Y., Stockwell, J. D., & Schroth, A. W. (2017b). Climate-driven changes in energy and mass inputs systematically alter nutrient concentration and stoichiometry in deep and shallow regions of Lake Champlain. *Biogeochemistry*, *133*(2), 201-217.

Ivanoff, D. B., Reddy, K. R., & Robinson, S. (1998). Chemical fractionation of organic phosphorus in selected Histosols[1]. *Soil Science*, *163*(1), 36-45.

Kaiser, K., & Guggenberger, G. (2000). The role of DOM sorption to mineral surfaces in the preservation of organic matter in soils. *Organic geochemistry*, *31*(7-8), 711-725.

Kaiser, K., & Zech, W. (2000). Dissolved organic matter sorption by mineral constituents of subsoil clay fractions. *Journal of Plant Nutrition and Soil Science*, *163*(5), 531-535.

Kellerman, A. M., Kothawala, D. N., Dittmar, T., & Tranvik, L. J. (2015). Persistence of dissolved organic matter in lakes related to its molecular characteristics. *Nature Geoscience*, *8*(6), 454.

Kemp, A. L. W., & Johnston, L. M. (1979). Diagenesis of organic matter in the sediments of Lakes Ontario, Erie, and Huron. *Journal of Great Lakes Research*, *5*(1), 1-10.

Koch, B. P., & Dittmar, T. (2006). From mass to structure: An aromaticity index for high-resolution mass data of natural organic matter. *Rapid communications in mass spectrometry*, *20*(5), 926-932.

Kritzberg, E. S., Cole, J. J., Pace, M. M., & Granéli, W. (2005). Does autochthonous primary production drive variability in bacterial metabolism and growth efficiency in lakes dominated by terrestrial C inputs?. *Aquatic Microbial Ecology*, *38*(2), 103-111.

Lalonde, K., Mucci, A., Ouellet, A., & Gélinas, Y. (2012). Preservation of organic matter in sediments promoted by iron. *Nature*, *483*(7388), 198.

Larsson, J. (2018). *eulerr: Area-Proportional Euler and Venn Diagrams with Ellipses*. R package version 4.1.0, https://cran.r-project.org/package=eulerr.

Levine, S. N., Lini, A., Ostrofsky, M. L., Bunting, L., Burgess, H., Leavitt, P. R., ... & Gilles, E. (2012). The eutrophication of Lake Champlain's northeastern arm: Insights from paleolimnological analyses. *Journal of Great Lakes Research*, *38*, 35-48.

Li, W., Joshi, S. R., Hou, G., Burdige, D. J., Sparks, D. L., & Jaisi, D. P. (2014). Characterizing phosphorus speciation of Chesapeake Bay sediments using

chemical extraction, ^{31}P NMR, and X-ray absorption fine structure spectroscopy. *Environmental science & technology*, *49*(1), 203-211.

Li, Y., Harir, M., Lucio, M., Kanawati, B., Smirnov, K., Flerus, R., ... & Hertkorn, N. (2016). Proposed guidelines for solid phase extraction of Suwannee River dissolved organic matter. *Analytical chemistry*, *88*(13), 6680-6688.

Llewelyn, J. M., Landing, W. M., Marshall, A. G., & Cooper, W. T. (2002). Electrospray ionization Fourier transform ion cyclotron resonance mass spectrometry of dissolved organic phosphorus species in a treatment wetland after selective isolation and concentration. *Analytical chemistry*, *74*(3), 600-606.

Magid, J., Tiessen, H., & Condron, L. M. (1996). Dynamics of organic phosphorus in soils under natural and agricultural ecosystems. In *Humic substances in terrestrial ecosystems* (pp. 429-466). Elsevier Sciene.

Mann, B. F., Chen, H., Herndon, E. M., Chu, R. K., Tolic, N., Portier, E. F., ... & Graham, D. E. (2015). Indexing permafrost soil organic matter degradation using high-resolution mass spectrometry. *PloS one*, *10*(6), e0130557.

Meyers, P. A., & Ishiwatari, R. (1993). Lacustrine organic geochemistry—an overview of indicators of organic matter sources and diagenesis in lake sediments. *Organic geochemistry*, *20*(7), 867-900.

Mitchell, A. M., & Baldwin, D. S. (2005). Organic phosphorus in the aquatic environment: Speciation, transformations and interactions with nutrient cycles. In *Organic phosphorus in the environment* (pp. 309-324). Wallingford, UK: CABI Publishing.

Perdue, E. M., & Ritchie, J. D. (2014). 7.8 - Dissolved organic matter in freshwaters. In *Treatise on Geochemistry, 2nd edn* (pp. 237-272). Oxford, UK: Elsevier Science.

Riedel, T., Zak, D., Biester, H., & Dittmar, T. (2013). Iron traps terrestrially derived dissolved organic matter at redox interfaces. *Proceedings of the National Academy of Sciences*, *110*(25), 10101-10105.

Rivas-Ubach, A., Liu, Y., Bianchi, T. S., Tolić, N., Jansson, C., & Paša-Tolić, L. (2018). Moving beyond the van Krevelen Diagram: A New Stoichiometric Approach for Compound Classification in Organisms. *Analytical chemistry*, *90*(10), 6152-6160.

Ruttenberg, K. C. (1992). Development of a sequential extraction method for different forms of phosphorus in marine sediments. *Limnology and oceanography*, *37*(7), 1460-1482.

Ryan, M. G., Melillo, J. M., & Ricca, A. (1990). A comparison of methods for determining proximate carbon fractions of forest litter. *Canadian Journal of Forest Research*, *20*(2), 166-171.

Schroth, A. W., Giles, C. D., Isles, P. D., Xu, Y., Perzan, Z., & Druschel, G. K. (2015). Dynamic coupling of iron, manganese, and phosphorus behavior in water and sediment of shallow ice-covered eutrophic lakes. *Environmental science & technology*, *49*(16), 9758-9767.

Serediak N.A., Prepas E.E., Putz G.J. (2014). 11.8 - Eutrophication of freshwater systems. In *Treatise on Geochemistry, 2nd edn* (pp. 305-323). Oxford, UK: Elsevier Science.

Sleighter, R. L., & Hatcher, P. G. (2007). The application of electrospray ionization coupled to ultrahigh resolution mass spectrometry for the molecular characterization of natural organic matter. *Journal of Mass Spectrometry*, *42*(5), 559-574.

Smith, L. (2009). *Missisquoi Bay sediment phosphorus cycling: the role of organic phosphorus and seasonal redox fluctuations.* (Graduate College Dissertations and Theses). Retrieved from https://scholarworks.uvm.edu

Smith, L., Watzin, M. C., & Druschel, G. (2011). Relating sediment phosphorus mobility to seasonal and diel redox fluctuations at the sediment–water interface in a eutrophic freshwater lake. *Limnology and Oceanography*, *56*(6), 2251-2264.

Søndergaard, M., Jensen, J. P., & Jeppesen, E. (2003). Role of sediment and internal loading of phosphorus in shallow lakes. *Hydrobiologia*, *506*(1-3), 135-145.

Sparling, G., Vojvodić-Vuković, M., & Schipper, L. A. (1998). Hot-water-soluble C as a simple measure of labile soil organic matter: the relationship with microbial biomass C. *Soil Biology and Biochemistry*, *30*(10-11), 1469-1472.

Schlesinger, W. H., & Bernhardt E. S. (2013). The Biosphere: The Carbon Cycle of Terrestrial Ecosystems. In *Biogeochemistry: An Analysis of Global Change, 3rd edn* (pp. 135-170). Academic Press.

Tfaily, M. M., Chu, R. K., Tolić, N., Roscioli, K. M., Anderton, C. R., Paša-Tolić, L., ... & Hess, N. J. (2015). Advanced solvent based methods for molecular characterization of soil organic matter by high-resolution mass spectrometry. *Analytical chemistry*, *87*(10), 5206-5215.

Turner, B. L., Cade-Menun, B. J., Condron, L. M., & Newman, S. (2005). Extraction of soil organic phosphorus. *Talanta*, *66*(2), 294-306.

Turner, B. L., Driessen, J. P., Haygarth, P. M., & Mckelvie, I. D. (2003). Potential contribution of lysed bacterial cells to phosphorus solubilisation in two rewetted Australian pasture soils. *Soil Biology and Biochemistry*, *35*(1), 187-189.

Valle, J., Gonsior, M., Harir, M., Enrich-Prast, A., Schmitt-Kopplin, P., Bastviken, D., Conrad, R., & Hertkorn, N. (2018). Extensive processing of sediment pore water dissolved organic matter during anoxic incubation as observed by high-field mass spectrometry (FTICR-MS). *Water research*, *129*, 252-263.

von Lützow, M., Kögel-Knabner, I., Ekschmitt, K., Flessa, H., Guggenberger, G., Matzner, E., & Marschner, B. (2007). SOM fractionation methods: relevance to functional pools and to stabilization mechanisms. *Soil Biology and Biochemistry*, *39*(9), 2183-2207.

Wattel-Koekkoek, E. J. W., Van Genuchten, P. P. L., Buurman, P., & Van Lagen, B. (2001). Amount and composition of clay-associated soil organic matter in a range of kaolinitic and smectitic soils. *Geoderma*, *99*(1-2), 27-49.

Wickham, H. (2016). *ggplot2: elegant graphics for data analysis*. Springer.

White, D. C., Davis, W. M., Nickels, J. S., King, J. D., & Bobbie, R. J. (1979). Determination of the sedimentary microbial biomass by extractible lipid phosphate. *Oecologia*, *40*(1), 51-62.

Williams, J. D. H., Jaquet, J. M., & Thomas, R. L. (1976). Forms of phosphorus in the surficial sediments of Lake Erie. *Journal of the Fisheries Board of Canada*, *33*(3), 413-429.

Chapter 3 - Seasonal processing of dissolved organic matter and organic phosphorus in a polymictic basin: implications for redox-driven eutrophication

Introduction:

Freshwater eutrophication is characterized by ecological trophic shifts from excess nutrient concentrations, namely nitrogen (N) and phosphorus (P), ultimately resulting in polluted terrestrial ecosystems and restriction of water resources (Smith et al., 1999). Aquatic primary producers readily consume surplus nutrients promoting unrestricted growth of phytoplankton and allowing for resilient cyanobacteria to outcompete the algal communities, forming extensive blooms of aggregated biomass (Mur et al., 1999). Development of these blooms has resulted in adverse consequences for aquatic and human health including reduction of water clarity, fish kills, and production of both unpleasant taste and odor compounds as well as harmful toxins (Paerl & Otten, 2013); expecting to increase globally due to temperature and hydrological effects promoted by climate change (O'Neil et al., 2012; Nazari-Sharabian et al., 2018). Anthropogenic nutrient pollution from point and non-point sources transports bioavailable P species into freshwaters which can be utilized by cyanobacteria to promote and sustain these bloom conditions (Paerl & Otten, 2013), particularly from inorganic orthophosphate (PO_4^{3-}). Additionally, dissolved organic P (DOP) originates from both allochthonous (terrestrial) and autochthonous (aquatic) sources serving as a potential pool of bioavailable P that can be mineralized largely by extracellular microbial enzymes and some abiotic processes (Baldwin et al., 2005). The breakdown of DOP produces both orthophosphate and dissolved organic matter (DOM) which are diffused into the water column, assimilated into biomass, or deposited with lake sediment. Freshwater DOM

consists of complex mixtures of organic molecules with various functional groups and like DOP, can be both terrestrial and aquatic, each producing unique chemical signatures (Dittmar & Stubbins, 2014). DOM is also an integral part of energy transfer in aquatic systems, representing a large portion of reactive carbon and having implications for the global transformation of organic carbon to CO_2 (Tranvik et al., 2009) as well as degradation processes that sequester refractory compounds in the sediment (Valle et al., 2018). As aquatic DOM is supplied by primary producers and consumed by microorganisms to meet energy demands, DOP is also produced and metabolized to fulfill various biological requirements. Therefore, in the context of eutrophication, the exchanges of phosphate groups between DOM and DOP link the aquatic C and P cycles together.

Internal loading is a means by which P species, both inorganic and organic, are released from the sediment into the water column and have been shown to drive eutrophic conditions in shallow freshwaters globally (Reynolds & Davies, 2001; Søndergaard et al., 2003; Li et al., 2015). Aquatic conditions beneath a cyanobacterial bloom can become anoxic resulting in dissolved oxygen depletion near the surface of the sediment (Rozan et al., 2002; Smith et al., 2011; Giles et al., 2016). Nutrient release under benthic anoxic conditions is driven by the activity of anaerobic microbial communities that couple the metabolic oxidation of organic matter to the reduction of Fe(III) and Mn(IV) (Lovley, 1991). In these lakes, available Fe(III) and Mn(IV) originate from poorly-crystalline (oxy)hydroxides with high adsorptive capacities for phosphate groups (Wang et al., 2013), and highly oxygenated DOM functional groups (Chassé & Ohno, 2016). Thus, the reductive dissolution of these minerals promotes the benthic desorption and release of P

species and DOM, fueling primary productivity in a positive feedback cycle where blooms are sustained from liberated nutrients and produce further anoxic conditions. (Søndergaard et al., 2003). The cycle breaks with the eventual bloom collapse from water column mixing or temperature changes (Paerl & Otten, 2013) restoring dissolved oxygen as the terminal electron acceptor in the bottom water, causing precipitation of Fe and Mn (oxy)hydroxides, and readsorption of P species and DOM (Reynolds & Davies, 2001; Smith et al., 2011), thereby recharging the sediment with nutrients.

Missisquoi Bay is a shallow, freshwater bay in Lake Champlain that experiences seasonal eutrophication driven by a similar internal loading mechanism (Smith et al., 2011). Cyanobacterial blooms occur during the summer months and become less frequent as the temperature decreases through fall. In winter the bay freezes over and creates a stratified water column with suboxic to hypoxic conditions in the bottom (Joung et al., 2017). Snowmelt in the spring discharges P, Fe, and organic C into the bay from its mostly agricultural watershed that supply the initial excess nutrients for cyanobacterial blooms to develop when water temperatures are sufficiently warm (Isles et al., 2017; Rosenberg & Schroth, 2017). The bay has been the target of several geochemical studies, including the use of long-term monitoring stations, resulting in abundant data regarding nutrient mobility and bioavailability (e.g. Smith et al., 2011; Giles et al., 2015; Schroth et al., 2015; Giles et al., 2016; Isles et al., 2017; Joung et al., 2017; Rosenberg & Schroth, 2017); however, the contributions of DOM and DOP to internal loading have not been addressed in detail.

Fourier transform-ion cyclotron mass spectrometry (FT-ICR MS) has been used extensively to characterize DOM in a multitude of freshwater lakes and rivers (e.g. Zhang

et al., 2014; Wagner et al., 2015; Gonsior et al., 2016) as well as incubated experiments (e.g. Dadi et al., 2017; Mostovaya et al., 2017; Valle et al., 2018). Historically, this method has not been applied to DOP analysis, in part due to the poor ionization efficiency of phosphate groups in electrospray and low natural abundance of P in natural waters (Cooper et al., 2005). In aquatic systems with elevated nutrient concentrations, FT-ICR MS has demonstrated its utility for describing the distribution of organic P molecular classes (Llewelyn et al., 2002; Brooker et al., 2018) and may become more widely used as resolution increases and tandem MS/MS techniques become more accessible. Although FT-ICR MS spectra provide an ultrahigh-resolution description of complex mixtures, they still lack the ability necessary for reliable quantification and detailed structural information (Hertkorn et al., 2007). Such structure-specific resolution for DOP would require coupling FT-ICR MS analysis with chromatographic separation techniques (Brabandere et al., 2008) and/or ^{31}P NMR spectroscopy (Cade-Menun, 2005). However, non-targeted FT-ICR MS data used in conjunction with manual SONDE sensor and electrochemical analyses, as employed in this study, can provide reliable information describing the seasonal and spatial distribution of different DOM pools, including organic P. The objectives of this study were: 1) to investigate the seasonal and spatial dynamics of DOM and DOP within Missisquoi Bay and 2) to compare between allochthonous and autochthonous contributions as well as short-term evolutions during changing redox conditions to the DOM pool. By answering these questions, we seek to gain a greater understanding of the over-arching cycling between the bioavailability of carbon, phosphorus, and iron driving eutrophication in freshwater lakes.

Methods:

Site description:

Missisquoi Bay is a shallow, eutrophic basin of Lake Champlain that shares a border with Vermont and Quebec. The bay experiences toxic cyanobacterial blooms in the late summer months due to internal nutrient loading and externally from its mostly agricultural watershed. The lake usually freezes completely during December with periodic thawing events throughout the winter until April when it melts entirely. The watershed of the bay is mostly forested (70%) with agricultural (25%) and urban (5%) inputs spanning a total of 3,100 km^2 (Joung et al., 2017). Nutrient loading is primarily supplied by three river systems: the Missisquoi, Pike, and Rock River from agricultural runoff.

Field sampling:

Water samples from Missisquoi Bay were collected into acid-washed plastic bottles during three different seasons throughout the water column using a peristaltic pump. Additionally, manual YSI SONDE cast data from the water column was collected for each sampling event. On May 17, 2017 the total depth of the bay was recorded at 4.1 m and water samples were taken at the surface (top), 2.0 m (middle), and 3.2 m (bottom). On September 11, 2017 the total depth was 3.5 m with samples collected at the surface (top), 1.0 m, 2.0 m (middle), 3.0 m, and 3.1 m (bottom). Surface water from the Missisquoi River was sampled on September 13, 2017 at the USGS gage station in Swanton, VT. On January 10, 2018 total water column depth was 3.3 m and sampled beneath ice cover at the surface (top), 2.0 m (middle), and 3.1 m (bottom). Sediment

cores for mesocosms were collected on the same days as water sampling was conducted. The cores were obtained using a gravity coring device into acrylic tubes (6.7 cm diameter) and transported to the laboratory on ice. Water samples were transported on ice, kept in the dark, and vacuum filtered through a 0.2 μm GF/F filter, that was precombusted at 450 °C for 5 hours, for solid phase extraction and FTICR-MS analysis. Water from September and January were collected employing trace metal techniques with Mn and Fe characterized as total dissolved (< 0.45 μm), truly dissolved (< 0.02 μm), and colloidal (total dissolved minus truly dissolved) and quantified using inductively coupled plasma mass spectrometry using methodology from Schroth et al. (2015).

Solid phase extractions:

Solid phase extraction (SPE) procedures were adapted from Dittmar et al. (2008). Samples were concentrated and desalted immediately after filtration through 0.2 μm GF/F filters to minimize hydrolysis and sample alterations. Filtered water samples (0.5 – 1.0 L) were then acidified to pH 2 with dropwise addition of HCl and extracted through an Agilent Bond Elut PPL column under air pressure. Columns were previously activated with 3 mL of methanol and washed with acidified water at pH 2. After extraction, columns were rinsed with acidified water at pH 2 and stored at -20 °C until analysis. The columns were then eluted with 5 mL of methanol and diluted accordingly for FT-ICR MS analysis. An axenic culture of *Synechocystis* sp. (15 mL, wild type) was also extracted using the same SPE procedure as the water samples to afford the extracellular organic matter (OM) associated with the cyanobacteria.

Fourier transform-ion cyclotron mass spectrometry:

Methanolic extracts were analyzed using a Bruker Solarix 12 Tesla (Bruker Daltonics, Bremen, Germany) Fourier Transform-Ion Cyclotron Resonance Mass Spectrometer (FT-ICR MS) with electrospray ionization in negative and positive mode. The concentrations of the samples were prepared in methanol using a microliter pump at a flow rate of 120 μL h^{-1} with a nebulizer gas pressure of 138 kPa and a drying gas pressure of 103 kPa. A source heater temperature of 200 °C was kept ensuring rapid desolvation of the ionized droplets. The spectra were zero filled to a processing size of 4 megawords in ESI(−) and ESI(+), and 500 scans were accumulated for each mass spectrum. All spectra were internally calibrated using an appropriate reference mass list to obtain a mass accuracy of less than 0.2 ppm. Data processing was conducted using Compass Data Analysis 4.0 (Bruker, Bremen, Germany) and formula assignment was processed by in-house software. The exact masses of the compounds were defined (FT-ICR MS), and their molecular composition was batch calculated by a software tool, written in-house (mass error: 0.2 ppm). The generated formulas were validated by setting sensible chemical constraints (N rule, oxygen-to-carbon (O/C) ratio ≤ 1, hydrogen-to-carbon (H/C) ratio ≤ 2n+2(C_nH_{2n+2}), element counts: C≤80, H unlimited, O≤60, N≤5, S≤1, P≤2) in conjunction with an automated theoretical isotope pattern comparison. Formulae with heteroatomic assignments in the range of N_{0-5}, S_{0-1}, and P_{0-2} were considered only if they had a corresponding ^{13}C peak and ion peaks with multiple assigned formulae were discarded.

Final molecular formula assignments were binned into groups containing CHO(P), CHON(P), CHOS(P) and CHONS(P) molecular compositions, which were used

to reconstruct the group-selective mass spectra. Chemical properties including aromaticity index (AI) and double bond equivalence (DBE)) were calculated according to Koch and Dittmar (2007) and average carbon oxidation state (CHO index) according to Mann et al. (2015). Molecular classes were also subject to CH_2 and HPO_3-based Kendrick mass defect (KMD) analysis for identification of homologous series that differ in structure by just one functional unit (CH_2 or HPO_3 group) (Hughey et al., 2001). Post processing and statistical analysis of the filtered mass lists were conducted using Microsoft Excel and R with the ggplot2 (Wickham, 2016), plotly (Sievert, 2018), vegan (Oksanen et al., 2019), and eulerr (Larsson, 2018) packages.

Transformed relative intensity index:

We developed a new semi-quantitative approach for the classification of molecular groups based on m/z peak intensities. The peak intensity and molecular class information for each assigned formula were combined to describe the contribution each molecular class has on the overall mass spectrum, since raw intensities alone may reflect ionization bias. This quantity is referred to as the transformed relative intensity index (TRII) and is conceptually similar to a pH scale, where differences of integer units represent changes in orders of magnitude. The computation begins by determining the relative intensity (R) of each formula in the sample, or the formula intensity divided by the total intensity of all assigned formulae. Next, categories are defined such as the molecular class by atomic composition (e.g. CHO, CHON, etc.) and the relative intensity of each formula within each category is summed and divided by the total number of

formula assignments for a given sample. This value is the relative intensity index (RII) and can be transformed using equation 3.1 to yield the TRII.

Equation 3.1 $$TRII = 100/-\log (RII)$$

The TRII typically describes a scale from 0 to 14 that allows for direct comparison of compounds between samples in the same ionization mode. However, unlike a pH scale, differences between integer TRII values do not correspond to linear differences between RII values. For instance, the lowest non-zero TRII integer for the Missisquoi Bay water column is 6 while the highest is 13 corresponding to RII values of 2.15e-17 and 2.03e-8, respectively.

Sediment core incubations:

Cores collected in May and September were reduced by bubbling nitrogen gas into the surface water for one week (3 days for the January core) while they were kept cool in a cold-water bath (5 °C) and obscured from light using aluminum foil sheets. An additional core from September had the surface water bubbled with air from an aquarium pump for one week while maintaining the same cold temperature (5 °C) but without light occlusion. The degree of reduction and oxidation for the cores was determined by detection of dissolved Mn(II) and Fe(II) at or above the sediment-water interface (SWI) using *in situ* cyclic voltammetry. Briefly, gold amalgam microelectrodes were constructed and polished according to the procedure from Brendel and Luther (1995) and used as the working electrodes. Cyclic voltammetry was conducted using a model DLK-

70 potentiostat (Analytical Instrument Systems, Inc.), an Ag/AgCl reference electrode, and a platinum wire counter electrode. The scan rate was 1000 mV/s over the potential range -0.1 V to -1.8 V with a 2 s deposition time. Ten scans were collected at each depth within the core and the resulting voltammograms were processed using in-house developed software. After analysis, 500 mL of the water was siphoned off and filtered through a precombusted 0.2 μm GF/F filter for solid phase extraction and FT-ICR MS analysis.

Evaluating organic phosphorus retention and ionization:

Select organic P compounds including, glucose-1-phosphate (G1P), adenosine-5'-monophosphate (AMP), and phenylphosphonic acid (PPA), were analyzed using FT-ICR MS to determine if common organic P molecules can be extracted, ionized, and detected in the mass spectra. Stock solutions were made by dissolving each compound in DI water and included 88 mg/L for G1P, 68 mg/L for AMP, and 103 mg/L for PPA. The solutions were extracted using the SPE procedure and the eluent was collected for total P quantification. The eluents were diluted 1:10 in DI water and analyzed on a Perkin Elmer ICP-OES for total P. Sample reproducibility, calculated from three measurements of the same sample, was within 5%. Percent retention was calculated as the stock concentration minus the eluted concentration divided by the stock concentration for each compound. The columns were extracted with methanol and analyzed using FT-ICR MS as described previously.

Results:

SONDE profiles and metal distributions:

The SONDE profiles for sampling dates in May (Figure 3.1A), September (Figure 3.1B), and January (Figure 3.1C) display dissolved oxygen, pH, temperature, and chlorophyll-a with depth with values provided in tables C-3.1, 3.2, 3.3. In May, temperature, dissolved oxygen, and pH all follow the same trend where they are relatively constant until 1.4 m and gradually decrease to the bottom with the greatest change occurring from 3.0 to 3.5 m. Chlorophyll-a reaches its maximum concentration of 11.2 µg/L at 1.4 m and then decreases down to 3.0 m. In contrast, pH and dissolved oxygen sharply increase just below the surface and then decrease below 0.5 m in September. Chlorophyll-a follows the same trend but achieves a maximum value of 3.5 µg/L at 1.3 m and then decreases until 3.0 m. The most stratified water column was in January. Dissolved oxygen decreased below 1.8 m until reaching suboxic conditions at the bottom (53.4% saturation) with temperature increasing from -0.5 °C from the surface to 3.0 °C at the bottom. Chlorophyll-a was not detected in January. Additional measurements of phycocyanin from blue-green algae (BGA) in all months and fluorescent dissolved organic matter (fDOM) concentrations in September and January are provided in tables C-3.2, 3.3. September bottom water had 9.86 and 30.68 µg/L of truly dissolved Fe and Mn, respectively, and 132.24 and 12.02 µg/L of colloidal Fe and Mn, respectively. In January the truly dissolved Fe and Mn were 6.61 and 89.34 µg/L, respectively, while colloidal fractions were 336.49 and 11.58 µg/L, respectively.

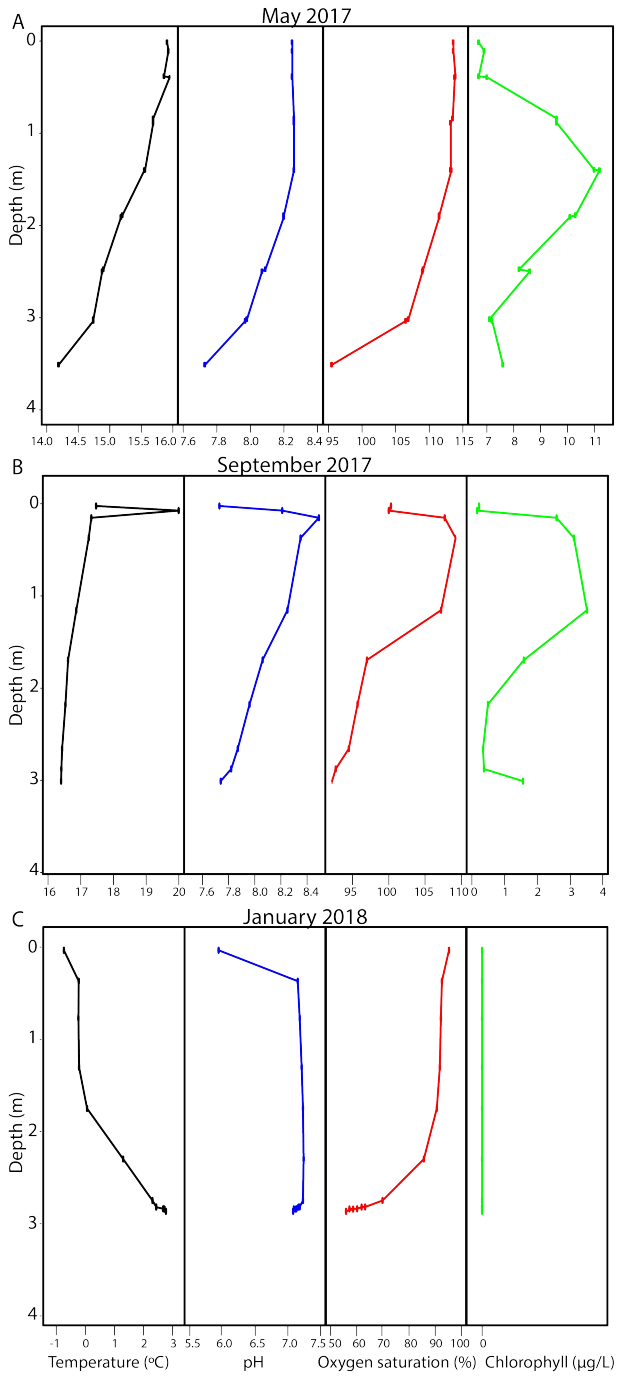

Figure 3.1 SONDE depth profiles of Missisquoi Bay in (A) May 2017, (B) September 2017, and (C) January 2018. Variables: Black, temperature; Blue, pH; Red, oxygen; Green, chlorophyll-a.

Organic P standards:

Concentrations of G1P, AMP, and PPA stock solutions were measured after elution through PPL columns and the percent retention on the column was calculated based on measured P (by ICP-OES) before and after the fluid passed through the column. G1P was retained at 30.5%, AMP at 3.5%, and PPA at 41.7%. When ionized in ESI neg, both G1P and PPA were identified within their mass spectra with corresponding ^{13}C peaks. However, neither AMP nor possible degradation products such as adenosine, glucose, G1P, or adenine were detected. When ionized in positive mode, the standards were absent from their spectra; however, adenosine was present in the AMP spectra indicating a possible hydrolysis of the phosphate group while in solution.

Water column DOM characteristics in ESI negative:

Assigned molecular formulae were initially separated into a non-P-containing (bulk DOM) and a P-containing (DOP) list for analysis and visualization of distinct classes. A visual matrix of the non-P-containing molecules are depicted in figure 3.2 using van Krevelen and Venn diagrams. A molecular lability boundary (MLB), defined by D'Andrilli et al. (2015) at H/C = 1.5 and representing compounds that are generally more bioavailable for microbial consumption (H/C $\geq$ 1.5), is depicted as a grey dashed line in the van Krevelen diagrams. Samples in each column are collected from the same time point while samples across each row are from the same depth. The water column in May shows high chemical diversity with respect to the top which shares the fewest assignments with the rest of the samples. It contains the fewest formulae assignments, but has a significant amount of CHONS compounds between 0.6 $\leq$ O/C $\leq$ 0.8 and 1.5 $\leq$ H/C

≤ 2.0 that are absent in the rest of May. May is also relatively enriched in CHO compounds compared to September which has more CHOS and CHON compounds, especially in the middle. The January surface water holds the highest number of unique assignments but still exhibits significant commonality with the water column. A large network of CHO and CHOS compounds occupy space above the MLB decreasing in number from the top to the bottom. In all three months, there is a considerable core of shared molecules that are conserved throughout the water column. However, molecules are less conserved across time. May contains the fewest unique compounds at each depth suggesting a lower commonality between the other months, while September and January both share more assignments with each other. Structural differences between molecular classes were also seen in homologous series of CHO and CHOS compounds. A CH_2-based Kendrick mass defect analysis revealed increasing alkyl chain length as time progressed from May to January (Figure C-3.1). Namely, the maximum number of CHO (Figure C-3.1A) and CHOS (Figure C-3.1B) molecules in a homologous series increased from May to January.

DOP molecular classes (CHOP, CHONP, CHOSP, and CHONSP) follow unique seasonal and spatial trends in ESI negative (Figure 3.3). In May there is a decrease in assignments through the water column and a compositional shift of molecules in the protein-like van Krevelen region in the top to more unsaturated and less oxygenated compounds towards the middle. There is also a decrease in CHOP-containing compounds to relatively more N and S-enriched P molecules as depth increases. DOP in September is characterized by more CHONP and CHONSP compounds, especially in the middle where there is a large increase in unsaturated molecules similar to May. Protein and

carbohydrate-like molecules above the MLB are present at all depths in small quantities. The distributions in January are akin to September but with fewer unsaturated compounds and more compounds above the MLB. Samples at each depth differ from the bulk DOM in that they are mostly unique to each sampling point and share minimal commonality. When commonality is present, more molecules are shared between the top and middle within each month, whereas only a few assignments are common temporally between September and January and negligible amounts with May.

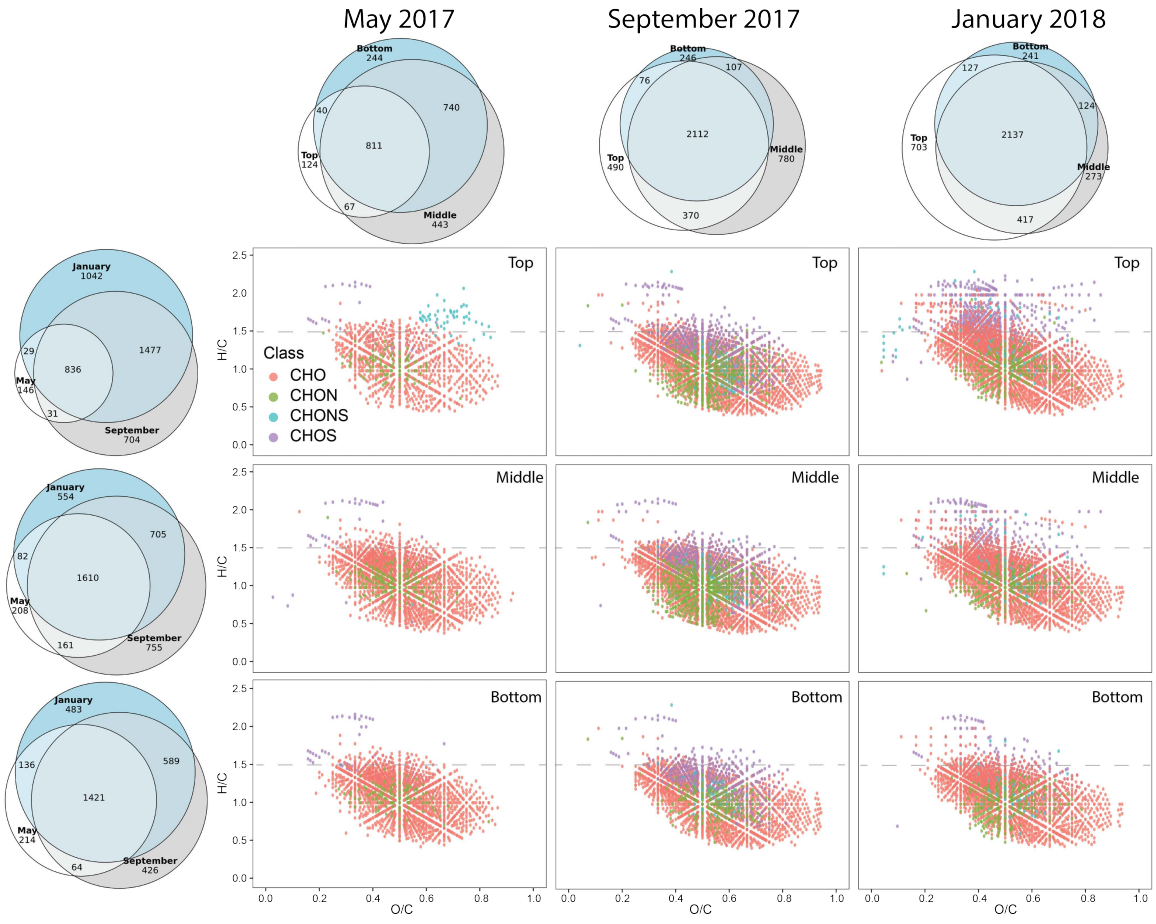

Figure 3.2. Van Krevelen diagram matrix of assigned non-P-containing formulae ionized in ESI negative from the Missisquoi Bay water column. A grey dashed line at H/C = 1.5 is representative of the MLB. Venn diagram sizes are proportional to the total number of constituents and correspond to samples in the water column of the same month (columns) and depths across different months (rows).

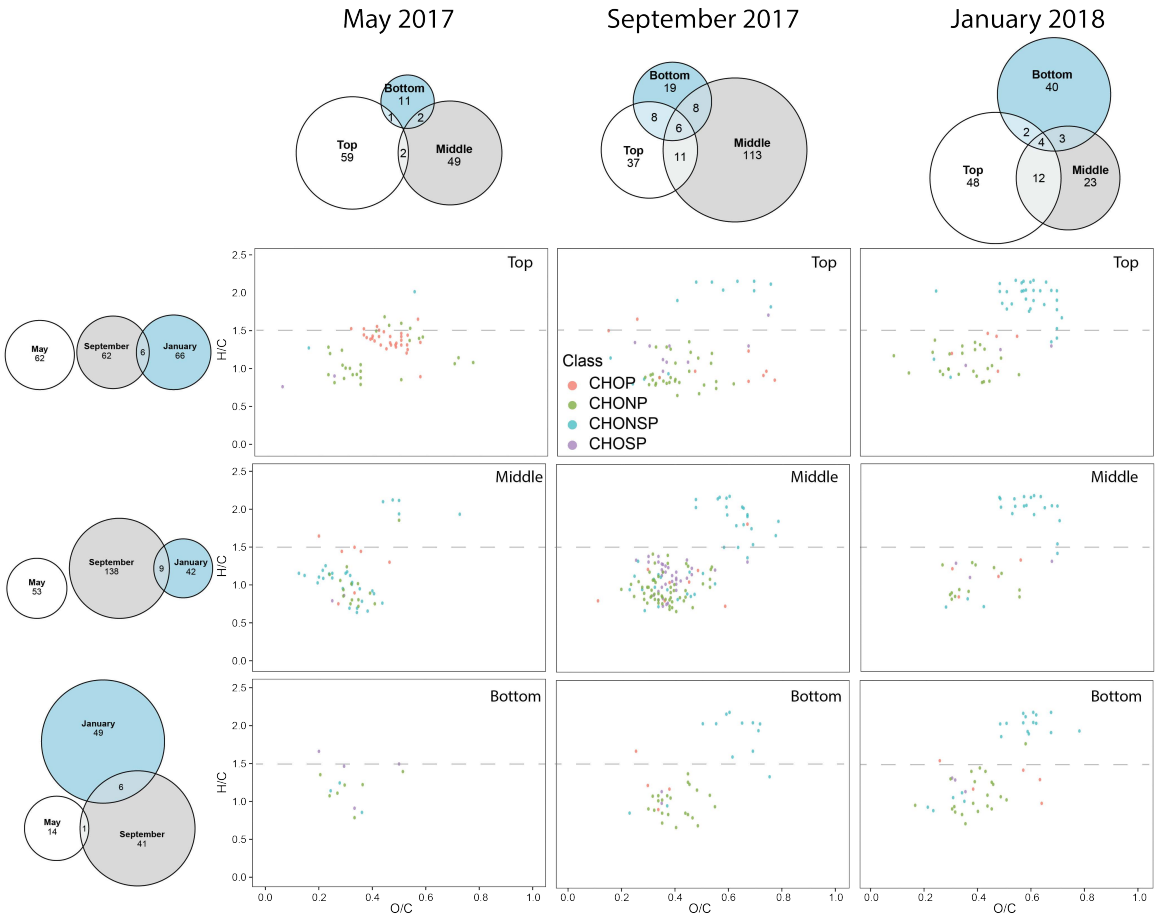

Figure 3.3. Van Krevelen diagram matrix of assigned P-containing formulae ionized in ESI negative from the Missisquoi Bay water column. Formatting and conventions are consistent with figure 3.2.

Assigned formulae were sorted into distinct molecular classes using a multidimensional stoichiometric compound classification (MSCC) scheme from Rivas-Ubach et al. (2018). Relative proportions of classes for each water column sample were calculated and included amino sugars, lipid-like, oxy-aromatic, and protein molecules as well as a "not matched" category that was not classified based on the parameters used (Figure 3.4). Carbohydrate and nucleotide categories were also included but constituted less than 0.5% of each sample and were omitted from figure 3.4. The dominant class for all samples is the broadly encompassing "oxy-aromatic" category that includes

unsaturated compounds with low H/C ratios, mainly polyphenols, and phytochemical compounds if they originate from plants (Rivas-Ubach et al., 2018). The next largest class are the lipid-like molecules, followed by proteins, and amino sugars. The May water column progressively decreases in lipid-like and protein content towards the bottom while increasing in oxy-aromatic compounds. The top sample contains the highest percentage of proteins (4.1%) and amino sugars (2.6%) out of all the samples analyzed from Missisquoi Bay. January follows a similar trend where lipid-like molecules decrease towards the bottom, but they occupy a greater portion of the molecular signatures (24.4-36.3%). Proteins, on the other hand, remain relatively constant. Molecular classes are the least spatially dynamic in September which have the highest percentages of oxy-aromatic compounds (73.8-75.6%) and lowest lipid-like compositions (19.6-22.1%). Proteins are also $\leq$ 0.8% of the total except for the 2.0 and 3.0 m samples where they increase to 1.9 and 1.7%, respectively. The “not matched” category is quite low for all samples ranging between 1.8 to 5.2% of all classifications and is still lower than reported values from Rivas-Ubach et al. (2018) that analyzed biological extracts.

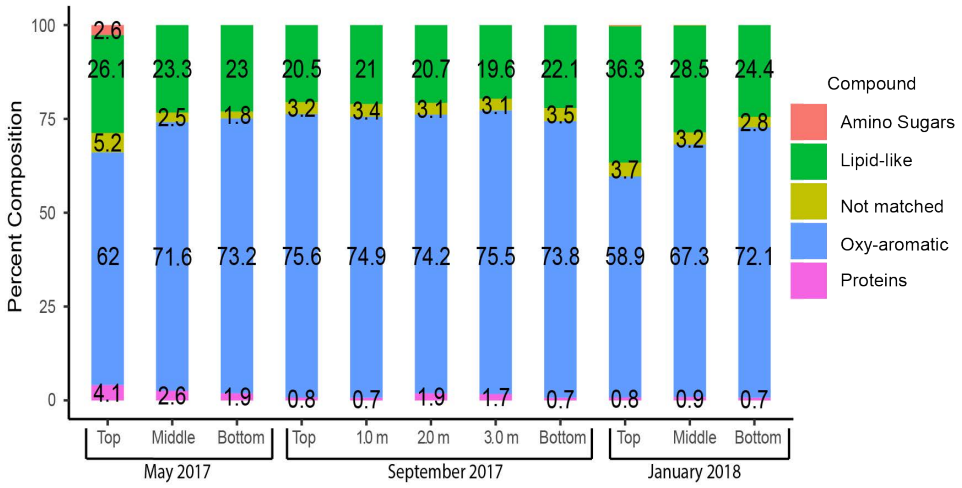

Figure 3.4. Stacked bar charts of molecular classes defined using MSCC from Missisquoi Bay ionized in ESI negative. Quantities are reported as percentages of molecules in each class relative to the total.

Water column DOM characteristics in ESI positive:

FT-ICR MS samples from the Missisquoi Bay water column were also analyzed in ESI positive and visualized in a van Krevelen matrix (Figure 3.5) consistent with the formatting of figure 3.1. Water from May is mainly composed of CHO compounds and almost entirely devoid of both CHON and CHOS molecules; however, they do contain a group of labile CHONS assignments consistent with protein-like signatures. There is low similarity within the water column and a significant decrease in assignments within the middle. September displays an increase in CHON and CHOS molecules but a disappearance of the protein-like CHONS cluster from May. The increase of CHOS compounds is most pronounced in the middle which has the greatest in the whole water column followed by a decrease in the bottom resulting in the absence of the CHOS group between $0.5 \leq H/C \leq 1.0$. January also contains many CHOS and CHON compounds in both the middle and bottom, but fewer in the surface. These samples also contain homologous series above the MLB consisting of CHO and CHON compounds that are

only present in January. Proportionally, DOM analyzed in ESI positive holds more unique compounds in each sample than in ESI negative, meaning less commonality within the water column and temporally. September and January contained the most shared assignments within each water column, whereas May had the fewest. Additionally, at each depth September and January had more compounds in common with each other than with May especially in the middle and the bottom, both in terms of relative amounts and total assignments.

In ESI positive, the distribution of DOP trends mimics the bulk DOM signatures in terms of seasonal commonality (Figure 3.6). The May water column consists of mainly CHOP, CHONP, and CHONSP compounds characteristic of unsaturated, protein, and lipid-like molecules. The assignments are largely unique to each depth with minimal commonality and are mostly distributed between the top and bottom water. In September and January there is a compositional shift of DOP to mostly CHOP compounds and some containing CHONP. The CHOP molecules occupy van Krevelen space consistent with protein and carbohydrate-like compounds above the MLB ($0.4 \leq O/C \leq 1.0$ and $1.5 \leq H/C \leq 2.0$) while the CHONP assignments cluster between $0.2 \leq O/C \leq 0.4$ and $1.0 \leq H/C \leq 1.5$ indicative of more unsaturated aliphatic molecules. In September this CHONP cluster decreases towards the bottom, while in January it increases. DOP compounds in both months display high commonality within the water column but still contain large amounts of unique assignments between depths. When comparing DOP compounds through time, May is compositionally distinct from September and January, sharing almost no assignments with either month. On the contrary, September and January share some assignments with each other at all three depths, more than in ESI negative.

Assignments from ESI positive were also grouped according to MSCC analysis into the same molecular classes described previously (Figure 3.7). Consistent with ESI negative, the dominant class remains as oxy-aromatic compounds with lipid-like molecules having the second-most abundance, but the contribution of oxy-aromatics is diminished with a greater contribution from the lipid-like molecules. Additionally, in ESI positive there are more molecules classified as amino sugars, proteins, and carbohydrates; DOM from May is highly characteristic of amino sugars (1.1-2.4%) and elevated protein content (4.9-7.1%) compared to the other seasons. In September carbohydrate molecules are present for the first time in stable amounts (0.7-1.0%) and proteins show minimal change (3.4-4.1%) while amino sugars are not detected. Lipid-like content decreases from the top (41.1%) to a minimum between 2.0 and 3.0 m (29.7-30.4%) before increasing again at the bottom (37.2%), complimented by an increasing trend for oxy-aromatic compounds. The January samples are compositionally similar to September containing the same molecular classes and no classified amino sugars. Lipid-like content decreases in the bottom followed by an increase of proteins and oxy-aromatics. The percentage of compounds in the "not matched" category is still low (1.8-6.4%) and consistent with the range found in ESI negative making MSCC a reasonable tool to classify DOM.

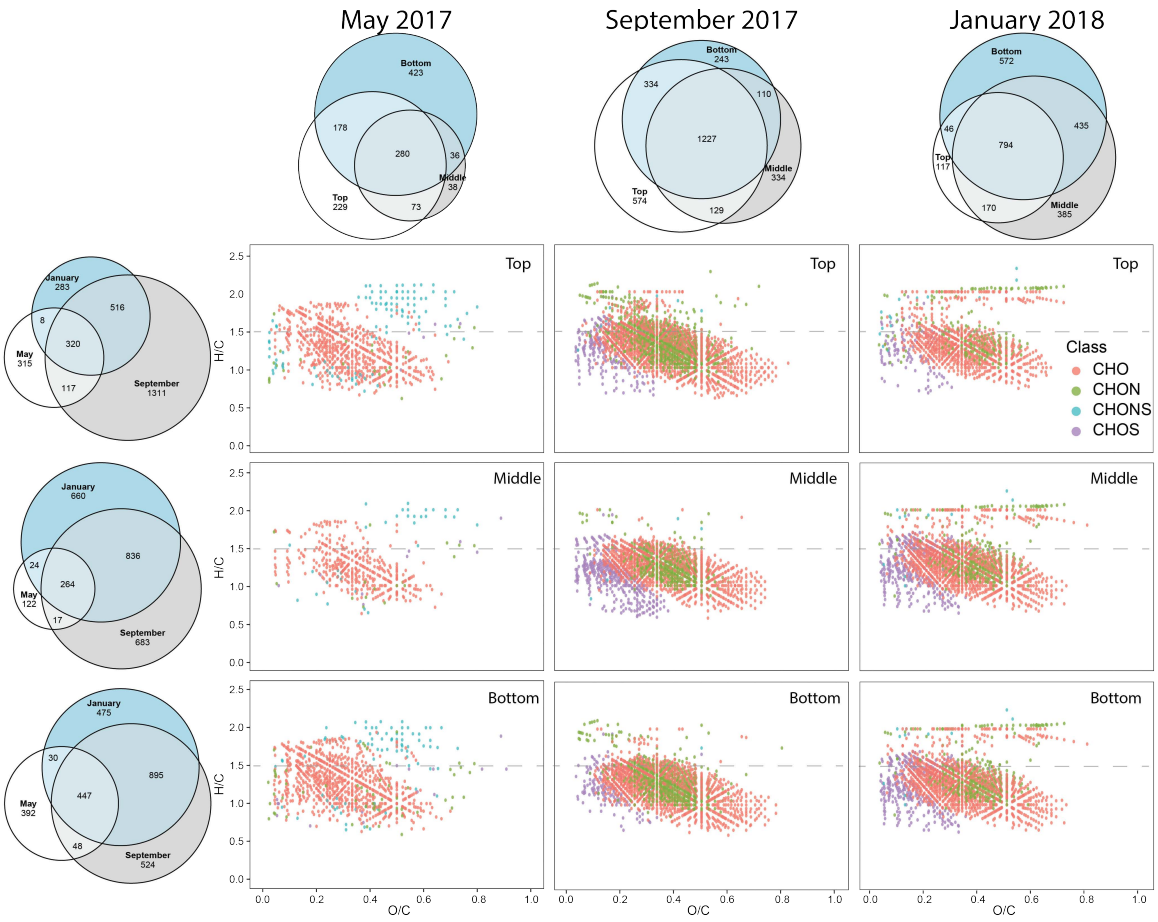

Figure 3.5. Van Krevelen diagram matrix of assigned non-P-containing formulae ionized in ESI positive from the Missisquoi Bay water column. Formatting and conventions are consistent with figure 3.2.

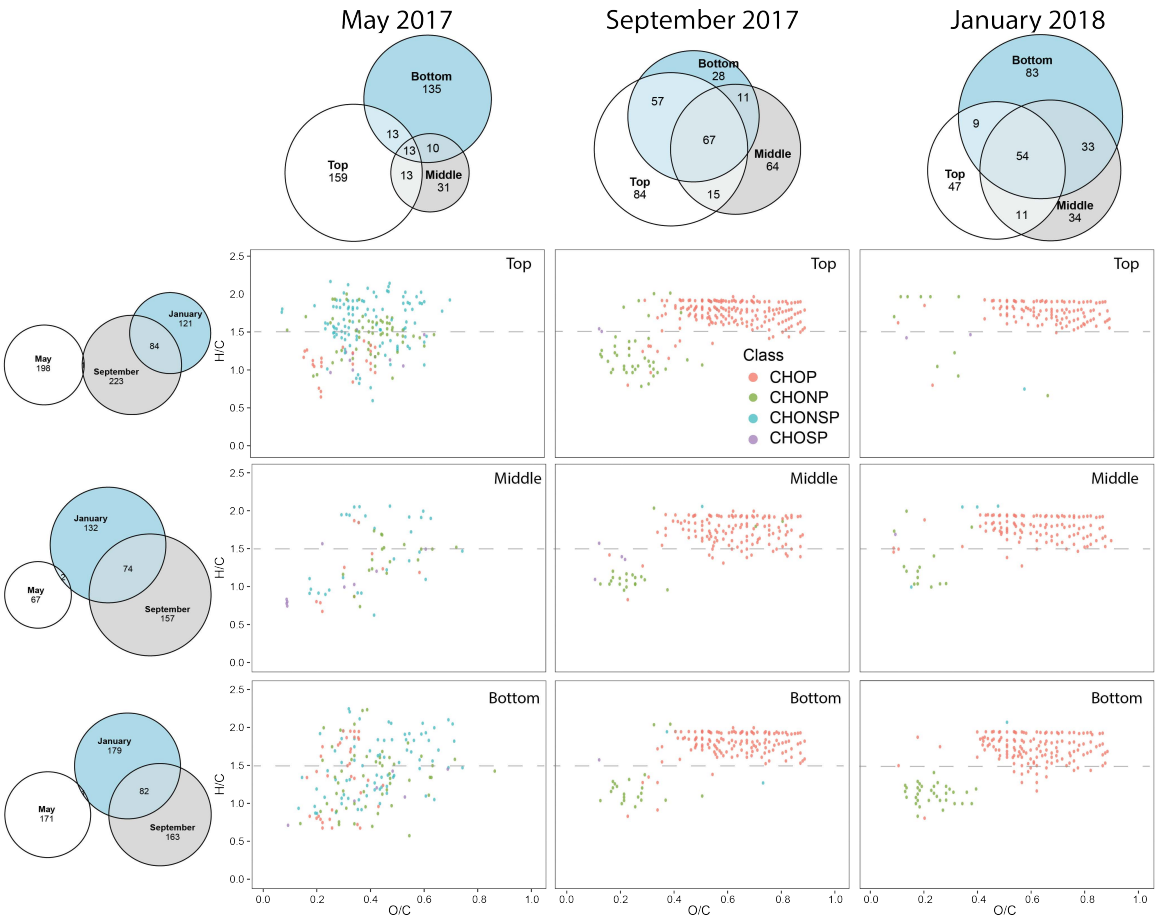

Figure 3.6. Van Krevelen diagram matrix of assigned P-containing formulae ionized in ESI positive from the Missisquoi Bay water column. Formatting and conventions are consistent with figure 3.2.

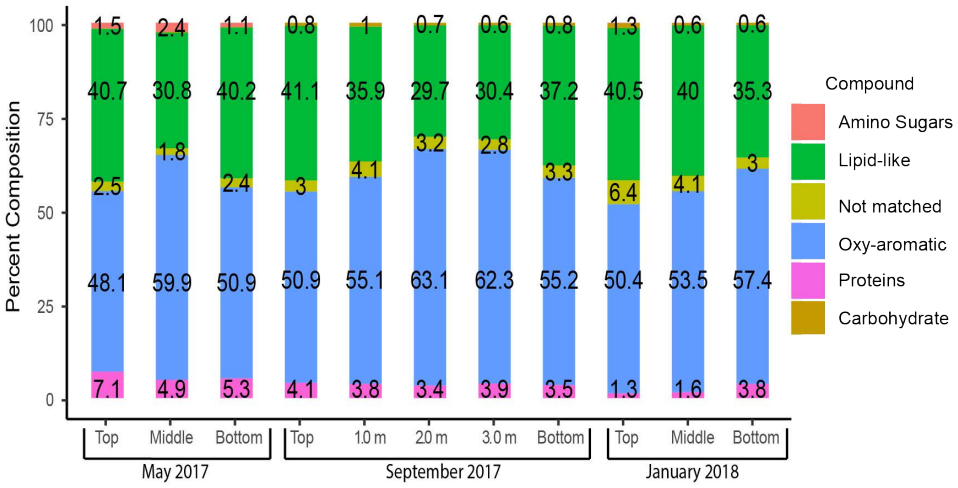

Figure 3.7. Stacked bar charts of molecular classes defined using MSCC from Missisquoi Bay ionized in ESI positive. Quantities are reported as percentages of molecules in each class relative to the total.

TRII analysis of Missisquoi Bay DOM:

TRII calculations provide insight into the total molecular contribution of compounds, taking into consideration the ion counts of each class. In ESI negative, CHO molecules overwhelmingly constitute each sample with significant signals from CHOS molecules (Figure 3.8A). In all samples except September 2.0 and 3.0 m, CHOS molecules are relatively more abundant than CHON, CHONS, and all P-containing molecules, especially in January which has the highest TRII value for CHOS. P-containing compounds are quantitatively similar to CHONS molecules but contribute more in the middle and bottom water of May and September. In addition, the September profiles of CHO, CHON, and P-containing compounds mirror the chlorophyll-a profile from figure 3.1. CHO molecules are also the highest contributing class in ESI positive spectra except for January where they are exceeded by CHOS molecules in the top and middle samples (Figure 3.8B). The trends for ESI positive are consistent with figure 3.5 where May samples have minimal heteroatom compositions and both September and

January have greater CHON and CHOS content. The spike in CHOS TRII values in September at 2.0 m is also consistent with the compositional increase of CHOS compounds in van Krevelen space (Figure 3.5). Contributions of P-containing compounds to the ESI positive spectra are much greater than in ESI negative, exceeding CHONS signals in all months.

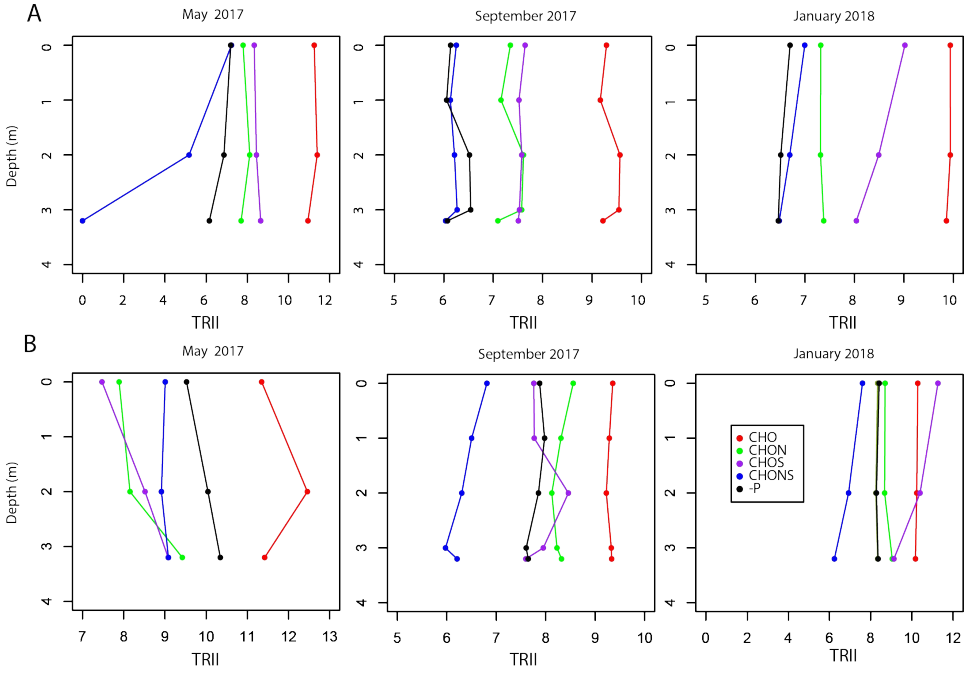

Figure 3.8. Depth profiles of the Missisquoi Bay water using TRII analysis for samples ionized in (A) ESI negative and (B) ESI positive modes. Colors are consistent with atomic class: Red, CHO; Green, CHON; Purple, CHOS; Blue, CHONS; Black, all P-containing molecules.

September 2017 DOM sources:

A water sample from the Missisquoi River and an axenic culture of cyanobacteria (*Synechocystis* sp.) was compared with surface water from September 2017 in ESI negative and positive to investigate the different contributions of organic matter to the bulk signature. MSCC revealed the dominant compound classes in the river sample are

oxy-aromatics followed by lipid-like molecules in both ionization modes (Figure 3.9A). In contrast, lipid-like molecules are more abundant in the cyanobacteria with the second highest class being oxy-aromatic compounds. Overall molecular diversity from cyanobacteria is high with amino sugars accounting for 1.1 to 1.4% of classified assignments and protein molecules being higher than in any water sample measured in this study (14-14.4%).

Non-P-containing DOM from the surface water in September most closely matched the water collected from the Missisquoi River in both ESI negative (Figure 3.9B) and ESI positive (Figure 3.9C) with some shared commonality with the cyanobacteria. In ESI negative top water DOM shared 64.6% of assignments with the just the river and a total of 80.7% when the molecules also common with cyanobacteria are considered. Commonality decreases in ESI positive; the top only shares 44.1% of its assignments with the river increasing to 53.3% after including the assignments also common to the cyanobacteria. A similar trend was observed with the P-containing dataset in both ESI negative (Figure 3.9D) and ESI positive (Figure 3.9E). The top and river DOP in ESI negative shared only 15 common molecules with each other and none with the cyanobacteria; meaning all samples were mainly composed of unique assignments. The ESI positive spectra also exhibited a high degree of uniqueness, but common elements were found between all three samples. The top water shares 31.8% of its DOP assignments just with the river and a total of 48.9% when those assignments also present in the cyanobacteria were included.

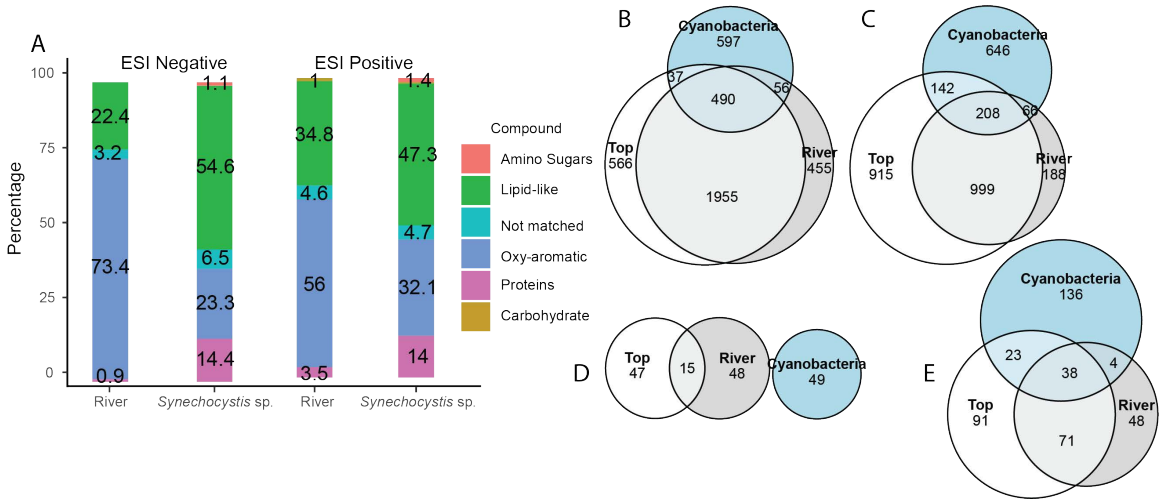

Figure 3.9. Potential DOM sources into Missisquoi Bay represented by the Missisquoi River and an axenic culture of cyanobacteria *(Synechocystis* sp.). (A) MSCC analysis in ESI negative and positive. Proportional Venn diagrams of the river, cyanobacteria, and September surface water depicting assignments for non-P-containing assignments in (B) ESI negative, (C) ESI positive, and P-containing assignments in (D) ESI negative and (E) ESI positive.

Incubated DOM:

Sediment cores collected from each water column sampling were subjected to reducing conditions by bubbling N_2 gas into the headspace to promote reductive dissolution of Fe(III) and Mn(IV) (oxy)hydroxides. In September 2017 an additional core was collected and subjected to oxic conditions by continuously bubbling the headspace with air. Electrochemical profiles were conducted using gold-amalgam microelectrodes to detect dissolved Mn(II), Fe(II), Fe(III)-complexed to organics, and O_2 species within the cores. Reducing conditions were achieved 3-7 days after incubation and were confirmed by the presence of Mn(II) and Fe(II) peaks and absence of O_2 at or above the (SWI) (Figure C-3.2). DOM from the reduced cores was analyzed using FT-ICR MS and compared to starting bottom water for each month to investigate chemical changes in the DOM signatures. Samples ionized in ESI negative displayed a trend of increased lability

with reduction (Figure 3.10A). In all months, reduction had the effect of increasing the proportion of compounds above the MLB relative to the bottom water. Changes in molecular functionality were also observed and resulted in positive increases in the proportion of lipid-like molecular assignments and a decrease in oxy-aromatic composition for all months. The greatest increase occurred in January while the smallest was in September. A similar outcome was observed in ESI positive where lability increased with respect to the percentage of molecules above the MLB (Figure 3.10B). The percentage of lipid-like molecules also increased while oxy-aromatics decreased but with larger differences than in ESI negative. Molecular compositions in ESI positive saw percent changes between 10 and 20% in September and January while all the changes in ESI negative were less than 10%. Percent changes can lead to ambiguity; for instance, a percent increase of a variable can be attributed to greater counts of that variable and/or a decrease in another. Additionally, absolute counts can be misleading if the number of assigned formulae vary from sample to sample. TRII analysis was conducted on the lipid-like and oxy-aromatic compounds detected in the bottom water and reducing incubations (Table C-3.4) revealing values for lipid-like molecules increased upon reduction and decreased in oxy-aromatic content in ESI positive. Similarly, all reduced samples in ESI negative had a higher TRII value for lipid-like compounds, but only January decreased in oxy-aromatic content, while May and September increased.

Changes in DOP were varied displaying different trends for ESI negative and positive. In both ionization modes the percent of assigned DOP formulae increased with reduction in May and September but not January. However, the total P contribution to the mass spectra increased upon reduction in negative but decreased in positive from the

TRII values (Table C-3.5). Overall, reduction resulted in an abundance of new DOP compounds absent from the bottom water with a greater proportion in ESI negative (Table C-3.5). Within each DOP class, diversity of compounds changed with reduction and did not follow any apparent trends other than the increase in CHOP molecules in all samples except for May ESI positive (Table C-3.5).

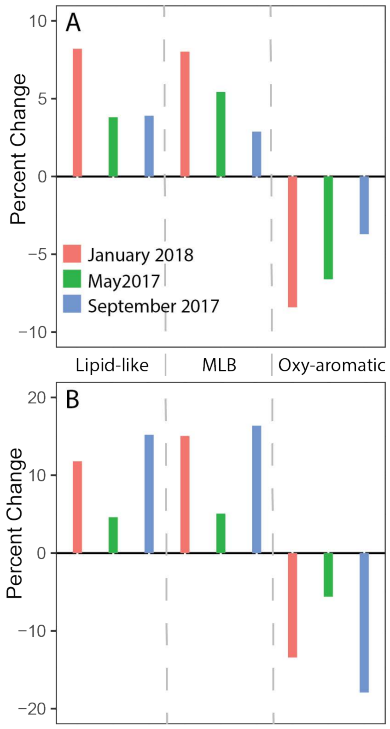

Figure 3.10. Percent changes in the content of Lipid-like, oxy-aromatic, and molecules above the MLB after reduction of sediment cores in (A) ESI negative and (B) ESI positive for all sampled months.

Discussion:

Seasonal evolution of DOM:

DOM was collected at three distinct time points from Missisquoi Bay to cover a range of differing seasonal conditions. The spring season is characterized by snowmelt and increased runoff from the watershed into the lake, late summer is considered the

"bloom" season with higher temperatures and a sustained period of cyanobacterial blooms marked by anoxia. In winter the lake freezes over and results in a stratified water column with reduced terrestrial input until a melting event remixes the water column (Schroth et al., 2015; Isles et al., 2017). In the context of this data, May represents the "pre-bloom" time point at the end of the spring melt and the beginning of summer with rising temperatures and increased phototrophic activity (Figure 3.1). September represents the end of the summer bloom season and January is characteristic of mid-winter frozen lake conditions. These descriptions are consistent with SONDE profiles taken at the time of sample collection (Figure 3.1, Table C-3.1. 3.2, 3.3). In May and September higher oxygen saturation and pH in the surface and elevated levels of BGA and chlorophyll-a towards the middle suggest algal and cyanobacterial photosynthetic activity. Although present in both months, the signals for both BGA and chlorophyll-a were higher overall in May than September indicating differences in primary productivity. Furthermore, BGA and chlorophyll-a correlate and follow the same trend except at the very surface of September where BGA is higher and shows a decreasing trend (Table C-3.2). This difference could be explained by the ability of buoyant cyanobacteria to outcompete phytoplankton and dominate the surface water during bloom season proliferation and extending into late summer (Huisman & Hulot, 2005), whereas in spring there is a greater abundance of other phytoplankton before the bloom onset (Bowling et al., 2015).

The common assignments in both ionization modes from the top, middle, and bottom water samples were combined in each month, and afforded 148 ions in May, 642 in September, and 467 in January. DOM originating from May contained 136 conserved

ions in September (91.9% of May) and 115 still present in January (77.7% of May) revealing a core of highly recalcitrant organic molecules. These are characteristic of the Missisquoi Bay watershed, remaining in the water column throughout the year and possibly ubiquitous in temperate lakes (Zark & Dittmar, 2018). However, this core of recalcitrant DOM is still relatively minor compared to the unique assignments found in each month from both ionization modes, meaning that each season has distinct processes that cycle DOM within the bay.

The progression from late spring to mid-winter is reflected in the chemical composition of water column DOM. May is disproportionately low in CHON and CHOS molecules and high in CHONS molecules, proteins, and amino sugars (Figure 3.2, 3.4, 3.5, 3.7, 3.8). The intrinsic properties of these CHONS molecules were also distinct since they mostly grouped above the MLB at higher O/C ratios while CHONS molecules from September and January were largely below the MLB at similar O/C ratios characteristic of more unsaturated molecules (Figure 3.2, 3.5). DOM derived from aquatic algae is distinct and characteristic of high protein and peptide content (Ly et al., 2017) with algal extracts found to have high molecular diversity of metabolites (Zhang et al., 2014). The higher content of proteins and amino sugars could be a result of increasing algal activity in May consistent with the high amount of measured chlorophyll-a. Although unique to May, the protein and CHONS signatures are still minimal compared to the contributions from CHO compounds and oxy-aromatics having signatures of terrestrial DOM (Kellerman et al., 2015). The compounds have TRII values above 10, while CHO molecules from September and January are at or below 10, suggesting they contribute more to the overall DOM signature in May (Figure 3.8). The bulk DOM assignments

demonstrate high spatial heterogeneity within the May water column; each depth contains large proportions of unique assignments in both ionization modes possibly from a combination of OM degradation and production, which is consistent with the differing limnological conditions at each depth (Figure 3.1, Table C-3.1).

From May to September there is a gain in CHON and CHOS molecules throughout the water column and higher proportions of shared molecules between each depth (Figure 3.2, 3.5). Spatial distributions of DOM within the water column from the TRII (Figure 3.8A) are also tied to biological interactions from SONDE profiles of chlorophyll-a and BGA (Figure 3.1B, Table C-3.2). TRII values decrease from the surface to middle and increase towards the bottom while chlorophyll-a follows the opposite trend. fDOM also increases with the TRII values at 2.0 and 3.0 m (Table C-3.2) and is accompanied by more proteins in ESI negative (Figure 3.4) and oxy-aromatics in ESI positive (Figure 3.7). These compositional shifts and increases of fDOM below the algal zone could be indicative of terrestrial DOM and production of algal DOM in the surface followed by heterotrophic consumption at 2.0 and 3.0 m producing unique fDOM compounds, characterized by humic-like substances from the processing of biomolecules (Dittmar & Stubbins, 2014). DOM progression during a summer bloom season revealed that post-bloom DOM produced more N-containing compounds from biological processing (Zhang et al., 2014), with various microalgae capable of distinct CHON, CHOS, and CHONS production (Bittar et al., 2015b; Mangal et al., 2016). Similarly, microbial and algal community activity can increase CHON, CHOS, and CHONS content and diversity in terrestrial streams (Kamjunke et al., 2017a). Consequently, the increase

of heteroatom-containing compounds in Missisquoi Bay through the summer is likely due to algal and microbial reworking of terrestrial DOM (Kellerman et al., 2105).

The transformations of DOM from September to January are less pronounced than during the summer, given the high degree of similarity between compounds, but still fundamentally shift the composition of DOM to more labile molecules (Figure 3.2, 3.5). Photochemical reactions result in the breakdown of aromatic molecules into smaller, aliphatic compounds proving to be a significant pathway for aquatic C cycling (Spencer et al., 2009; Stubbins et al., 2010); however, ice cover limits the photodegradation of these compounds (D'Andrilli et al., 2013). In January, the lake is protected from sunlight by an ice sheet attenuating the breakdown of terrestrial aromatic compounds from spring and summer which may contribute to the high commonality of compounds between September and January. An increase of CHOS (Figure 3.2, 3.5, 3.8) and lipid-like (Figure 3.4) composition is accompanied by a stratified water column and absence of both BGA and chlorophyll-a (Figure 3.1, Table C-3.3). The increase in CHOS content is likely biological since reactive sulfur species (e.g. HS-, polysulfides, thiosulfate) were not detected with electrochemistry making abiotic sulfurization unlikely. Changes in these molecular signatures underneath the ice could be explained by a combination of processes including less terrestrial input and a shift in surface microbial activity from phototrophy to heterotrophy resulting in mineralization of residual algal biomass and less overall OM. This is supported by lower concentrations of fDOM than in September correlating to lower DOC concentrations (Ditmmar & Stubbins, 2014), and winter oxygen consumption in Missisquoi Bay from respiration (Schroth et al., 2015) (Table C-3.2, 3.3). While the distinct contributions of phototrophic and heterotrophic bacteria to

DOM composition is still unknown, heterotrophic bacteria have been shown to decompose algal DOM in the presence of terrestrial DOM (Morling et al., 2017) and produce diverse metabolites that are reflected in the overall signature of freshwaters (Romano et al., 2014). Heterotrophic microbial activity could produce the unique labile compounds in January since phototrophs are inactive in the winter while the observed compositional DOM shift is indicative of microbial activity (Einsiedl et al., 2007; D'Andrilli et al., 2013; Feng et al., 2016). Labile aliphatic compounds would be degraded faster with respect to unsaturated and phenolic compounds (Kamjunke et al., 2017b; Mostovoya et al., 2017) meaning they must have been produced recently from algal lysis and will likely continue to decompose through spring. Increases in CHO and CHOS homologous series from May to January are also suggestive of systematically processed DOM (Figure C-3.1) with various phytoplankton shown to produce networks of CHOS compounds occupying the same van Krevelen space (Mangal et al., 2016). In contrast, terrestrial oxy-aromatic compounds are still the main molecular class in January (Figure 3.4, 3.7) either through baseflow riverine input or retention of recalcitrant compounds from the previous seasons but are proportionally less than in the other months.

DOP compounds were found to be highly labile with each month containing primarily unique assignments (Figure 3.3, 3.6) suggesting a high organic P turnover in Missisquoi Bay. Internal cycling is compartmentalized with large differences in P quality due to physical (temperature and mixing), chemical (pH, oxygen, metals), and biological (bacteria and algae) factors at each depth (Figure 3.1A-C). Within individual water columns, DOP commonality between depths was also low, especially in ESI negative (Figure 3.3) and further supports the compartmentalized water column in terms of P

cycling. DOP molecules are related to the bulk DOM through biotic and abiotic transformations which can occur on the order of days (Killberg-Thoreson et al., 2013). Aquatic degradation primarily occurs through enzymatic cleavage of phosphate groups but can also through abiotic hydrolysis or photolysis, while natural synthesis of DOP is biological (Baldwin et al., 2005; Turner, 2005). DOP assignments were subjected to KMD analysis of HPO_3 unit loss/addition pairs and confirmed that many of the compounds were linked to precursor DOM molecules within the Missisquoi Bay water samples either by HPO_3 removal or biological HPO_3 assimilation (Figure C-3.3). This supports the assertion that DOP in Missisquoi Bay is potentially labile but also that much of it (assignments without identified precursors) is still poorly characterized, especially in ESI negative. Though quantification of the DOP contribution to the inorganic P pool was outside the scope of this study, it is still feasible that they support cyanobacterial growth during the summer bloom season when inorganic P is in high demand (Whitton et al., 1991), given their lability and the structural transformations.

While the DOP contribution to individual mass spectra remained relatively constant throughout the year (except in May, ESI positive) (Figure 3.8A,B), the chemical compositions were quite diverse. In ESI positive, September and January displayed networks of CHOP molecules in the carbohydrate and protein region of the van Krevelen diagram that are absent in May (Figure 3.6). This provides further evidence of DOM transformation during the summer bloom season resulting in fundamentally different DOP molecules that continue through mid-winter. The differences in DOP composition for May could be due to the recent spring runoff and anthropogenic input of agricultural/urban DOP from the surrounding watershed (Rosenberg & Schroth, 2017),

consistent with DOP observations from other world rivers (Wagner et al., 2015). Summer transformations also occur in ESI negative, although to a lesser extent, where there is an overall increase in assigned DOP and networks of protein-like CHONSP molecules in September and January (Figure 3.3). Clusters of CHONP molecules with an H/C ratio of about 1 to 1.3 were also abundant (particularly in September at mid depth) (Figure 3.3, 3.6) analogous to similar biolabile molecules from intracellular cyanobacterial OM that have been suggested to represent fragments or subunits of DNA/RNA (Bittar et al., 2015b), which are often the main forms of aquatic DOP. (Baldwin, 2013). Such diverse assignments of DOP molecules are not uncommon in the Great Lakes region; Brooker et al. (2018) detected hundreds of assorted DOP compounds in the Lake Erie watershed, while Minor et al. (2012) found many N- and S- containing DOP assignments in the oligotrophic Lake Superior, suggesting these distributions may be universal to temperate watersheds.

Source contributions:

DOM and DOP compositions in Missisquoi Bay are a result of terrestrial input, microbial production, and redox-dependent sediment mobility. Simplified endmember analysis was done with a riverine sample, cyanobacterial extract, and reduced sediment cores to compare the contributions of each source and sink to the water column signatures. Microbial community analysis of Missisquoi Bay is incomplete, so it is not certain whether *Synechocystis* sp. is present, however it was chosen as a representative of the cyanobacterial community because it is one of the most studied cyanobacteria and can grow both in the light and dark (Červený et al., 2015). Although September and May both

had BGA and chlorophyll-a in the water column, cyanobacteria were strictly compared to September because the surface sample had more formulae assignments and was sampled after the summer bloom period, likely retaining cyanobacterial DOM. Since the cyanobacteria sample was water-soluble and extracted using the SPE method in the same way as the DOM samples, the ions had the same potential to be found in the water column spectra, and thus could be compared directly with the samples. As expected, the river water afforded DOM signatures consistent with terrestrial sources (Kellerman et al., 2015; Wagner et al., 2015; Gonsior et al., 2016), while the cyanobacteria had greater chemical diversity and proportions of labile compounds characteristic of biomolecular signatures (Rivas-Ubach et al., 2018) (Figure 3.9A). Most of the compounds in the surface water from September were also present in the river in ESI negative with a substantial amount also in ESI positive (Figure 3.9B,C). Extending into the water column, riverine DOM was highly resistant to degradation with 63% and 65% of the river DOM assignments present in the bottom water in ESI negative and positive, respectively (Figure C-3.4A). The total ions common to both negative and positive modes also followed the same trend but with a greater retention of riverine DOM with 74% of the river assignments. This resistance of riverine DOM to aquatic degradation agrees with the widely accepted river continuum model where more refractory compounds are transported from the river, while much of the unique upstream riverine DOM assignments are absent due to degradation (Vannote et al., 1980). While the surface water DOM in ESI negative was almost entirely composed of terrestrial DOM, the same water in ESI positive had almost half its total assignments as unique and exclusively shared many compounds with the cyanobacteria (Figure 3.9C). The cyanobacterial sample

shared many ions with both the river and surface water but had greater amounts of unique assignments possibly reflecting labile DOM that would be processed in natural waters, especially extracellular organics that are highly susceptible to photodegradation (Bittar et al., 2015b). Assuming high solar irradiance during the summer, photodegradation during the bloom season could contribute to the unique surface compounds in September, with evidence of eutrophic lake DOM compositions being influenced by algal DOM photoproducts (Bittar et al., 2015a), which would be absent from the sampled extracellular cyanobacterial OM. The uniqueness of the cyanobacteria signatures could also be due to the lower volume extracted through the PPL columns compared to DOM samples, (15 mL vs 1 L, respectively) resulting in the retention of less polar molecules (Li et al., 2016). Overall variability in surface water compositions and endmember sources (especially in ESI positive) reflect the complex interactions of terrestrial DOM with autochthonous DOM, particularly microbial reworking of OM (Ward et al., 2013; Zark & Dittmar, 2018).

On the other hand, DOP compounds were highly dispersed in ESI negative with minimal similarity between the top and river and more commonality in ESI positive with most of the river DOP shared between the two endmembers (Figure 3.9D,E). The low amount of riverine DOP common with the surface is not surprising given that lateral transport has been shown to process DOP in wetlands, resulting in the retention of a only small number of recalcitrant compounds (Llewelyn et al., 2002). Aquatic degradation of DOP was more severe than the bulk DOM; only 1.6% and 27.3% of the original riverine DOP was detected in the bottom in ESI negative and positive, respectively (Figure C-3.4B) with the greatest decreases occurring in the surface during transport to the bay

followed by diffusion from the surface to the middle. Consequently, terrestrial DOP may not be as important as particulates to the organic P fraction that is deposited and released from the sediment during anoxia, but rather consumed in the surface water releasing inorganic P. Autochthonous sources seem to be the leading DOP contributor below the surface during oxic conditions, since most assigned formulae are unique at each depth and given the increase of DOP formulae at 2.0 m in ESI negative (Figure 3.3, 3.6). To illustrate, studies have shown that the particulate fraction contains both more inorganic and organic P from mixed sources, possibly enriched in bioavailable phospholipids and DNA derivatives (Shinohara et al., 2012), that assimilate with the sediment and can contribute to internal P loading through remobilization (Broberg & Persson, 1988; Uusitalo et al., 2003; Bai et al., 2015). Thus, the surface of the sediment becomes rich in biogenic organic P and over time influences the composition of the bottom water DOP (Ahlgren et al., 2005).

This interplay between deposition and transfer of previously particulate P into the dissolved fraction supplies organic P to the benthic DOP pool for uptake by anaerobic-tolerant microorganisms, however the contribution of this pool to phytoplankton in deep lakes is thought to be minimal unless it is mobilized by water column mixing (Reynolds & Davies, 2001). Transport of organic P between the dissolved and particulate fraction is still poorly understood with both constituents having different polarities and structural features (Turner, 2005; Baldwin, 2013), but may provide a link to the differences of DOP quality seen at each depth. Regardless, both ionization modes suggest that a substantial amount of DOP is transferred into Missisquoi Bay from the river and consumed in the surface, but other surface processes are responsible for producing unique DOP signatures

that would have otherwise been degraded during transport (Figure C-3.4B), given the high proportion of unique DOP in the ESI negative river. Other mechanisms reflecting the uniqueness of the DOP water column pool could include structural degradation of the riverine compounds through photolysis, or microbial production as evidenced by the commonality with cyanobacteria in ESI positive (Figure 3.9E).

Bottom water DOM composition and interactions are more dependent on sediment mobility and resuspension with the most recalcitrant fraction arriving from the surface (Meyers & Ishiwatari, 1993). Specifically, the DOM signature is a result of the interplay between sorption processes of redox-dynamic waters by associations with Fe minerals (Lalonde et al., 2012; Chassé & Ohno, 2016; Riedel et al., 2013; Dadi et al., 2017) as well as microbial processing (Kamjunke et al., 2017b; Mostovaya et al., 2017; Valle et al., 2018). In Missisquoi Bay, all bottom water displayed an increase in lipid-like and labile compounds upon reduction, while the percent composition of oxy-aromatics decreased (Figure 3.10A,B). This was confirmed by the increase in TRII values for lipid-like molecules and a decrease in oxy-aromatics except in ESI negative during May and September where oxy-aromatic TRII values increased (Table C-3.4.). Desorption of DOM from mineral surfaces has been shown to release larger, aromatic and oxygenated molecules into the solution (Chassé & Ohno, 2016; Coward et al., 2018); however, this trend was not observed for most incubated samples, indicating that desorption is not the dominant process for bottom water DOM cycling. Shifts to more bioavailable compounds are consistent with microbial degradation of DOM with similar anoxic incubations reporting degradation of labile compounds and shifts to smaller, less-oxygenated molecules (Valle et al., 2018). Although these discrete trends are masked by the

complexity of DOM in both ionization modes, assignments common to both modes clearly follow this same trend. In all incubated samples there was a decrease in mass, O/C ratio, AI, and DBE while the H/C ratio increased (Figure C-3.5; Table C-3.6), consistent with microbial DOM properties (Kujawinski et al., 2004;). The gain in lipid-like molecules within all samples is contrary to the trend Valle et al. (2018) observed. However, their incubations were conducted for 40 days during which time DOC sources can become limiting and showed evidence of methanogenesis which hydrolyzes these compounds. In contrast, Missisquoi Bay incubations ran for 7 days at most with an absence of methane indicating no direct evidence of methanogenesis. The lability increase in Missisquoi Bay upon reduction is best explained by microbial signatures from active Mn(IV)- and Fe(III)-reducing bacteria, while the TRII increase of oxy-aromatics in May and September ESI negative is from stronger desorption processes. Desorption would have a lesser effect in January where the bottom water is already suboxic upon collection (Figure 3.1C) and enriched in oxy-aromatics relative to the rest of the January water column (Figure 3.4, 3.7). Consequently, the January sediment would contain fewer aromatic organics than the already oxic May and September sediment, desorbing less during the incubations. Overall, the effect of microbial DOM processing seems to be the dominant mechanism during rapid anoxic periods in Missisquoi Bay, whereas desorption of oxygenated and aromatic molecules does occur, but to a lesser extent.

Both inorganic and organic P have high adsorptive affinities for oxide minerals and are also released upon reductive dissolution (Baldwin et al., 2005; Celi & Barberis, 2005; Smith et al., 2011). Although the quantification of DOP was not tracked during incubations, the chemical signatures displayed variability between the bottom water with

the incubated core. Increases in unique DOP compounds after reduction (Table C-3.5) can be linked to a combination of desorption and biological release of organic P from mineral dissolution and changes in microbial communities (Ahlgren et al., 2011). Consistent with the bulk DOM, the January sediment was already suboxic and depleted of DOP at the time of collection, releasing proportionally less assigned compounds from the sediment during the incubations (Table C-3.5). However, DOP degradation in January was evident with more HPO_3 KMD pairs in the bottom water and a sizable increase upon reduction (16 pairs in the bottom, 24 after reduction) suggesting the transformations of organic P in the winter could be a source for inorganic P in the spring (Shinohara et al., 2017). Dynamic chemical compositions in the water can also reflect the organic P content in the underlying sediment. In a previous study, mild extractions of Missisquoi Bay sediment revealed the abundance of labile CHOP molecules associated with mineral surfaces (see Ch 2) possibly related to the increase in released CHOP compounds from these experiments (Table C-3.5). All DOP compositions shifted to lower mass and DBE distributions following reduction (data not shown), much like the commonly ionized bulk DOM indicating a similar biological mechanism for DOP release, stronger than the effect of desorption. Variability in overall DOP composition between reduced samples is likely due to different biological transformations in the sediment and particulate deposition over the course of the bloom season manifesting in changes in the molecular compositions (Giles et al., 2015). Further quantitative and structural analysis is needed to assess trends in DOP mobility during anoxic periods.

A holistic approach to DOM and DOP cycling in Missisquoi Bay:

Raw mass spectra are information-dense. They contain data regarding bulk ionization and molecular signatures from each sample but make larger scale relationships between multiple samples difficult to conceptualize. Combining water column, source (river and cyanobacteria), and empirical (incubations) data through ordination provides a holistic visualization of how DOM is processed and transferred through time in Missisquoi Bay. Non-metric multidimensional scaling (NMDS) was chosen to construct a "seasonal map" of Missisquoi Bay DOM, in part due to its ecological robustness and the minimal assumptions it makes regarding the distribution and linearity of the input data (Paliy & Shankar, 2016). Many of the same distinguishing characteristics of each sample can be seen when multiple variables are collapsed into two dimensions, particularly between samples in negative (Figure 3.11A) and positive (Figure 3.11B) ionization modes. In ESI negative, May is clearly distinct from the September and January by NMDS2 which corresponds to variables consistent with terrestrial DOM (e.g. higher AI, DBE, O/C etc.). May DOM is also spread along NMDS1 with the top water being more influenced by organic N and P content, similar to 2.0 and 3.0 m samples from September. Progressing to September and January up NMDS2, the samples are more driven by S and N-containing compounds, as well as higher H/C ratios, especially in January which has greater contributions from sulfurized compounds. Here again the riverine influence on the top and 1.0 m samples is apparent and illustrates the differences in DOM signatures through the water column as 2.0 and 3.0 m are more driven by heteroatom content consistent with the excursion of fDOM (Table C-3.2), TRII values (Figure 3.8) and increase in protein molecules (Figure 3.7). In contrast, the biplot for ESI positive

expresses more of the compositional differences between the samples (Figure 3.11B). The high amount of CHO compounds and diverse DOP assignments are reflected in May along NMDS1, also with high atomic N/P and P/C ratios. In contrast, September is characteristic of more oxygenated compounds originating from the river and CHON/CHOP molecules pushing September further away along NMDS1. January is more distinct from September in ESI positive than negative, again influenced by higher H/C and S/C ratios but also reflecting more microbial signatures represented by the cyanobacterial extract.

In general, both ionization modes convey a progression of DOM from May to January with a shift away from terrestrial CHO compounds to more labile CHOS molecules with higher H/C ratios. September and January are compositionally similar, at least when compared against May, but September still contains a significant contribution from terrestrial/riverine DOM despite its unique N and P-molecular content. Interestingly, both ordinations indicate that the bottom water in January is more like the top, 1.0 m, and bottom water from September than the same water column in January. This could be due to the redox conditions in January at the time of sampling. The bottom water in January was less oxic (53% oxygen saturation), had significantly higher concentrations of truly dissolved Mn and colloidal Fe than in September, and comparable amounts of fDOM to the September surface and bottom. The suboxic conditions could have prompted the long-term reductive dissolution of poorly crystalline Mn(IV) and Fe(III) (oxy)hydroxides releasing terrestrial DOM compositionally similar to September into the bottom water that was previously bound to minerals and metal complexes (Christl & Kretzschmar, 2007; Riedel et al., 2012; Riedel et al., 2013; Dadi et al., 2017).

In contrast, reductive incubations of the bottom water cores create short-term, highly anoxic conditions resulting in more reductive dissolution (Figure C-3.2) with varying effects on the DOM composition, but generally overshadow the desorption effect with increases in the lability and microbial signatures (see previous section). Holistically speaking, this is especially evident in ESI positive and in a biplot of common ions combined from both ionization modes where both September and January reduced water move further away from their bottom water starting compositions and closer to the microbial extract endmember (Figure 3.11B, Figure C-3.6). Therefore, the reducing conditions in the water column experienced during a rapid oxygen-depletion event (such as a bloom) are different than long term reduction from suboxic conditions in the winter (Shukle, personal communication.) and are reflected in the analyzed DOM compositions. Although reduction does change the DOM and DOP compositions in May, it is less significant than in the other months. Differences in May sediment reactivity are likely due to a combination of environmental conditions at the time of collection and experimental factors during incubation. Differences in benthic geochemical composition and microbial efficiency prior to the bloom season (Smith et al., 2011; Giles et al., 2015; Giles et al., 2016) as well as sedimentation from the spring runoff season (Rosenberg & Schroth, 2017) could contribute to the sediment's capacity for DOM release. Similarly, experimental variations in DOM expression during the incubations are also possible due to weaker reducing conditions seen from the lower amounts Mn(II) and Fe(II) above the SWI (Figure C-3.2A).

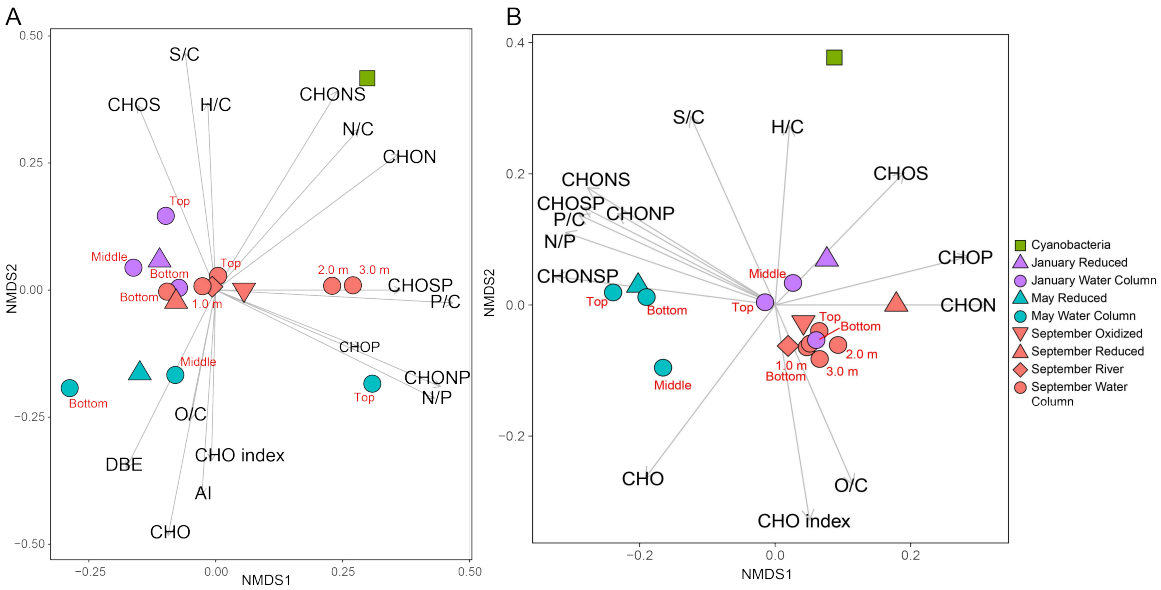

Figure 3.11. NMDS biplots of water samples from this study using data obtained from individual mass spectra. Distances calculated using Bray-Curtis dissimilarity matrices (k=2, stress < 0.1) for samples in (A) ESI negative and (B) ESI positive.

Ionization biases and recommendations:

Samples were ionized in both modes to cover the wide range of possible compounds expressed by each mode and to improve detection of aliphatic and carbohydrate-like molecules (Ohno et al., 2016). Ionization efficiencies varied between negative and positive, but overall produced more assignments in negative partly due to adduct formation in positive spectra (Sleighter & Hatcher, 2007). The quality of DOM from each ionization mode was quite different with ESI positive selecting for more N-containing molecules and aliphatics while negative was enriched in aromatic and carboxylic groups (Sleighter & Hatcher, 2007; Ohno et al., 2016). When samples were compared within each ionization mode, ESI negative generally highlighted the similarities between samples, while ESI positive displayed the uniqueness of samples, probably due to the conserved nature of aromatic DOM ionized in negative, while the labile, biological signatures were highly varied in positive depending on their source

(Figure 3.2, 3.5). This is also seen in figure 3.11A where the riverine DOM and September surface DOM are located near the origin of the vectors in negative, suggesting they represent the average composition of the variables, whereas the seasonal clusters in figure 3.11B are more distinct in positive and further from the origin, driven more by differences.

Perhaps one of the greatest differences between ionization modes was seen in the distribution of DOP compounds (Figure 3.3, 3.6). In general, negative mode resulted in more unsaturated N- and S-containing DOP compounds, while positive mode ionized mostly saturated CHOP compounds, except in May (see discussion above). DOP compounds are not ionized efficiently in ESI, especially when in complex mixtures and competing for charge with other highly-ionizable compounds (Cooper et al., 2005). However, analysis of these molecules using ESI-FT-ICR MS in aquatic systems has still been successful (e.g. Llewelyn et al., 2002; Sleighter et al., 2009; Brooker et al., 2018). In this study, solid phase extraction efficiencies of model DOP compounds was low (3.5-41.7%) owing to the selectivity of PPL columns for non-polar molecules (Li et al., 2016). However, G1P and PPA were detected in ESI negative meaning this method could be used to detect certain biologically relevant DOP compounds. The ionization efficiency differences of the standards between positive and negative further illustrate the diverse quality of DOP compounds each method reveals, especially in natural waters when ion suppression from DOM adds another level of analytical complexity. Some studies have reported greater detection of DOP using ESI negative (e.g. Gonsior et al., 2011; Minor et al., 2012; Ohno et al., 2016) and thus used to justify analysis of DOP solely using ESI negative (see Brooker et al., 2018). However, this only holds true if the assumption is

made that all DOM and DOP is homogeneous, which is not the case. For instance, Gonsior et al. (2011) only detected CHOP and CHOS molecules in marine water using ESI negative, whereas both classes were abundant in ESI positive in freshwater Missisquoi Bay (Figure 3.5, 3.6). Therefore, the decision of whether to ionize DOP compounds in positive or negative mode will depend on the DOM composition and chemical properties of the sample, potentially yielding different distributions and shared compounds between the two modes. Both ionizations should be considered and analyzed for a particular sample matrix to select the best way to represent the DOP distribution in natural waters.

Conclusion:

In short, DOM in May 2017 was characterized by abundant terrestrial signatures and the beginnings of a shift towards algal DOM compositions with many unique DOP compounds. The progression through the summer bloom period transformed much of the DOM and DOP resulting in more heteroatom-containing DOM with strong similarities to riverine input. The transition into winter resulted in less dramatic transformations of existing DOM with bottom suboxic water retaining many of the same late summer terrestrial signatures, but more diverse molecules with higher atomic S content above the suboxic transition zone, likely due to a shift towards heterotrophy. While the bulk DOM shared many of the same ions spatially and seasonally, a significant number of unique compounds were produced in each sample. In contrast, DOP was highly dissimilar, spatially and temporally, indicating a compartmentalized water column in terms of P cycling and a greater amount of terrestrial degradation in the surface water compared to

the non-P-containing molecules. Overall DOM composition in Missisquoi Bay is strongly influenced by both allochthonous and autochthonous sources that are transformed through both biological processing and abiotic mechanisms such as photodegradation and sorption. These transformations couple the cycles of aquatic carbon, phosphorus, and iron demonstrating the power of redox-driven physical and chemical reactions in terrestrial waters.

References:

Ahlgren, J., Reitzel, K., De Brabandere, H., Gogoll, A., & Rydin, E. (2011). Release of organic P forms from lake sediments. *Water research*, *45*(2), 565-572.

Ahlgren, J., Tranvik, L., Gogoll, A., Waldebäck, M., Markides, K., & Rydin, E. (2005). Sediment depth attenuation of biogenic phosphorus compounds measured by ^{31}P NMR. *Environmental Science & Technology*, *39*(3), 867-872.

Bai, X. L., Zhou, Y. K., Sun, J. H., Ma, J. H., Zhao, H. Y., & Liu, X. F. (2015). Classes of dissolved and particulate phosphorus compounds and their spatial distributions in the water of a eutrophic lake: a ^{31}P NMR study. *Biogeochemistry*, *126*(1-2), 227-240.

Baldwin, D. S. (2013). Organic phosphorus in the aquatic environment. *Environmental Chemistry*, *10*(6), 439-454.

Baldwin, D., Howitt, J., & Beattie, J. (2005). Abiotic degradation of organic phosphorus compounds in the environment. In *Organic phosphorus in the environment* (pp. 75-88). Wallingford, UK: CABI Publishing.

Bittar, T. B., Stubbins, A., Vieira, A. A., & Mopper, K. (2015a). Characterization and photodegradation of dissolved organic matter (DOM) from a tropical lake and its dominant primary producer, the cyanobacteria Microcystis aeruginosa. *Marine Chemistry*, *177*, 205-217.

Bittar, T. B., Vieira, A. A., Stubbins, A., & Mopper, K. (2015b). Competition between photochemical and biological degradation of dissolved organic matter from the cyanobacteria Microcystis aeruginosa. *Limnology and Oceanography*, *60*(4), 1172-1194.

Bowling, L. C., Blais, S., & Sinotte, M. (2015). Heterogeneous spatial and temporal cyanobacterial distributions in Missisquoi Bay, Lake Champlain: an analysis of a 9 year data set. *Journal of Great Lakes Research*, *41*(1), 164-179.

Brendel, P. J., & Luther, G. W. I. (1995). Development of a gold amalgam voltammetric microelectrode for the determination of dissolved Fe, Mn, O2, and S (-II) in porewaters of marine and freshwater sediments. *Environmental Science & Technology*, *29*(3), 751-761.

Broberg, O., & Persson, G. (1988). Particulate and dissolved phosphorus forms in freshwater: composition and analysis. *Hydrobiologia*, *170*(1), 61-90.

Brooker, M. R., Longnecker, K., Kujawinski, E. B., Evert, M., & Mouser, P. J. (2018). Discrete Organic Phosphorus Signatures are Evident in Pollutant Sources within a Lake Erie Tributary. *Environmental science & technology*, *52*(12), 6771-6779.

Cade-Menun, B. J. (2005). Characterizing phosphorus in environmental and agricultural samples by ^{31}P nuclear magnetic resonance spectroscopy. *Talanta*, *66*(2), 359-371.

Celi, L., & Barberis, E. (2005). Abiotic stabilization of organic phosphorus in the environment. In *Organic phosphorus in the environment* (pp. 113-132). Wallingford, UK: CABI Publishing

Červený, J., Sinetova, M., Zavřel, T., & Los, D. (2015). Mechanisms of high temperature resistance of Synechocystis sp. PCC 6803: an impact of histidine kinase 34. *Life*, *5*(1), 676-699.

Chassé, A. W., & Ohno, T. (2016). Higher molecular mass organic matter molecules compete with orthophosphate for adsorption to iron (oxy) hydroxide. *Environmental science & technology*, *50*(14), 7461-7469.

Christl, I., & Kretzschmar, R. (2007). C-1s NEXAFS spectroscopy reveals chemical fractionation of humic acid by cation-induced coagulation. *Environmental science & technology*, *41*(6), 1915-1920.

Cooper, W. T., Llewelyn, J. M., Bennett, G. L., Stenson, A. C., & Salters, V. J. (2005). Organic phosphorus speciation in natural waters by mass spectrometry. In *Organic phosphorus in the environment* (pp. 45-74). Wallingford, UK: CABI Publishing.

Coward, E. K., Ohno, T., & Plante, A. F. (2018). Adsorption and Molecular Fractionation of Dissolved Organic Matter on Iron-Bearing Mineral Matrices of Varying Crystallinity. *Environmental science & technology*, *52*(3), 1036-1044.

D'Andrilli, J., Cooper, W. T., Foreman, C. M., & Marshall, A. G. (2015). An ultrahigh-resolution mass spectrometry index to estimate natural organic matter lability. *Rapid Communications in Mass Spectrometry*, *29*(24), 2385-2401.

D'Andrilli, J., Foreman, C. M., Marshall, A. G., & McKnight, D. M. (2013). Characterization of IHSS Pony Lake fulvic acid dissolved organic matter by electrospray ionization Fourier transform ion cyclotron resonance mass spectrometry and fluorescence spectroscopy. *Organic geochemistry*, *65*, 19-28.

Dadi, T., Harir, M., Hertkorn, N., Koschorreck, M., Schmitt-Kopplin, P., & Herzsprung, P. (2017). Redox Conditions Affect Dissolved Organic Carbon Quality in

Stratified Freshwaters. *Environmental science & technology*, *51*(23), 13705-13713.

De Brabandere, H., Forsgard, N., Israelsson, L., Petterson, J., Rydin, E., Waldebäck, M., & Sjöberg, P. J. (2008). Screening for organic phosphorus compounds in aquatic sediments by liquid chromatography coupled to ICP-AES and ESI-MS/MS. *Analytical chemistry*, *80*(17), 6689-6697.

Dittmar, T., & Stubbins, A. (2014). 12.6 - Dissolved organic matter in aquatic systems. In *Treatise on Geochemistry, 2nd edn* (pp. 125-156). Oxford, UK: Elsevier Science.

Dittmar, T., Koch, B., Hertkorn, N., & Kattner, G. (2008). A simple and efficient method for the solid-phase extraction of dissolved organic matter (SPE-DOM) from seawater. *Limnology and Oceanography: Methods*, *6*(6), 230-235.

Einsiedl, F., Hertkorn, N., Wolf, M., Frommberger, M., Schmitt-Kopplin, P., & Koch, B. P. (2007). Rapid biotic molecular transformation of fulvic acids in a karst aquifer. *Geochimica et Cosmochimica Acta*, *71*(22), 5474-5482.

Feng, L., Xu, J., Kang, S., Li, X., Li, Y., Jiang, B., & Shi, Q. (2016). Chemical composition of microbe-derived dissolved organic matter in cryoconite in Tibetan Plateau glaciers: insights from Fourier transform ion cyclotron resonance mass spectrometry analysis. *Environmental science & technology*, *50*(24), 13215-13223.

Giles, C. D., Isles, P. D., Manley, T., Xu, Y., Druschel, G. K., & Schroth, A. W. (2016). The mobility of phosphorus, iron, and manganese through the sediment–water

continuum of a shallow eutrophic freshwater lake under stratified and mixed water-column conditions. *Biogeochemistry*, *127*(1), 15-34.

Giles, C. D., Lee, L. G., Cade-Menun, B. J., Hill, J. E., Isles, P. D., Schroth, A. W., & Druschel, G. K. (2015). Characterization of organic phosphorus form and bioavailability in lake sediments using ^{31}P nuclear magnetic resonance and enzymatic hydrolysis. *Journal of environmental quality*, *44*(3), 882-894.

Gonsior, M., Peake, B. M., Cooper, W. T., Podgorski, D. C., D'Andrilli, J., Dittmar, T., & Cooper, W. J. (2011). Characterization of dissolved organic matter across the Subtropical Convergence off the South Island, New Zealand. *Marine Chemistry*, *123*(1-4), 99-110.

Gonsior, M., Valle, J., Schmitt-Kopplin, P., Hertkorn, N., Bastviken, D., Luek, J., ... & Enrich Prast, A. (2016). Chemodiversity of dissolved organic matter in the Amazon Basin. *Biogeosciences*, *13*(14), 4279-4290.

Hertkorn, N., Ruecker, C., Meringer, M., Gugisch, R., Frommberger, M., Perdue, E. M., ... & Schmitt-Kopplin, P. (2007). High-precision frequency measurements: indispensable tools at the core of the molecular-level analysis of complex systems. *Analytical and bioanalytical chemistry*, *389*(5), 1311-1327.

Hughey, C. A., Hendrickson, C. L., Rodgers, R. P., Marshall, A. G., & Qian, K. (2001). Kendrick mass defect spectrum: a compact visual analysis for ultrahigh-resolution broadband mass spectra. *Analytical Chemistry*, *73*(19), 4676-4681.

Huisman, J., & Hulot, F. D. (2005). Population dynamics of harmful cyanobacteria. In *Harmful cyanobacteria* (pp. 143-176). Dordrecht, NL: Springer.

Isles, P. D., Xu, Y., Stockwell, J. D., & Schroth, A. W. (2017). Climate-driven changes in energy and mass inputs systematically alter nutrient concentration and stoichiometry in deep and shallow regions of Lake Champlain. *Biogeochemistry*, *133*(2), 201-217.

Joung, D., Leduc, M., Ramcharitar, B., Xu, Y., Isles, P. D., Stockwell, J. D., ... & Schroth, A. W. (2017). Winter weather and lake-watershed physical configuration drive phosphorus, iron, and manganese dynamics in water and sediment of ice-covered lakes. *Limnology and Oceanography*, *62*(4), 1620-1635.

Kamjunke, N., Nimptsch, J., Harir, M., Herzsprung, P., Schmitt-Kopplin, P., Neu, T. R., ... & Woelfl, S. (2017a). Land-based salmon aquacultures change the quality and bacterial degradation of riverine dissolved organic matter. *Scientific reports*, *7*, 43739.

Kamjunke, N., von Tümpling, W., Hertkorn, N., Harir, M., Schmitt-Kopplin, P., Norf, H., ... & Herzsprung, P. (2017b). A new approach for evaluating transformations of dissolved organic matter (DOM) via high-resolution mass spectrometry and relating it to bacterial activity. *Water research*, *123*, 513-523.

Kellerman, A. M., Kothawala, D. N., Dittmar, T., & Tranvik, L. J. (2015). Persistence of dissolved organic matter in lakes related to its molecular characteristics. *Nature Geoscience*, *8*(6), 454.

Killberg-Thoreson, L., Sipler, R. E., & Bronk, D. A. (2013). Anthropogenic nutrient sources supplied to a Chesapeake Bay tributary support algal growth: a bioassay and high-resolution mass spectrometry approach. *Estuaries and coasts*, *36*(5), 966-980.

Koch, B. P., Dittmar, T., Witt, M., & Kattner, G. (2007). Fundamentals of molecular formula assignment to ultrahigh resolution mass data of natural organic matter. *Analytical Chemistry*, *79*(4), 1758-1763.

Kujawinski, E. B., Del Vecchio, R., Blough, N. V., Klein, G. C., & Marshall, A. G. (2004). Probing molecular-level transformations of dissolved organic matter: insights on photochemical degradation and protozoan modification of DOM from electrospray ionization Fourier transform ion cyclotron resonance mass spectrometry. *Marine Chemistry*, *92*(1-4), 23-37.

Lalonde, K., Mucci, A., Ouellet, A., & Gélinas, Y. (2012). Preservation of organic matter in sediments promoted by iron. *Nature*, *483*(7388), 198.

Larsson, J. (2018). *eulerr: Area-Proportional Euler and Venn Diagrams with Ellipses*. R package version 4.1.0, https://cran.r-project.org/package=eulerr.

Li, Y., Harir, M., Lucio, M., Kanawati, B., Smirnov, K., Flerus, R., ... & Hertkorn, N. (2016). Proposed guidelines for solid phase extraction of Suwannee River dissolved organic matter. *Analytical chemistry*, *88*(13), 6680-6688.

Llewelyn, J. M., Landing, W. M., Marshall, A. G., & Cooper, W. T. (2002). Electrospray ionization Fourier transform ion cyclotron resonance mass spectrometry of dissolved organic phosphorus species in a treatment wetland after selective isolation and concentration. *Analytical chemistry*, *74*(3), 600-606.

Lovley, D. R. (1991). Dissimilatory Fe (III) and Mn (IV) reduction. *Microbiological reviews*, *55*(2), 259-287.

Ly, Q. V., Maqbool, T., & Hur, J. (2017). Unique characteristics of algal dissolved organic matter and their association with membrane fouling behavior: a review. *Environmental Science and Pollution Research*, *24*(12), 11192-11205.

Mangal, V., Stock, N. L., & Guéguen, C. (2016). Molecular characterization of phytoplankton dissolved organic matter (DOM) and sulfur components using high resolution Orbitrap mass spectrometry. *Analytical and bioanalytical chemistry*, *408*(7), 1891-1900.

Mann, B. F., Chen, H., Herndon, E. M., Chu, R. K., Tolic, N., Portier, E. F., ... & Graham, D. E. (2015). Indexing permafrost soil organic matter degradation using high-resolution mass spectrometry. *PloS one*, *10*(6), e0130557.

Meyers, P. A., & Ishiwatari, R. (1993). Lacustrine organic geochemistry—an overview of indicators of organic matter sources and diagenesis in lake sediments. *Organic geochemistry*, *20*(7), 867-900.

Minor, E. C., Steinbring, C. J., Longnecker, K., & Kujawinski, E. B. (2012). Characterization of dissolved organic matter in Lake Superior and its watershed using ultrahigh resolution mass spectrometry. *Organic Geochemistry*, *43*, 1-11.

Morling, K., Raeke, J., Kamjunke, N., Reemtsma, T., & Tittel, J. (2017). Tracing aquatic priming effect during microbial decomposition of terrestrial dissolved organic carbon in chemostat experiments. *Microbial ecology*, *74*(3), 534-549.

Mostovaya, A., Hawkes, J. A., Dittmar, T., & Tranvik, L. J. (2017). Molecular determinants of dissolved organic matter reactivity in lake water. *Frontiers in Earth Science*, *5*, 106.

Mur, R., Skulberg, O. M., & Utkilen, H. (1999). CYANOBACTERIA IN THE ENVIRONMENT. In *Toxic Cyanobacteria In Water: A Guide To Their Public Health Consequences, Monitoring And Management* (pp. 15-40). CRC Press.

Nazari-Sharabian, M., Ahmad, S., & Karakouzian, M. (2018). Climate change and eutrophication: A short review. *Engineering, Technology and Applied Science Research*, *8*(6), 3668-3672.

O'neil, J. M., Davis, T. W., Burford, M. A., & Gobler, C. J. (2012). The rise of harmful cyanobacteria blooms: the potential roles of eutrophication and climate change. *Harmful algae*, *14*, 313-334.

Ohno, T., Sleighter, R. L., & Hatcher, P. G. (2016). Comparative study of organic matter chemical characterization using negative and positive mode electrospray ionization ultrahigh-resolution mass spectrometry. *Analytical and bioanalytical chemistry*, *408*(10), 2497-2504.

Oksanen, J., Blanchet, F. G., Kindt, R., Legendre, P., Minchin, P. R., O'hara, R. B., ... & Oksanen, M. J. (2013). Package 'vegan'. *Community ecology package, version*, *2*(9).

Paerl, H. W., & Otten, T. G. (2013). Harmful cyanobacterial blooms: causes, consequences, and controls. *Microbial ecology*, *65*(4), 995-1010.

Paliy, O., & Shankar, V. (2016). Application of multivariate statistical techniques in microbial ecology. *Molecular ecology*, *25*(5), 1032-1057.

Reynolds, C. S., & Davies, P. S. (2001). Sources and bioavailability of phosphorus fractions in freshwaters: a British perspective. *Biological reviews*, *76*(1), 27-64.

Riedel, T., Biester, H., & Dittmar, T. (2012). Molecular fractionation of dissolved organic matter with metal salts. *Environmental Science & Technology*, *46*(8), 4419-4426.

Riedel, T., Zak, D., Biester, H., & Dittmar, T. (2013). Iron traps terrestrially derived dissolved organic matter at redox interfaces. *Proceedings of the National Academy of Sciences*, *110*(25), 10101-10105.

Rivas-Ubach, A., Liu, Y., Bianchi, T. S., Tolić, N., Jansson, C., & Paša-Tolić, L. (2018). Moving beyond the van Krevelen Diagram: A New Stoichiometric Approach for Compound Classification in Organisms. *Analytical chemistry*, *90*(10), 6152-6160.

Romano, S., Dittmar, T., Bondarev, V., Weber, R. J., Viant, M. R., & Schulz-Vogt, H. N. (2014). Exo-metabolome of Pseudovibrio sp. FO-BEG1 analyzed by ultra-high resolution mass spectrometry and the effect of phosphate limitation. *PloS one*, *9*(5), e96038.

Rosenberg, B. D., & Schroth, A. W. (2017). Coupling of reactive riverine phosphorus and iron species during hot transport moments: impacts of land cover and seasonality. *Biogeochemistry*, *132*(1-2), 103-122.

Rozan, T. F., Taillefert, M., Trouwborst, R. E., Glazer, B. T., Ma, S., Herszage, J., ... & Luther III, G. W. (2002). Iron-sulfur-phosphorus cycling in the sediments of a shallow coastal bay: Implications for sediment nutrient release and benthic macroalgal blooms. *Limnology and Oceanography*, *47*(5), 1346-1354.

Schroth, A. W., Giles, C. D., Isles, P. D., Xu, Y., Perzan, Z., & Druschel, G. K. (2015). Dynamic coupling of iron, manganese, and phosphorus behavior in water and

sediment of shallow ice-covered eutrophic lakes. *Environmental science & technology*, *49*(16), 9758-9767.

Shinohara, R., Hiroki, M., Kohzu, A., Imai, A., Inoue, T., Furusato, E., ... & Miura, S. (2017). Role of organic phosphorus in sediment in a shallow eutrophic lake. *Water Resources Research*, *53*(8), 7175-7189.

Shinohara, R., Imai, A., Kawasaki, N., Komatsu, K., Kohzu, A., Miura, S., ... & Tomioka, N. (2012). Biogenic phosphorus compounds in sediment and suspended particles in a shallow eutrophic lake: a ^{31}P-nuclear magnetic resonance (^{31}P NMR) study. *Environmental science & technology*, *46*(19), 10572-10578.

Sievert, C. (2018) *plotly for R*. https://plotly-book.cpsievert.me

Sleighter, R. L., & Hatcher, P. G. (2007). The application of electrospray ionization coupled to ultrahigh resolution mass spectrometry for the molecular characterization of natural organic matter. *Journal of Mass Spectrometry*, *42*(5), 559-574.

Sleighter, R. L., McKee, G. A., & Hatcher, P. G. (2009). Direct Fourier transform mass spectral analysis of natural waters with low dissolved organic matter. *Organic Geochemistry*, *40*(1), 119-125.

Smith, L., Watzin, M. C., & Druschel, G. (2011). Relating sediment phosphorus mobility to seasonal and diel redox fluctuations at the sediment–water interface in a eutrophic freshwater lake. *Limnology and Oceanography*, *56*(6), 2251-2264.

Smith, V. H., Tilman, G. D., & Nekola, J. C. (1999). Eutrophication: impacts of excess nutrient inputs on freshwater, marine, and terrestrial ecosystems. *Environmental pollution*, *100*(1-3), 179-196.

Søndergaard, M., Jensen, J. P., & Jeppesen, E. (2003). Role of sediment and internal loading of phosphorus in shallow lakes. *Hydrobiologia*, *506*(1-3), 135-145.

Spencer, R. G., Stubbins, A., Hernes, P. J., Baker, A., Mopper, K., Aufdenkampe, A. K., ... & Six, J. (2009). Photochemical degradation of dissolved organic matter and dissolved lignin phenols from the Congo River. *Journal of Geophysical Research: Biogeosciences*, *114*(G3).

Stubbins, A., Spencer, R. G., Chen, H., Hatcher, P. G., Mopper, K., Hernes, P. J., ... & Six, J. (2010). Illuminated darkness: molecular signatures of Congo River dissolved organic matter and its photochemical alteration as revealed by ultrahigh precision mass spectrometry. *Limnology and Oceanography*, *55*(4), 1467-1477.

Tranvik, L. J., Downing, J. A., Cotner, J. B., Loiselle, S. A., Striegl, R. G., Ballatore, T. J., ... & Kortelainen, P. L. (2009). Lakes and reservoirs as regulators of carbon cycling and climate. *Limnology and Oceanography*, *54*(6 part 2), 2298-2314.

Turner, B. L. (2005). Organic phosphorus transfer from terrestrial to aquatic environments. In *Organic phosphorus in the environment* (pp. 269-294). Wallingford, UK: CABI Publishing.

Uusitalo, R., Turtola, E., Puustinen, M., Paasonen-Kivekäs, M., & Uusi-Kämppä, J. (2003). Contribution of particulate phosphorus to runoff phosphorus bioavailability. *Journal of Environmental Quality*, *32*(6), 2007-2016.

Valle, J., Gonsior, M., Harir, M., Enrich-Prast, A., Schmitt-Kopplin, P., Bastviken, D., Conrad, R., & Hertkorn, N. (2018). Extensive processing of sediment pore water dissolved organic matter during anoxic incubation as observed by high-field mass spectrometry (FTICR-MS). *Water research*, *129*, 252-263.

Vannote, R. L., Minshall, G. W., Cummins, K. W., Sedell, J. R., & Cushing, C. E. (1980). The river continuum concept. *Canadian journal of fisheries and aquatic sciences*, *37*(1), 130-137.

Wagner, S., Riedel, T., Niggemann, J., Vähätalo, A. V., Dittmar, T., & Jaffé, R. (2015). Linking the molecular signature of heteroatomic dissolved organic matter to watershed characteristics in world rivers. *Environmental science & technology*, *49*(23), 13798-13806.

Wang, X., Liu, F., Tan, W., Li, W., Feng, X., & Sparks, D. L. (2013). Characteristics of phosphate adsorption-desorption onto ferrihydrite: comparison with well-crystalline Fe (hydr) oxides. *Soil Science*, *178*(1), 1-11.

Ward, N. D., Keil, R. G., Medeiros, P. M., Brito, D. C., Cunha, A. C., Dittmar, T., ... & Richey, J. E. (2013). Degradation of terrestrially derived macromolecules in the Amazon River. *Nature Geoscience*, *6*(7), 530.

Whitton, B. A., Grainger, S. L. J., Hawley, G. R. W., & Simon, J. W. (1991). Cell-bound and extracellular phosphatase activities of cyanobacterial isolates. *Microbial Ecology*, *21*(1), 85-98.

Wickham, H. (2016). *ggplot2: elegant graphics for data analysis*. Springer.

Zark, M., & Dittmar, T. (2018). Universal molecular structures in natural dissolved organic matter. *Nature communications*, *9*(1), 3178.

Zhang, F., Harir, M., Moritz, F., Zhang, J., Witting, M., Wu, Y., ... & Hertkorn, N. (2014). Molecular and structural characterization of dissolved organic matter during and post cyanobacterial bloom in Taihu by combination of NMR spectroscopy and FTICR mass spectrometry. *Water research*, *57*, 280-294.

Coda

An approach using traditional geochemical techniques (sediment extractions, electrochemistry, SONDE profiling etc.) was combined with Fourier Transform-Ion Cyclotron Resonance Mass Spectrometry (FT-ICR MS) for a high-resolution study of the organic matter and organic P compositions of Missisquoi Bay, VT. Specifically, the objective of this project was to qualitatively assess the potential contributions of organic P to the labile P fraction and the role of seasonal abiotic and biotic processes in cycling the dissolved organic matter in a eutrophic basin, both through internal and external loading. The sediment was found to contain a variety of labile and some recalcitrant organic compounds through parallel chemical extractions. Stronger chemical extractants (strong acid/base) afforded both organic matter and organic P that were associated with mineral phases and considered more refractory. Extractions with milder reagents (acetic acid/$NaHCO_3$) selected for more labile molecules associated with microbially-derived compounds. Additionally, the milder reagents extracted greater amounts of organic P formulae than the stronger extractants, revealing lipid-like compounds that could mobilize into the water column from the sediment thereby providing a source of bioavailable P. By identifying a subset of both sedimentary non-P and P-containing molecules after the summer bloom season, these extractions complemented previous work that tracked seasonal changes in organic P classes through the bloom season. This work was also novel from an analytical standpoint, whereby accessible reagents were able to chemically fractionation lake sediment organic matter. Previous studies of organic matter have focused on soil or mineral chemical extractions with limited FT-ICR MS applications to lake sediment. Moreover, these fractionations allow the investigator to

select extractants to study specific organic matter functionalities (i.e. HCl for resistant terrestrial material, $NaHCO_3$ for labile compounds).

As the bay experienced physical changes from the progression of seasons, so too did the overall organic matter follow in chemical and compositional diversity. Both the organic P and the bulk DOM displayed an evolution from being mostly terrestrial in late spring to biolabile and of aquatic origin by midwinter. The most dramatic changes occurred between the spring runoff and the late summer bloom period, accompanied by the appearance of many N and S-containing compounds and homogeneity within the water column. However, the progression from September to January was less severe with many of the same compounds shared between the two sampling points and a gain in organic matter aliphaticity and overall lability. Potential sources in the form of riverine water (external) and cyanobacterial DOM (internal) were compared to the organic signatures in September to evaluate relative contributions. Riverine water shared most of its assignments with the surface water and decreased with commonality towards the bottom, particularly with organic P which had lost almost all shared compounds through the water column. Cyanobacteria also shared strong similarities with the surface water but afforded many unique molecules not seen in the natural water, suggesting cell presence and eventual death yields a significant pool of both reactive and more labile organic molecules. Sediment cores were collected at each season and subjected to short-term anoxic incubations to better understand the mobility of DOM and organic P during oxygen-depletion events, such as blooms. The incubations resulted in mixed chemical signatures with both desorption and biological processing affecting the overall organic geochemistry, though the latter process was more dominant. These combined samples

and experiments offered a unique glimpse into the seasonal cycling of organic species within a eutrophic lake. To date, this is the first study to emphasize FT-ICR MS analysis of organic P compounds within a shallow lake, both spatially and temporally, in both electrospray ionization modes. This work also synthesizes many different analytical procedures to provide complementary geochemical information, such as coupling FT-ICR MS for organic speciation to electrochemistry for monitoring redox conditions.

These combined chapters culminated in a greater understanding of the quality and mobility of both the organic matter and organic P within Missisquoi Bay, enriching an extensive body of literature. They also provide a solid foundation for future work within Missisquoi Bay and many other similar freshwaters around the world. While the chemical formulas of organic P were well defined, future work would benefit from combining FT-ICR MS spectra with ^{31}P NMR analysis to gain structural information of the dissolved water column fraction as well as including quantitative measurements of organic and inorganic P concentrations to monitor lability and bioavailability. The particulate fraction should also be addressed by extracting seston left over on the filters after passing through sampled water and analyzing them with FT-ICR MS to compare with the dissolved fraction. This comparison could identify a previously unknown pool of hydrophobic organic P associated with particles and microbial surfaces, supplying orthophosphate into the water column during times of high productivity or settling to the bottom and adding to the redox-active organic P. Additionally, the organic compositions of the watershed may provide evidence for the loading of specific organic P compounds into the bay and their potential to supply orthophosphate to microorganisms. Since the watershed is composed of urban, agricultural, and forested areas supplying nutrient loading through

three rivers (see Ch 1), organic P is expected to be quite diverse; however, much is still unknown about the stability of these molecules during transport. In the sediment, a sequential extraction protocol to isolate organic P and organic matter by their chemical functionality (see Ch 2) with minimal overlap between fractions while maintaining the porewater species would be beneficial to many different limnological studies. Isolating subsets of each fraction by precipitating thiols, sulfates, and phosphate groups with metal cations would add greater certainty in identifying organic matter functional groups and could reveal previously occluded compounds that were unavailable due to ion suppression in electrospray ionization.

Consequently, the work in these presented chapters displays clear intellectual originality and a high degree of applicability to further work on Missisquoi Bay and various other freshwater ecosystems.

Appendix A

Procedure for extracting and analyzing freshwater DOM with FT-ICR MS.

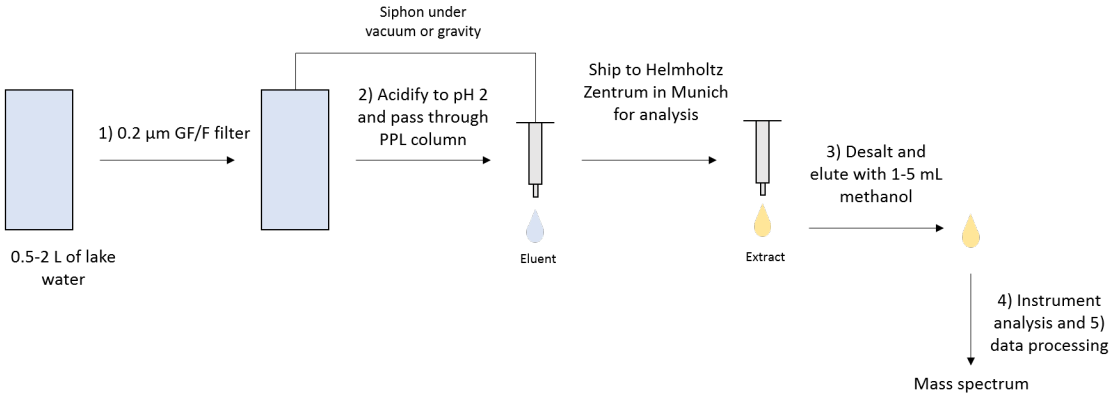

1) Water is immediately filtered through an oven baked (5 h at 450 °C) glass fiber filter (0.2 µm).
2) Filtered water is acidified to pH 2 using HCl and passed through a PPL column to concentrate and desalt the DOM.
3) The column is rinsed, dried, and the bound DOM is eluted with methanol as the extract.
4) The extract is diluted as necessary and introduced to the instrument through ESI.
5) Ion counts are acquired and result in a mass spectrum after proper calibration.

Appendix B

Supplemental figures and tables for chapter 2.

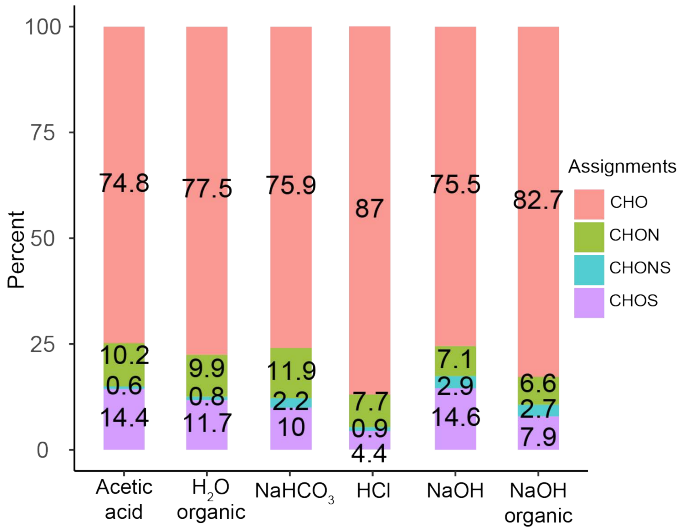

Figure B-2.1. Bar charts depicting percent composition of non-P-containing molecules from each extraction. Values are computed percentages relative to the total assigned non-P-containing formulae.

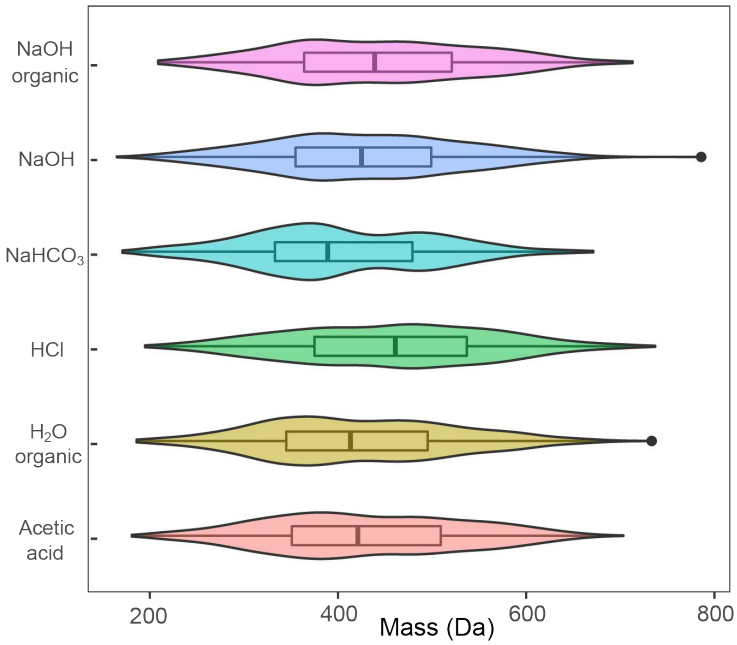

Figure B-2.2. Violin plots of the measured mass distribution from the non-P-containing assigned molecules. Box plots are embedded in the violin plot and represent the median with associated interquartile range (IQR).

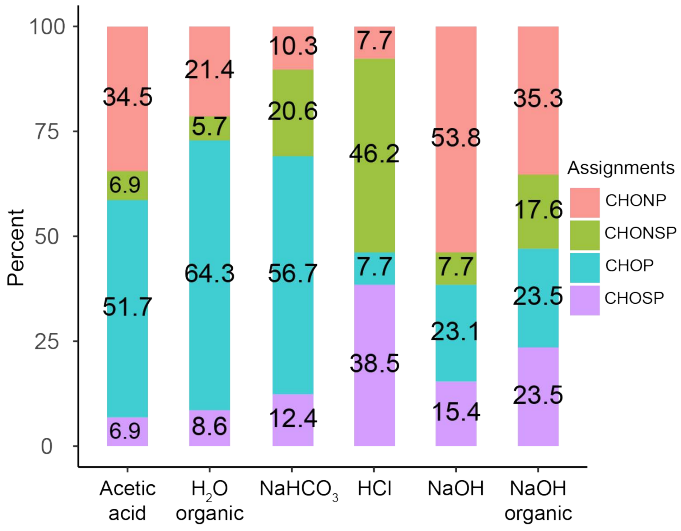

Figure B-2.3. Bar charts depicting percent composition of P-containing molecules from each extraction. Values are computed percentages relative to the total assigned P-containing formulae.

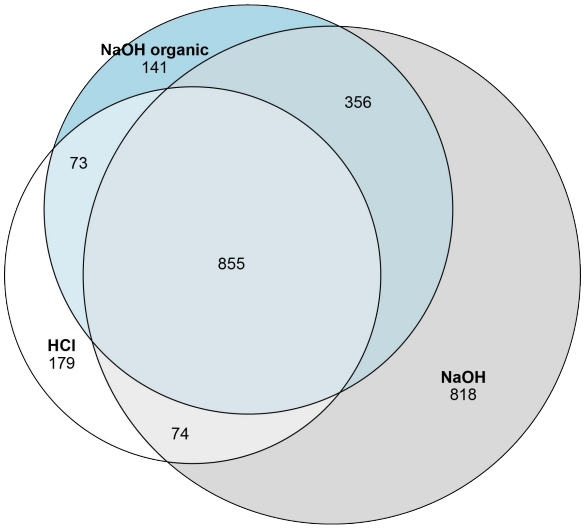

Figure B-2.4. Triple Venn diagram of non-P-containing assigned molecules for the HCl, NaOH, and organic NaOH extracts. Circle areas are scaled to total assignments and numbers represent assigned molecular formulae. The figure was generated using the eulerr R package (Larsson, 2018).

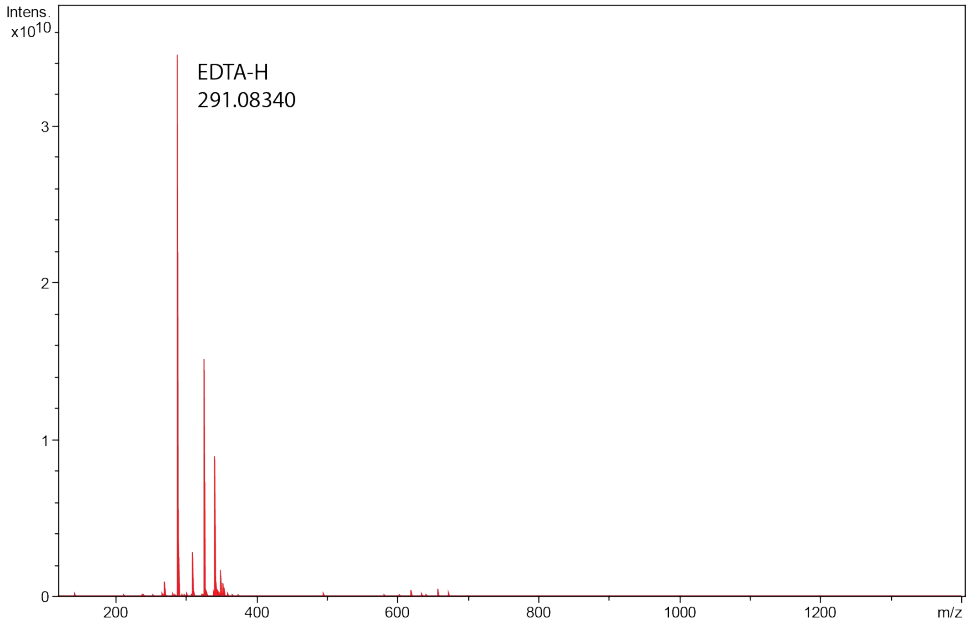

Figure B-2.5. ESI negative mass spectrum of Missisquoi Bay sediment extracted with 0.5 M NaOH and 0.025 M EDTA. The EDTA ion is present at m/z 291.08340.

Sample	**Acetic acid**	**H_2O organic**	**HCl**	**$NaHCO_3$**	**NaOH**
H_2O organic	1103 (27.6%)				
HCl	586 (16.4%)	138 (5.0%)			
$NaHCO_3$	782 (22.3%)	862 (31.8%)	80 (3.5%)		
NaOH	1274 (28.3%)	581 (15.7%)	929 (28.3%)	440 (13.7%)	
NaOH organic	782 (20.4%)	261 (8.6%)	928 (35.6%)	177 (7.0%)	1211 (34.3%)

Table B-2.1. Pairwise similarities of non-P-containing molecules from each extraction. Numbers indicate total shared assigned formulae between any two samples. Numbers in () indicate the percentage of shared assigned formulae between any two samples.

Sample	Mean M/Z	Median M/Z	SD M/Z	Mean H/C	Median H/C	Mean O/C	Median O/C	Mean AI	Median AI	Mean DBE	Median DBE
H_2O organic	422.1155	413.3273	102.1086	1.52	1.53	0.35	0.33	-0.19	-0.09	12.60	12
HCl	455.9055	461.0573	107.5681	0.82	0.78	0.67	0.67	-0.34	0.00	25.44	24
$NaHCO_3$	401.765	389.1606	97.36321	1.56	1.57	0.34	0.33	-0.20	-0.10	11.72	12
NaOH organic	442.7791	438.9943	104.8972	0.88	0.83	0.61	0.61	-0.16	0.00	24.18	24
NaOH	427.191	425.015	102.3387	1.04	0.96	0.56	0.56	-0.20	-0.08	20.88	20
Acetic acid	429.2715	421.1174	104.9322	1.33	1.36	0.45	0.44	-0.18	-0.13	16.12	16

Table B-2.2. Computed average values of molecular properties from the non-P-containing molecules. M/Z is the measured mass/charge reported in Daltons (Da), SD represents 1σ standard deviation.

Sample	**Acetic acid**	**H_2O organic**	**HCl**	**$NaHCO_3$**	**NaOH**
H_2O organic	7 (7.0%)				
HCl	1 (2.4%)	1 (1.2%)			
$NaHCO_3$	7 (5.6%)	12 (7.2%)	1 (0.9%)		
NaOH	1 (2.4%)	0 (0%)	0 (0%)	0 (0%)	
NaOH organic	2 (4.3%)	2 (2.3%)	0 (0%)	2 (1.8%)	1 (3.3%)

Table B-2.3. Pairwise similarities of P containing molecules from each extraction. Numbers indicate total shared assigned formulae between any two samples. Numbers in () indicate the percentage of shared assigned formulae between any two samples.

Sample	Mean M/Z	Median M/Z	SD M/Z	Mean H/C	Median H/C	Mean O/C	Median O/C	Mean AI	Median AI	Mean DBE	Median DBE
H_2O organic	471.1866	472.2126	110.8051	1.66	1.67	0.37	0.36	-0.83	-0.29	11.43	10
$NaHCO_3$	472.111	469.1997	113.616	1.62	1.65	0.38	0.36	-0.84	-0.21	12.56	10
Acetic acid	441.1407	431.1841	106.9601	1.56	1.61	0.34	0.32	-0.50	-0.14	13.45	12
HCl	583.897	573.0544	108.1734	1.03	1.10	0.51	0.44	-1.09	0.00	28.62	24
NaOH	469.7053	471.0487	63.96969	1.08	0.96	0.42	0.43	0.07	0.36	23.85	26
NaOH organic	484.1207	481.0807	108.4136	0.91	0.87	0.41	0.43	0.33	0.31	27.88	28

Table B-2.4. Computed average values of molecular properties from the P containing molecules. M/Z is the measured mass/charge reported in Daltons (Da), SD represents 1σ standard deviation.

Appendix C

Supplemental figures and tables for chapter 3.

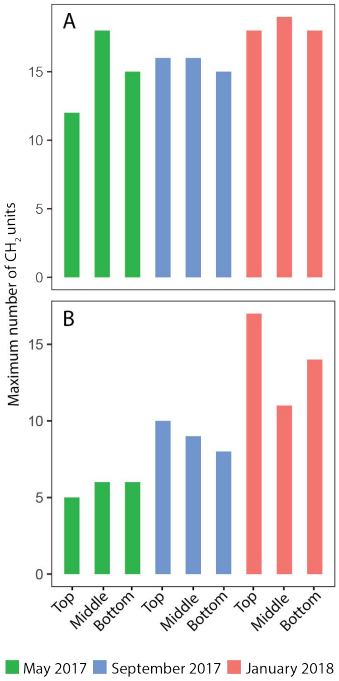

Figure C-3.1. Bar plots depicting CH_2-based Kendrick mass defect analysis of water column DOM from Missisquoi Bay in ESI negative. Bar height indicates the maximum number of molecules in a CH_2-based homologous series for (A) CHO compounds and (B) CHOS compounds.

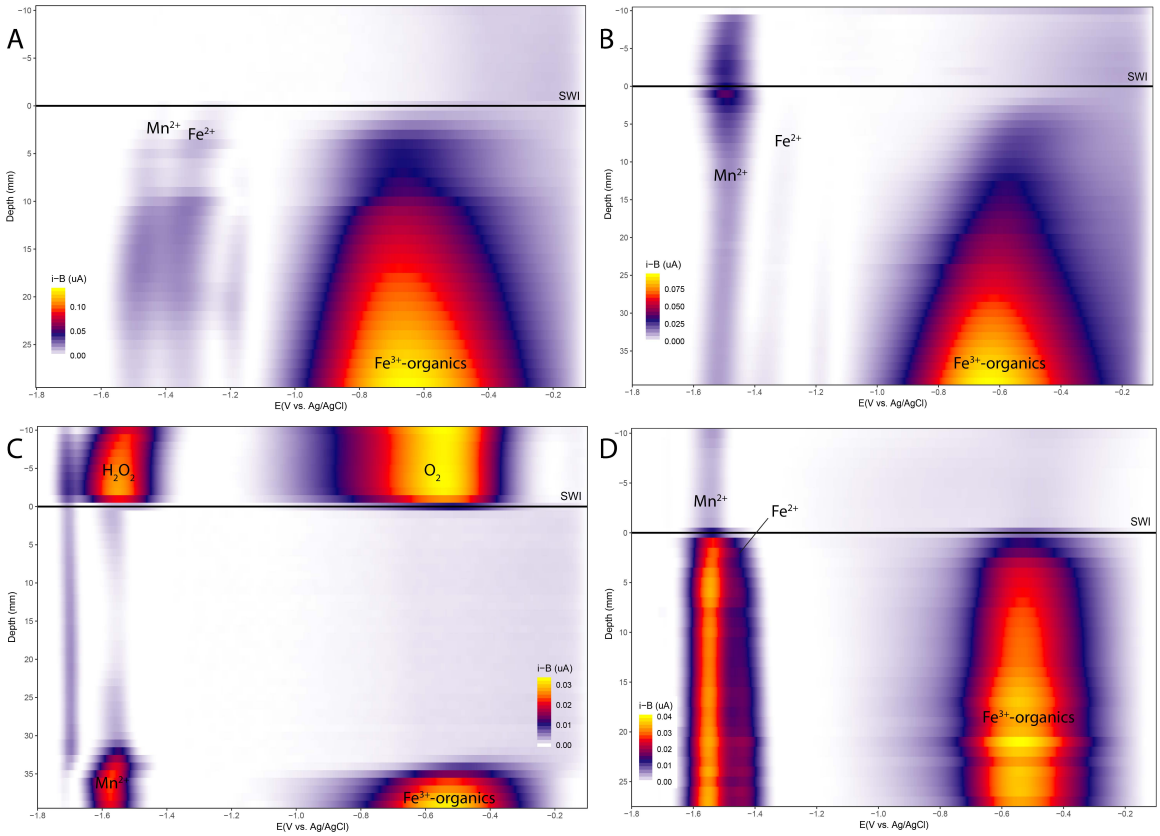

Figure C-3.2. Heat maps of electroactive chemical species from profiled Missisquoi Bay sediment cores. Colors are scaled to measured current intensity which is proportional to chemical concentration. Chemical species are electroactive on the Hg-amalgam at a specific potential referenced to a Ag/AgCl electrode; for details see Brendel and Luther (1995). The sediment-water interface (SWI) is depicted by a solid black line at depth=0. Profiles correspond to (A) reducing, May 2017; (B) reducing, September 2017; (C) oxic, September 2017; (D) reducing, January 2018.

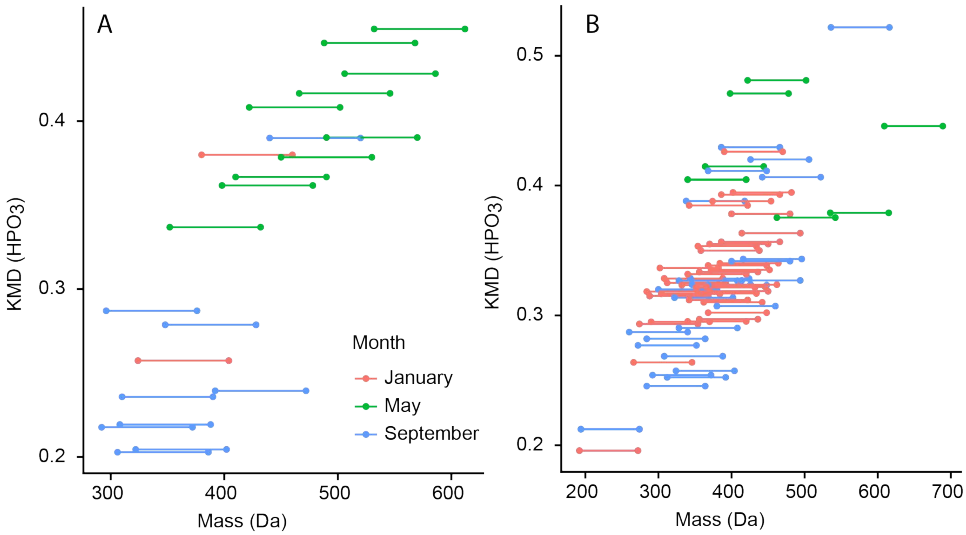

Figure C-3.3. HPO_3-based Kendrick mass defect analysis of all water samples taken from Missisquoi Bay. Connecting lines indicate a DOP molecule and a potential precursor in (A) ESI negative and (B) ESI positive.

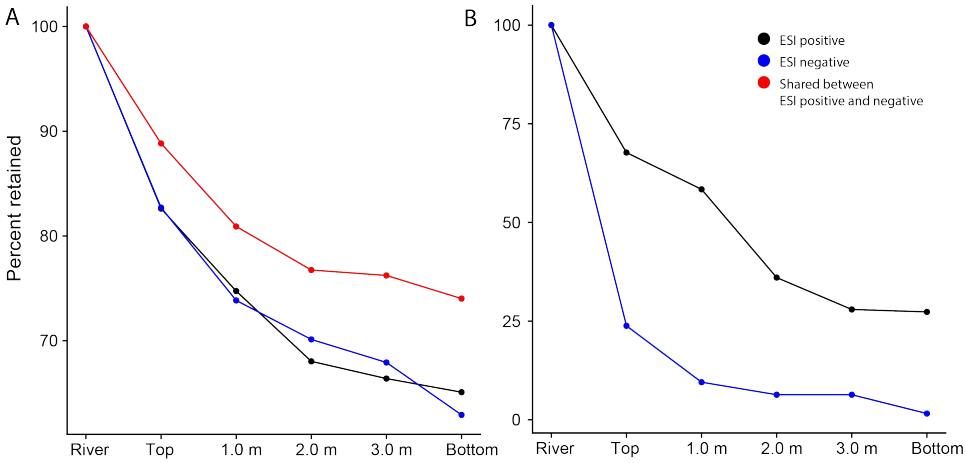

Figure C-3.4. Percent of original riverine DOM assignments present in the September water column at each depth for (A) Non-P-containing formulae and (B) P-containing formulae.

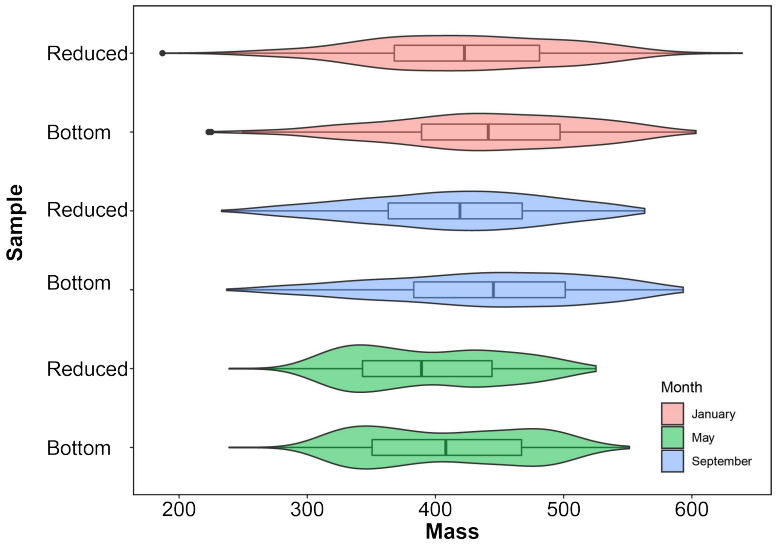

Figure C-3.5. Violin-box plots of the mass distribution of ions common to both ESI negative and positive before (Bottom) and after (Reduced) incubations. Box plots are embedded in the violin plot and represent the median with associated interquartile range (IQR).

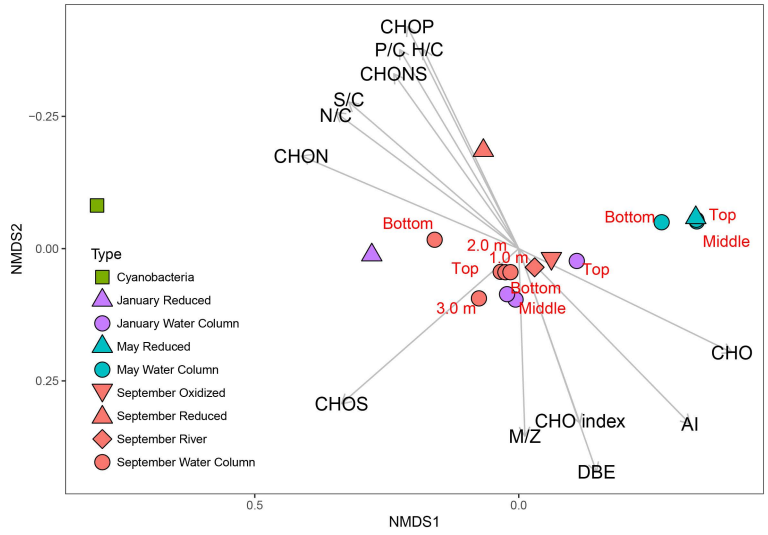

Figure C-3.6. NMDS biplot of water samples with ions found in both ESI negative and positive from this study using data obtained from individual mass spectra. Distances calculated using Bray-Curtis dissimilarity matrices (k=2, stress < 0.1).

Depth (m)	Temp (ºC)	pH	ODO%	ODO (mg/L)	Chlorophyll-a (RFU)	Chlorophyll-a (µg/L)	BGA (RFU)
0.014	15.91	8.25	113.6	11.23	1.6	6.7	0.6
0.107	15.93	8.25	113.6	11.22	1.6	6.9	0.6
0.383	15.86	8.25	113.9	11.27	1.6	6.7	0.5
0.392	15.95	8.25	113.8	11.24	1.7	7	0.6
0.839	15.69	8.26	113.5	11.28	2.3	9.6	0.7
0.886	15.69	8.26	113.2	11.24	2.3	9.6	0.6
1.397	15.56	8.26	113.2	11.27	2.6	11	0.8
1.401	15.55	8.26	113.3	11.28	2.7	11.2	1
1.89	15.2	8.2	111.5	11.19	2.5	10.3	0.8
1.907	15.18	8.2	111.5	11.2	2.4	10.1	0.9
2.476	14.9	8.09	109.1	11.02	2	8.2	0.7
2.498	14.88	8.07	109	11.02	2.1	8.6	0.7
3.017	14.74	7.98	106.9	10.83	1.7	7.1	0.5
3.036	14.74	7.97	106.5	10.8	1.7	7.2	0.5
3.511	14.19	7.73	95.5	9.79	1.8	7.6	0.6

Table C-3.1. Manual SONDE data collected in May 2017. Optical dissolved oxygen (ODO) is recorded in concentration units (mg/L) and percent saturation (%). Blue green algae (BGA) is reported in relative fluorescent units (RFU) of phycocyanin and was not calibrated to concentrations (µg/L) at time of collection.

Depth (m)	Temp (ºC)	pH	ODO%	ODO (mg/L)	Chlorophyll -a (RFU)	Chlorophyll -a (µg/L)	BGA (RFU)	BGA (µg/L)	fDOM (QSU)
0.168	17.469	8.21	100	9.09	0.04	0.16	0.51	0.37	1.49
0.218	19.993	7.73	100.3	9.59	0.02	0.22	0.42	0.44	2.01
0.296	17.323	8.49	107.7	10.34	0.78	2.59	0.23	0.2	64.89
0.515	17.244	8.35	109.2	10.5	0.94	3.12	0.25	0.22	65.26
1.298	16.864	8.25	107.2	10.38	1.07	3.52	0.15	0.13	67.29
1.838	16.612	8.06	97	9.45	0.47	1.59	0.04	0.04	74.98
2.32	16.532	7.96	95.7	9.34	0.12	0.49	0	0.01	75.78
2.801	16.43	7.87	94.5	9.24	0.08	0.34	-0.01	0	74.41
3.02	16.407	7.82	92.7	9.07	0.08	0.37	0	0.01	74
3.152	16.399	7.74	92.2	9.02	0.46	1.56	0.11	0.1	54.35

Table C-3.2. Manual SONDE data collected in September 2017. Optical dissolved oxygen (ODO) is recorded in concentration units (mg/L) and percent saturation (%). Blue green algae (BGA) and fluorescent dissolved organic matter (fDOM) are included.

Depth (m)	Temp (ºC)	pH	ODO%	ODO (mg/L)	Chlorophyll -a (µg/L)	BGA (µg/L)	fDOM (QSU)
0.092	-0.472	5.94	101.7	15.05	0	1.19	2.27
0.427	0.038	7.15	99.4	14.51	0	0	40.99
0.829	0.028	7.18	98.8	14.43	0	0	40.55
1.361	0.051	7.21	98.3	14.35	0	0	40.74
1.808	0.326	7.23	97.5	14.12	0	0	42.52
2.356	1.567	7.24	93.8	13.13	0	0	57.86
2.806	2.575	7.23	73.3	9.97	0	0	56.59
2.876	2.707	7.18	63.7	8.64	0	0	56.1
2.877	2.703	7.16	61.7	8.37	0	0	55.97
2.896	2.944	7.13	59.6	8.03	0	0	41.47
2.899	2.991	7.12	57.4	7.72	0	0	53.09
2.897	2.976	7.09	55.2	7.44	0	0	54.14
2.923	3.038	7.08	53.4	7.18	0	0	54.47
2.923	3.039	7.08	53.4	7.18	0	0	54.49

Table C-3.3. Manual SONDE cast collected in January 2018. Optical dissolved oxygen (ODO) is recorded in concentration units (mg/L) and percent saturation (%). Blue green algae (BGA) and fluorescent dissolved organic matter (fDOM) are included.

	Lipid-like	Oxy-aromatic
ESI negative		
May 2017	9.546510 / 9.661448	10.721038/ 10.919225
September 2017	8.164625 / 9.031749	9.504273 / 9.801926
January 2018	8.900784 / 9.233204	10.211237 / 10.171121
ESI positive		
May 2017	10.620676 / 11.640433	11.396202 / 11.190034
September 2017	9.232678 / 9.633901	9.629550 / 9.123812
January 2018	9.773516 / 10.131157	10.463452 / 9.870015

Table C-3.4. Calculated TRII values for lipid-like and oxy-aromatic compounds before and after reduction of sediment cores from Missisquoi Bay. First value indicates bottom water, the following value indicates reduced core water. Note the increase in oxy-aromatics in May and September ESI negative.

	TRII (P-containing)	% CHOP	% CHOSP	% CHONP	% CHONSP	% DOP of total DOM	Ions common with bottom water	Ions produced after reduction
ESI negative								
May 2017	6.155349 / 6.703960	28.6 / 45.5	0 / 0	50.0 / 36.4	21.4 /18.2	0.8 / 1.8	3	30
September 2017	6.074761 / 6.654995	9.8 / 25.9	4.9 / 7.4	53.7 / 44.4	31.7 / 22.2	1.6 / 1.8	7	47
January 2018	6.458641 / 6.381507	10.2 / 25	6.1 / 3.8	42.9 / 44.2	40.8 / 26.9	1.8 / 1.6	5	47
ESI positive								
May 2017	10.343646 / 9.837602	21.1 / 10.0	3.5 / 6.7	30.4 / 29.3	45.0 / 54.0	15.7 / 16.4	36	114
September 2017	7.645945 / 7.413148	84.7 / 93.5	0.6 / 0.6	12.9 / 5.3	1.8 / 0.6	7.8 / 8.2	92	77
January 2018	8.361944 / 8.312998	80.4 / 87.1	0 / 1.8	19 / 9.9	0.6 / 1.2	8.8 / 7.8	80	91

Table C-3.5. DOP compositions of Missisquoi Bay before and after redox incubations for ESI negative and positive. % CHOP, % CHOSP, % CHONP, and % CHONSP are percentages of all P-containing assignments. % DOP is the percentage of P-containing molecules relative to all assigned formulae. First value indicates bottom water, the following value indicates reduced core water.

Sample	H/C	O/C	AI	DBE
May	1.17 / 1.20	0.41 / 0.40	0.082 / 0.027	20 / 18
September	1.18 / 1.25	0.44 / 0.42	0.0022/ -0.040	18 / 16
January	1.18 / 1.23	0.42 / 0.40	0.043 / 0.00076	20 / 18

Table C-3.6. Changes in H/C, O/C, AI, and DBE values before and after reduction for ions common to both ESI negative and ESI positive. All values are computed medians except for AI which are the computed means. First value indicates bottom water, the following value indicates reduced core water.

Curriculum Vitae

Martin Roman Kurek

Education

- Indiana University-Purdue University Indianapolis (IUPUI) (August 2017 – July 2019)
  Master of Science in Geology
  Advisor: Dr. Gregory Druschel

- IUPUI (August 2013 – May 2017)
  Bachelor of Science in Chemistry, ACS certified with highest distinction
  Minors in Geochemistry and Mathematics

Research and teaching experience

- IUPUI (2017-2019)
  Graduate researcher
  Aqueous geochemistry research in the Earth Science department concerning organic phosphorus and dissolved organic matter including instrumental analysis, field sampling, and experimental design.

- IUPUI (2015 – 2017)
  Organic chemistry lab II teaching assistant
  Lead lab activities, graded assignments and lab reports, monitored students' experiments, and tutored students in the department resource center.

- IUPUI (2015-2017)
  Undergraduate researcher
  Aqueous geochemistry research in the Earth Science department focusing on stable isotopic analysis and electrochemistry of inorganic sulfur species including instrumental analysis, field sampling, and experimental design.

- IUPUI (2014-2015)
  Undergraduate researcher
  Organic synthesis research in the Chemistry and Chemical Biology department including preparation, syntheses, purification, and analysis of pharmaceutical molecules.

Scholarships and awards

- IUPUI University graduate student fellowship (2017-2018)
- Outstanding Undergraduate Analytical Chemistry Student Award (2017)
- Marilyn S. Morrison Scholarship (2016)
- NSF REU Fellowship recipient (2016)

- Cressy T. Haven Scholarship (2016)
- Loren T. Jones Memorial Research Scholarship (2015)
- UROP research grant recipient (2014)
- School of Science Scholar's List (2014-2017)
- Dean's Science Scholar scholarship (2013-2017)
- Dean of Faculty's scholarship (2013-2017)

Select presentations

- Kurek, M. R., Harir, M., Shukle, J. T., Wilkes, A., Leduc, M., Schroth, A. W., Schmitt-Kopplin, P., & Druschel, G. K. Understanding organic phosphorus cycling in redox-dynamic eutrophic systems. Poster. *Goldschmidt Geochemistry Conference, Boston, August 2018.*

- Kurek, M. R., Harir, M., Shukle, J. T., Wilkes, A., Leduc, M., Schroth, A. W., Schmitt-Kopplin, P., & Druschel, G. K. A multi-analytical approach for studying organic phosphorus cycling in freshwater systems. Poster. *Gordon Research Symposium and Conference, Galveston, January 2018.*

- Kurek, M. R., Harir, M., Shukle, J. T., Wilkes, A., Leduc, M., Schroth, A. W., Schmitt-Kopplin, P., & Druschel, G. K. Ultra-high resolution mass spectrometry as a tool to study freshwater phosphate cycling. Poster. *Midwest Geobiology Symposium, Indianapolis, September 2017.*

- Kurek, M. R., Druschel, G. K., & Gilhooly III, W. P. The Effects of Surfactants on Colloidal, Nanoparticulate, and Dissolved Sulfur. Poster. *1st Geobiology Society Conference, Banff, June 2017*.

- Kurek, M. R., Gilhooly III, W. P., & Druschel, G. K. A Novel Method to Reduce and Quantify Elemental Sulfur. Poster. *GSA North Central Section Meeting*, *Pittsburgh, March 2017.*

Publications

- Kurek, M. R., Harir, M., Shukle, J. T., Druschel, G. K., Wilkes, A., Leduc, M., Schroth, A. W., & Schmitt-Kopplin, P. (in prep). Seasonal processing of dissolved organic matter and organic phosphorus in a polymictic basin: implications for redox-driven eutrophication.

- Kurek, M. R., Harir, M., Shukle, J. T., Druschel, G. K., Schroth, A. W., & Schmitt-Kopplin, P. (in prep). Chemical fractionation of organic matter and organic phosphorus extractions from freshwater lake sediment.

- Kafantaris, F. C., Crane, E. J., Kurek, M. R., Nuzzio, D., & Druschel, G. K. (in prep). Electroanalytical chemistry of elemental sulfur.

- Kurek, M. R., Gilhooly III, W. P., Druschel, G. K., O'Beirne, M. D., & Werne, J. P. (2018). The use of dithiothreitol for the quantitative analysis of elemental sulfur concentrations and isotopes in environmental samples. *Chemical Geology*, *481*, 18-26.

- Miao, J., Yang, K., Kurek, M., & Ge, H. (2015). Palladium-Catalyzed Site-Selective Fluorination of Unactivated C (sp3)–H Bonds. *Organic letters*, *17*(15), 3738-3741.